Rational chemical applications of explosion-graphene

by

Jose Jesus Covarrubias

A.S. Chemistry, Seward County Community College, 2014
B.S. Biochemistry, Kansas State University, 2017

AN ABSTRACT OF A DISSERTATION

submitted in partial fulfillment of the requirements for the degree

DOCTOR OF PHILOSOPHY

Department of Chemistry
College of Arts and Sciences

KANSAS STATE UNIVERSITY
Manhattan, Kansas

2021

Abstract

Cancer is a very complex disease that has zero respect for humans; it affects every human being no matter what age, gender, race, or ethnicity they come from. It is among the leading causes of deaths worldwide. In the United States alone, it is the second leading cause of death. On average, there are approximately 4 new cancer cases and 1 death every minute. For this reason, researchers have explored the use of several materials in the development of novel strategies to fight cancer. Fortunately, thanks to the extraction of graphene (a honeycomb sheet of carbon atoms) and the discovery of its extraordinary properties in 2004, graphene became the wonder material of the 21st century due to its unique properties, including excellent electrical and thermal conductivity, optical transparency, and mechanical strength. For this reason, many researchers were inspired to explore the possibility of using graphene in cancer applications; however, it has been difficult to take complete advantage of graphene's exceptional properties because large-scale production methods are neither simple nor economical. For this reason, the goal of this dissertation was to overcome one of the greatest challenges in mass-producing high-quality graphene materials in a reproducible way at low cost that could be easily modified and used in a variety of areas such as nanoelectronics, sensors, batteries, supercapacitors, and in biomedicine including cancer applications. Therefore, we have synthesized the first known turbostratic core/shell graphene oxide which is designed to incorporate the unique physical and materials properties of graphene into numerous materials. This was accomplished by oxidizing high-quality explosion synthesized few-layer graphene by means of Fenton oxidation. Additionally, the reaction was successfully scaled up from 1.0 g batch to 200g per batch maintaining all of graphene's extraordinary properties intact because only the surface layers of few-layer graphene get oxidized during Fenton oxidation. Furthermore, we have developed a

graphene-based nanobiosensor for the early detection of lung cancer, which causes the highest number of deaths than any other type of cancer in the United States. Based on the results, our graphene-based nanobiosensor was able to detect biomarkers down to the sub-femtomolar level after 1 hour of incubation. This presents a promising opportunity to detect lung cancer at a much earlier stage. This is very important in lung cancer detection because cancer survival significantly increases when it is detected at stages 0, 1 compared to 3 or 4.

Rational chemical applications of explosion-graphene

by

Jose Jesus Covarrubias

A.S. Chemistry, Seward County Community College, 2014
B.S. Biochemistry, Kansas State University, 2017

A DISSERTATION

submitted in partial fulfillment of the requirements for the degree

DOCTOR OF PHILOSOPHY

Department of Chemistry
College of Arts and Sciences

KANSAS STATE UNIVERSITY
Manhattan, Kansas

2021

Approved by:

Co-Major Professor
Dr. Paul Smith

Approved by:

Co-Major Professor
Dr. Stefan H. Bossmann

Copyright

Abstract

Cancer is a very complex disease that has zero respect for humans; it affects every human being no matter what age, gender, race, or ethnicity they come from. It is among the leading causes of deaths worldwide. In the United States alone, it is the second leading cause of death. On average, there are approximately 4 new cancer cases and 1 death every minute. For this reason, researchers have explored the use of several materials in the development of novel strategies to fight cancer. Fortunately, thanks to the extraction of graphene (a honeycomb sheet of carbon atoms) and the discovery of its extraordinary properties in 2004, graphene became the wonder material of the 21st century due to its unique properties, including excellent electrical and thermal conductivity, optical transparency, and mechanical strength. For this reason, many researchers were inspired to explore the possibility of using graphene in cancer applications; however, it has been difficult to take complete advantage of graphene's exceptional properties because large-scale production methods are neither simple nor economical. For this reason, the goal of this dissertation was to overcome one of the greatest challenges in mass-producing high-quality graphene materials in a reproducible way at low cost that could be easily modified and used in a variety of areas such as nanoelectronics, sensors, batteries, supercapacitors, and in biomedicine including cancer applications. Therefore, we have synthesized the first known turbostratic core/shell graphene oxide which is designed to incorporate the unique physical and materials properties of graphene into numerous materials. This was accomplished by oxidizing high-quality explosion synthesized few-layer graphene by means of Fenton oxidation. Additionally, the reaction was successfully scaled up from 1.0 g batch to 200g per batch maintaining all of graphene's extraordinary properties intact because only the surface layers of few-layer graphene get oxidized during Fenton oxidation. Furthermore, we have developed a

graphene-based nanobiosensor for the early detection of lung cancer, which causes the highest number of deaths than any other type of cancer in the United States. Based on the results, our graphene-based nanobiosensor was able to detect biomarkers down to the sub-femtomolar level after 1 hour of incubation. This presents a promising opportunity to detect lung cancer at a much earlier stage. This is very important in lung cancer detection because cancer survival significantly increases when it is detected at stages 0, 1 compared to 3 or 4.

Table of Contents

List of Figures

List of Tables

Acknowledgements

I want to thank my advisor, Dr. Stefan H. Bossmann for all of his guidance, motivation, support, and help during these past 7 years. Thank you for giving me the opportunity to explore what the world of research was like as an undergraduate and for taking me on as a graduate student a couple of years later. There are not enough words to express how grateful I am to have had the best mentor and role model throughout this journey. Thank you very much for always being there, and most importantly for not letting me throw the towel all those times I would come into your office ready to quit. You always found the right words to lift me up and motivate me to continue to work hard.

I also want to thank Katrin Bossmann, for all your support all these years. Thank you very much for always taking the time to message me just to check how things were going. I am grateful to have been able to work with you and to be part of the first article from KSU to get published on the Leonardo journal. Thank you for always posting all of those amazing art creations, they truly are inspiring!

I would also like to thank Dr. Deryl Troyer, Dr. Tej Shrestha, and Marla Pyle for giving me the opportunity to do a summer internship in their laboratory and introducing me to the cell world. I enjoyed every minute of it. Thank you for all your attention and for always being willing to help me with anything I needed.

Also, I want to thank Dr. Todd Carter, the main reason why I ended up going to Kansas State University. Thank you for convincing me to have a plan B in case plan A (pharmacy school) did not work. Thank you for your endless support even until this day.

I would like to thank my committee members Dr. Daniel Higgins, Dr. Christopher Culbertson, Dr. Punit Prakash, Dr. Paul Smith, and Dr. A. Lorena Passarelli for their time, support, and suggestions.

A big thank you also goes to Dr. Hongwang Wang, for taking the time and dedication to discuss with me in detail all the work we were doing when I was an undergraduate. He was an inspiration why I wanted to go graduate school.

I would also like to thank the professors, faculty, and staff from the Department of Chemistry. Specially, I want to thank James Hodgson and Tobe Eggers for helping and ensuring that everything (apparatus or glassware) was running smooth.

Also, I would like to thank all former and current members of the Bossmann research group (aka the Bossmannites)! A big thanks to Kayla, for always been there supporting each other as we suffered together throughout classes, research, and cumes. Also, I want to thank the undergraduates that worked with me, Azzy Minjarez, Steven Eschliman, and Laura Soto. Thank you for all of your hard work and all the help in the lab. It was a great pleasure to have worked with you, and I am excited to see where life takes you all next.

In the same way, I want to thank the undergraduate research programs that gave me the opportunity to be funded for my undergraduate summers to stay involved in research. Special thanks to Bridges to the Future, Developing Scholars Program, McNair Scholars Program, and Kansas Idea Network of Biomedical Research Excellence (K-INBRE) program. Thank you as well to Anita Cortez for her support and advice and for always pointing me in the right direction when I needed help.

A huge thank you also goes to my sweet girlfriend, Dr. Pamela L. Maynez. Thank you for your unconditional support and love all these years. Thank you for accompanying me to my

conferences, for listening to me when I needed to vent, and for always motivating me to keep going and to not give up. But above all thank you for introducing me to Dr. Bossmann.

Lastly, I would like to thank my beloved family! Thank you to my two older brothers (two of my biggest role models) Julian and Salvador Covarrubias for their unconditional support, advice, and love, and for always being there at all times ready to jump and help at any time no matter what the situation is. Of course, a huge thanks goes to my sister, my best friend, my accomplice, and role model. Thank you for opening so many doors, and for always being there through thick and thin. Thanks for always motivating me to give my best. Since we were little kids, you have always been ahead leading the way, guiding, and helping me to get up when I fall. I remember that I always hated being compared to you but now it fills me with pride, and I presume to everyone that I am Obdulia's little brother. I also want to thank my 5 nephews, the most loving children in the world who follow me and admire my work, and that more than nephews for me it is as if they were my own children. Thank you also to my sisters-in-law and my brother-in-law (Maria Elena, Miriam, y Ricardo) for their support.

Finally, thank you so much to my loving parents, who are responsible for me being here today. Thank you for all your sacrifices, for the scolding and the punishments that led me to be the man I am nowadays. Thank you, mom and dad, for having made that difficult decision in July 2006, in the middle of the world cup, to bring us to the United States. This achievement is because of you who without thinking gave me everything, worked and sacrificed a lot to help my siblings and me move forward, you should feel proud to see your children succeed. I know I gave you a lot of headaches, but you always had the wisdom and right way to guide me to this day. Gracias papa y mama los amo!!! This doctorate is not only mine, thank you to all and God who were and are important pieces for me to have made it to this day. Si se pudo!!!

Dedication

To my loving parents Julian and Obdulia Covarrubias, they are my heroes because they worked hard and made a lot of sacrifices for my siblings and me so we could have a better future. None of this would have been possible if my parents did not take the decision in 2006 to migrate to the United States. Also, I want to dedicate this to God, for blessing me with the family, friends, and parents that supported me and made this journey possible!

Chapter 1 - Graphene-based materials: The newly emerging enemy of cancer

1. Importance of Cancer Research

Cancer is a very complex disease that has zero respect for humans; it affects every human being no matter what age, gender, race, or ethnicity they come from. Cancer is a disease caused by the uncontrolled growth and division of abnormal cells in the body.[1,2] This uncontrolled cell growth leads to the formation of large masses of tissues called tumors, often classified as benign or malignant tumors, and can occur almost anywhere in the human body. Benign tumors do not spread into nearby tissues and usually do not grow back once removed, whereas malignant tumors can spread into nearby tissues to form new tumors and sometimes grow back when removed.[1] Overall, cancer death rate has continued to decline thanks to the advancement in the development of more effective treatments for cancer; however, to date, there is no way to prevent cancer because there are several factors that have been associated to increase cancer risk. It is well known that cancer is caused by gene mutations; however, there are several reasons known to trigger these mutations, varying from person to person. A gene mutation can affect a healthy cell in the following ways: it can make mistakes when repairing DNA errors, allow rapid growth, and fail to stop uncontrolled cell growth.[2] Some mutations can be either inherited from parents, which there is no control over, or occur after birth, where factors could be modifiable (e.g., smoking, radiation, carcinogens, poor nutrition).[2]

Unfortunately, cancer is among the leading causes of deaths worldwide. In the United States alone, it is the second leading cause of death after heart disease.[3] In 2019, statistics showed that there were approximately 16.9 million cancer survivors living in the United States, and this number is expected to reach 22.2 million by 2030.[1,4] Cancer has not only impacted many

lives worldwide, but it has also had a great economic impact. In 2015, the estimated cancer-related medical cost in the United States alone was $183 billion, and this number is expected to increase to approximately $246 billion by 2030.[1,4] However, the projection could be much higher because of the growing cost of prescription medicines. Last but not least, statistics showed that in 2021 in the United States alone there will be approximately 1,898,160 new cancer cases and 608,570 cancer deaths.[4] That is approximately four new cancer cases and one death per minute. To put it into perspective, the United States population is expected to grow by approximately 1.9 million in 2021. This means that for nearly every new person (either born or migrated to the United States), there will be one diagnosed with cancer.[5] Because of these reasons, researchers have been intensively exploring ways to create safer and more effective methods to fight cancer.

2. Graphene's history, structure and properties

Throughout the years, researchers have explored the use of several materials in the development of novel strategies to fight cancer. Most of these materials require extensive modifications in order for these to be useful for bio-applications: they must have unique properties such as water stability, good biocompatibility and nontoxicity, and facile conjugation to biological molecules.[6] Fortunately, in 2004, two physicists from the University of Manchester, Andre Geim and Konstantin Novoselov, isolated graphene (G) from a piece of graphite simply using adhesive tape, and discovered that it had a unique combination of extraordinary properties.[7] G is a honeycomb sheet of carbon atoms that is one atom-thick, and it is the building block for other materials (e.g. graphite, carbon nanotubes, and fullerene).[7,8] The reason G was considered the wonder material of the 21st century was due to its remarkably unique properties, including excellent electrical and thermal conductivity, optical transparency and mechanical strength.[8,9] G is considered to be the toughest 2D material; it is harder than diamond or steel but

lighter than aluminum and more elastic than rubber.[8,9] Not only this, but G's electrical conductivity is 13x better than copper, its electron mobility is 100x faster than silicon, its heat conductivity is 2x better than diamond, and it has a large surface area.[8,9] Because of the ground-breaking experiments performed on G, Geim and Novoselov received the Nobel Prize in Physics in 2010. Their discovery of G's unique properties inspired many researchers to explore the possibility of using graphene in different areas such as nanoelectronics, sensors, batteries, supercapacitors, and in biomedicine including cancer applications.[7-10]

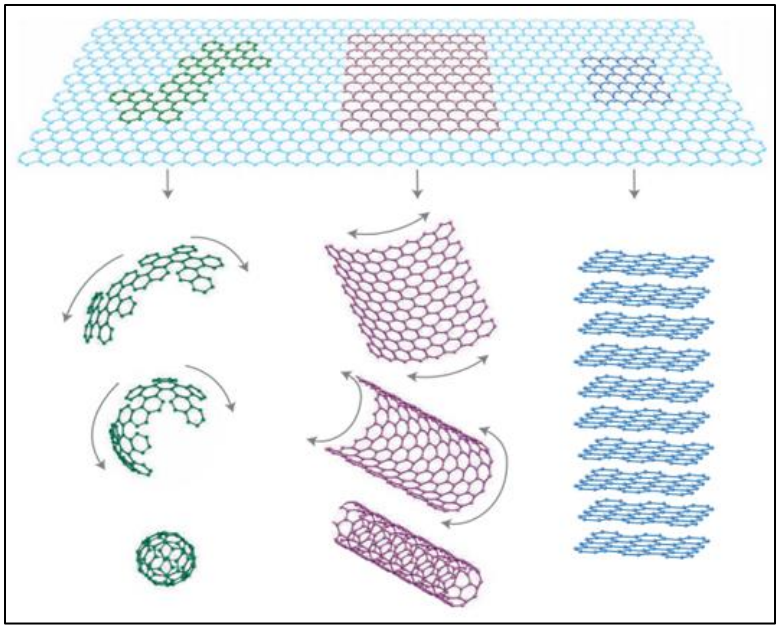

Figure 1-1 Graphene: Mother of all graphitic forms.[8]

3. Synthesis progress of graphene and its derivatives

After the discovery of graphene, several strategies have been developed to synthesize graphene with hopes of achieving large-scale production methods to take complete advantage of G's amazing properties. Most of the strategies developed to produce graphene can be grouped into two categories: "bottom up" and "top down" methods. The bottom-up method, or "construction" method, involves synthesizing graphene

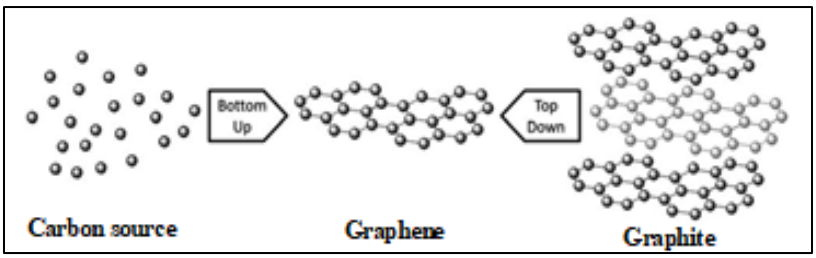

Figure 1-2 "Top" vs "Bottom" methods for graphene synthesis.[11]

from carbon-containing materials, whereas the top down method, or "destruction" method, involves synthesizing graphene via exfoliation of graphite (isolation of layers).[11] However, taking complete advantage of G's exceptional properties has been difficult since large-scale production methods are neither simple nor economical. Despite this, the largest issue remains in maintaining sheet separation of G to prevent irreversible agglomeration and restacking of sheets forming multilayer graphite. As a solution to this issue, researchers have been looking for ways to make processable G that would not only help in preventing aggregation but also improve water stability without needing surfactant or polymeric stabilizers.[12] Therefore, oxidizing G to make graphene oxide (GO), which is decorated with oxygen-containing hydrophilic groups, became an alternative for overcoming these issues.[12] Both agglomeration and water stability issues must be improved in order for any material to be useful in biomedical applications.[13] In general, GO is synthesized by some variation of either the Brodie, Hummers, or Staudenmaier methods. Staudenmaier and Brodie methods use a combination of potassium chlorate with nitric and/or sulfuric strong acids, whereas Hummers method uses a combination of potassium permanganate, sulfuric acid, and sodium nitrate.[14] Even though the reason why GO came about was because it could be easily reduced back to G, recent studies demonstrated that GO could be used as an independent nanomaterial due to its unique properties.[14] Due to the limitations on traditional cancer therapies, such as lack of specificity and toxicity, G and GO have been explored to create safer and more effective methods to fight cancer thanks to their unique properties.[13,15] In this report, we will discuss how graphene based materials have been used to

develop more effective ways to battle cancer, more specifically in applications in cancer diagnosis and therapies.

4. Graphene-based materials in cancer diagnosis

Regardless of the recent advances in the fight against cancer, it is still considered one of the leading causes of deaths worldwide. Being able to detect cancer early is the first line of defense against this awful disease. That is why researchers have been intensively investigating ways to create reliable, cost-effective and less invasive methods for early cancer detection and better prognosis. Early cancer detection does not only increase survival rates dramatically, but it also helps to find better treatments that can prevent the spread of cancer to nearby tissues while reducing risk of adverse side effects. Nowadays, electrochemical sensors have been viewed as a great alternative to develop early cancer detection biosensors because of the advantages of rapid detection, cost effectiveness, high sensitivity and specificity.[16] That is because current methods for detecting tumors, such as histological and immunological methods, are expensive, have a long turnaround time, and require experienced personnel.[16] For this reason, researchers have been investigating ways to create faster and safer ways to detect cancer at an early stage using electrochemical sensors. Roberts, A. *et. al.* developed a new ultrasensitive electrochemical biosensor for urokinase plasminogen activator receptor (uPAR) detection, a biomarker of cancer, based on graphene nanosheets (GNs), a Fluorine-doped tin oxide (FTO) electrode, and monoclonal uPAR antibody (uPAR-Ab) (Figure 1.3).[17] The FTO-electrode was chosen over ITO (Indium tin oxide) electrodes because this is less expensive and more chemically stable, and it has a high electrical conductivity. Similarly, GNs were chosen as the suitable nanomaterial due to their excellent electrochemical properties and high surface-to-volume ratio. Also, due to the specific immunological interaction between an antibody and a specific antigen, antibodies have

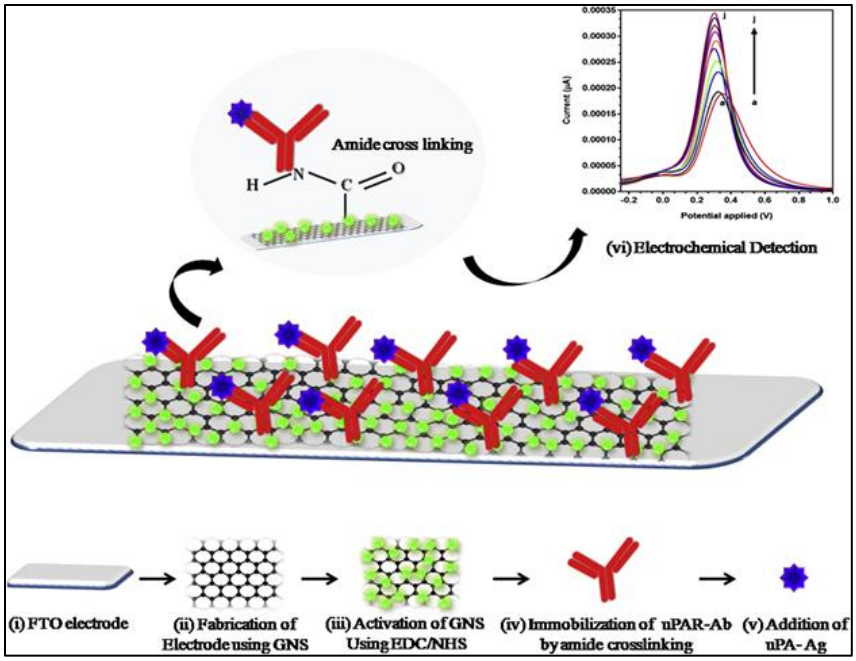

Figure 1-3 Schematic illustration of fabrication procedure of FTO-GNS/uPAR-Ab immunosensor.[17]

been used as a biosensing tool for fast detection of various analytes in biological samples and provide sensors with high specificity and sensitivity.[17] For this reason, uPAR-Ab was used as the recognition element for the specific detection of uPA antigen (uPA-Ag). In brief, their GNs were synthesized from graphite powder, which was oxidized by a modified Hummer's method, followed by sonication and autoclave for four hours to produce reduced graphene oxide nanosheets (GNs). Next, GNs were activated using carbodiimide chemistry, followed by fabrication of GNs on the FTO electrode via physisorption at room temperature to obtain high electrical conductivity. Lastly, the FTO-GNs/uPAR-Ab immunosensor was fabricated by coupling uPAR-Ab with activated GNs using EDC-NHS as a heterobifunctional crosslinker. Their results demonstrated that, under optimum conditions, the proposed sensor showed a linear detection range of 1 fM to 1 uM with a detection limit of 4.8 fM in standard and a rapid response time of 35 seconds. Furthermore, their immunosensor showed good reproducibility, repeatability, and storage stability in which up to 75% of initial activity was observed up to 4 weeks. Therefore, their developed immunosensor demonstrated that using GNs, due to the fast conduction of electrons, helped increase the sensitivity of the sensor and overcome the issues with response time. These

promising results indicated that GNs can be used to develop highly efficient sensors for early detection of cancer.

5. Graphene-based materials in cancer therapy

If detecting cancer early fails, the next line of defense is to find the most optimal way to treat it. The type of treatment typically depends on the type of cancer and how advanced it is. Sadly, cancer treatments available to date such as chemotherapy, which uses drugs to kill cancer cells, and radiation therapy, which uses X-rays to kill cancer cells, often come with terrible side effects. These side effects occur because such treatments not only kill cancer cells, but also kill or slow growth of healthy cells, leading to the weakening of the immune system, thus causing adverse complications (e.g., hair loss, infections, fertility effects, fatigue, nausea, seizures, and low blood counts).[18] For this reason, researchers have been intensively exploring ways to create targeted delivery systems that will help improve efficacy while reducing adverse side effects.

5.1. MRI & Targeted Drug Delivery

In recent years, targeted drug delivery in combination with imaging strategies have been explored as a great alternative to develop multifunctional cancer treatments that could monitor progression of tumors and provide treatment at the same time. Unfortunately, the development of an efficient theranostic agent with improved loading of drug and diagnostic agents, low cytotoxicity, controlled release profile and efficient targeting delivery has been a major challenge. However, with the discovery of graphene, researchers are exploring ways to take advantage of G's large surface area to overcome this challenge and create better theranostic agents with improved loading of drugs, diagnostic agents, and targeting groups. Not long ago, Foroushani, M. S. et. al. developed a theranostic system based on GO integrated with polydopamine (PDA), bovine serum albumin (BSA), a pentetic acid manganese-based (DTPA-

Mn(II)) contrast agent, folic acid (FA), and the 5-fluorouracil (5Fu) anticancer drug for targeting colon cancer cells (Figure 1.4).[19] GO was selected as a platform for drug delivery due to its large surface area and ease of surface functionalization, which is used to load anticancer drugs, diagnostic agents and targeting groups. PDA was used to stabilize and protect the reduced graphene oxide (RGO), which also helps to bind BSA and FA onto the RGO-PDA surface. BSA was used for two reasons: 1) it plays an important role in drug delivery due to its high cellular uptake in tumor and inflamed tissues, and 2) it plays an antifouling role to block excess active sites to prevent adsorptions of unwanted materials on the surface. Similarly, FA was used as a targeting agent for folate receptors, typically overexpressed on cancer cells. Finally, DTPA-Mn(II) was used as a contrast agent for MRI and 5Fu as a model of an anticancer drug. In short, their GO was synthesized from graphite powder using a modified Hummers' method. Next, GO was dispersed in a PBS buffer with a pH of 8.5 by using an ultrasonic bath; afterwards, GO was functionalized with PDA at 60 C for 24 hours to form RGO-PDA. From there, the loading of BSA and FA on the surface of RGO-PDA was done at room temperature for 24 hours in PBS with a pH of 8.5. BSA and FA were attached via Michael addition and/or Schiff base reactions, forming RGO-PDA-BSA/FA. Subsequently, DTPA was covalently immobilized onto the nanoplatform surface via chemical reaction between -COOH of

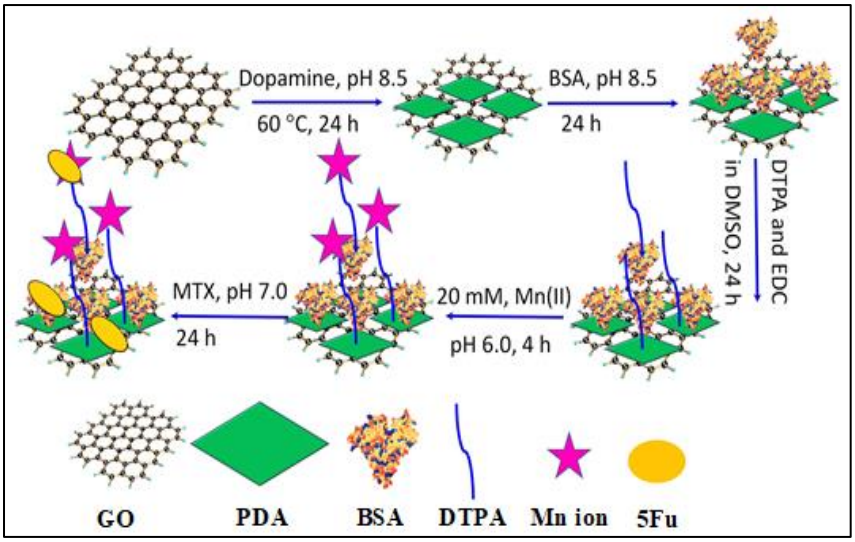

Figure 1-4 Schematic illustration for step-by-step modification of GO surface by PDA, BSA, DTPA-Mn(II), and 5Fu compounds.[19]

DTPA and -NH_2 groups of the surface using EDC as an activator. Next, complexation of Mn(II) was performed by mixing $MnCl_2$ and RGO-PDA-BSA/FA-DTPA in distilled water with a pH adjusted to 6.0 for 4 hours. Finally, 5Fu was loaded to the nanocarrier to form RGO-PDA-BSA/FA-DTPA-MN(II)/5Fu by mixing the nanocarrier with an aqueous solution of 5Fu with a pH of 7.0 at a mass ratio of 5Fu to the nanocarrier powder of 2:1.[19] After characterizing their theranostic system, they moved on to do *in-vitro* and *in-vivo* studies. Their results demonstrated that their theranostic system enhanced the contrast of cancer cells, had high biocompatibility, and was able to deliver the 5Fu anticancer drug into CT-26 tumors, which was shown to successfully inhibit the growth of tumors (Figure 1.5). Therefore, their results demonstrated that it is possible to use G-based materials to develop theranostic systems for both enhancement of contrast and inhibition of cancer cell growth.

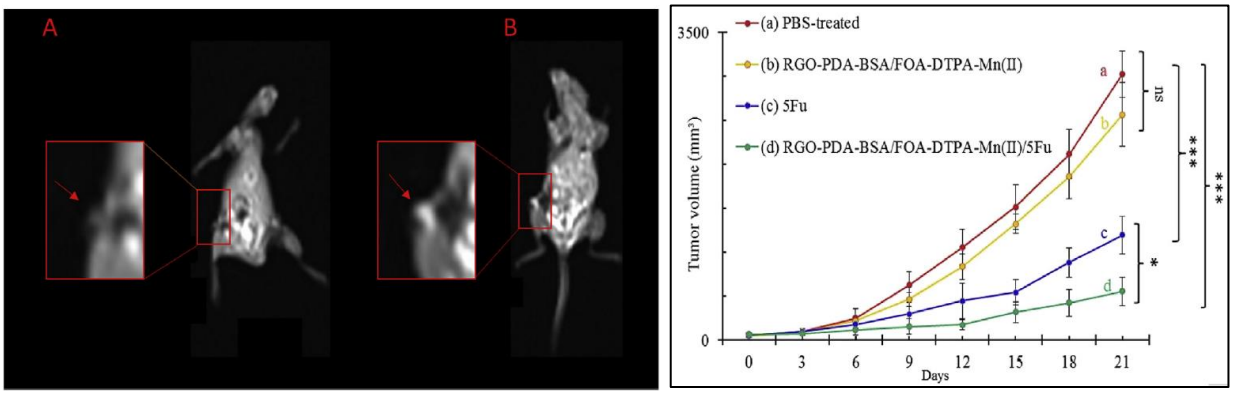

Figure 1-5 T_1 MRI images and drug delivery efficacy of RGO-PDA-BSA/FOA-DTPA-Mn(II)/5Fu system.[19]

5.2. Photodynamic Therapy & Targeted Drug Delivery

In the search for developing effective cancer treatments, photothermal therapy (PTT) has been considered a promising strategy for cancer therapy, which is a light-based therapy that kills cancerous cells by heat generated from absorbed near-infrared (NIR) light energy. However, one of the main issues in PTT is finding a good photothermal agent that will prevent heat from

filtering out and damaging the surrounding tissue. Nevertheless, previous studies have demonstrated that GO can serve as a photothermal agent with low cytotoxicity.[20,21] For this reason, researchers have been exploring ways to combine GO's photothermal property with drug delivery mechanisms to create multifunctional cancer therapies. Recently, Liang, J. *et. al.* developed a targeted nanocomplex based on GO integrated with targeted FA, the chemotherapeutic drug doxorubicin (DOX), and the photosensitizer methylene blue (MB).[22] In brief, their nanoscale-GO (NGO) was synthesized from graphite powder based on a modified Hummer's method by ultrasonication. Next, NGO was carboxylated with chloroacetic acid and sodium hydroxide to introduce more carboxyl groups to obtain carboxylated nanoscale-GO (NCGO). Subsequently, FA was linked to NCGO by a classical amide reaction between -NH_2

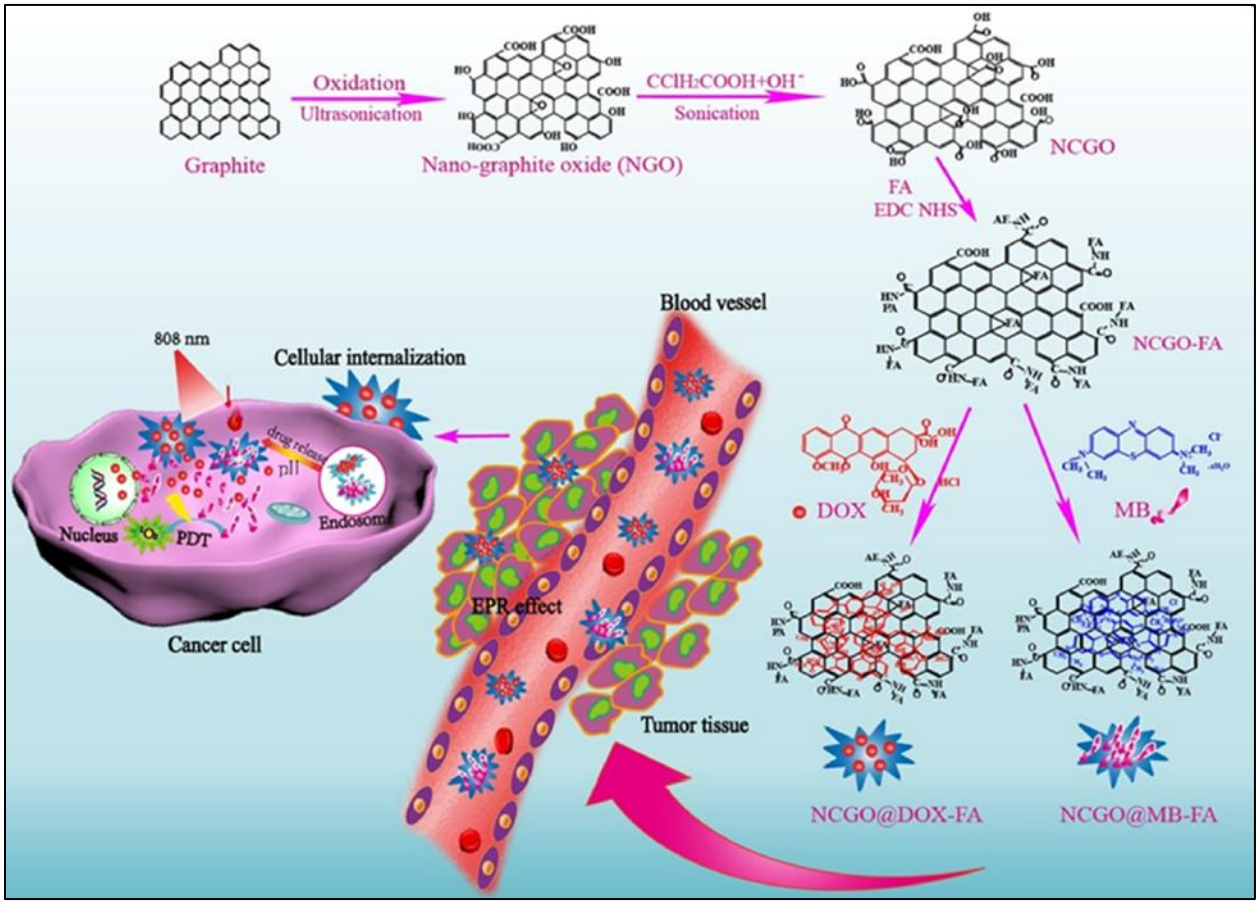

Figure 1-6 Schematic illustration of fabrication of NCGO@DOX-FA and NCGO@MB-FA.[22]

groups in FA and -COOH groups of NCGO using EDC/NHS coupling in a 0.5% sodium bicarbonate solution ($NaHCO_3$) with a pH of 8.0, at room temperature for 24 hours. Finally, MB and DOX were separately loaded to the nanocarrier by mixing a certain amount of nanocarrier with different concentrations of DOX or MB, forming NCGO@DOX-FA and NCGO@MB-FA through π−π stacking, electrostatic attractions, and/or hydrophobic interactions (Figure 1.6).[22] Their results demonstrated their nanoplatform had targeting specificity, a high-load content of drugs, an excellent photothermal conversion efficiency and photostability, a pH and thermal dual-responsive drug release behaviors, and an excellent hemocompatibility (Figure 1.7). As a result, their nanoplatform showed promising results as a potential candidate for photothermal-photodynamic or photothermal-chemo synergistic therapy for cancer applications. Therefore, once again, it was shown that graphene-based materials can not only be used to develop drug delivery platforms but can also be used for therapy due to the materials' excellent photothermal conversion efficiency.

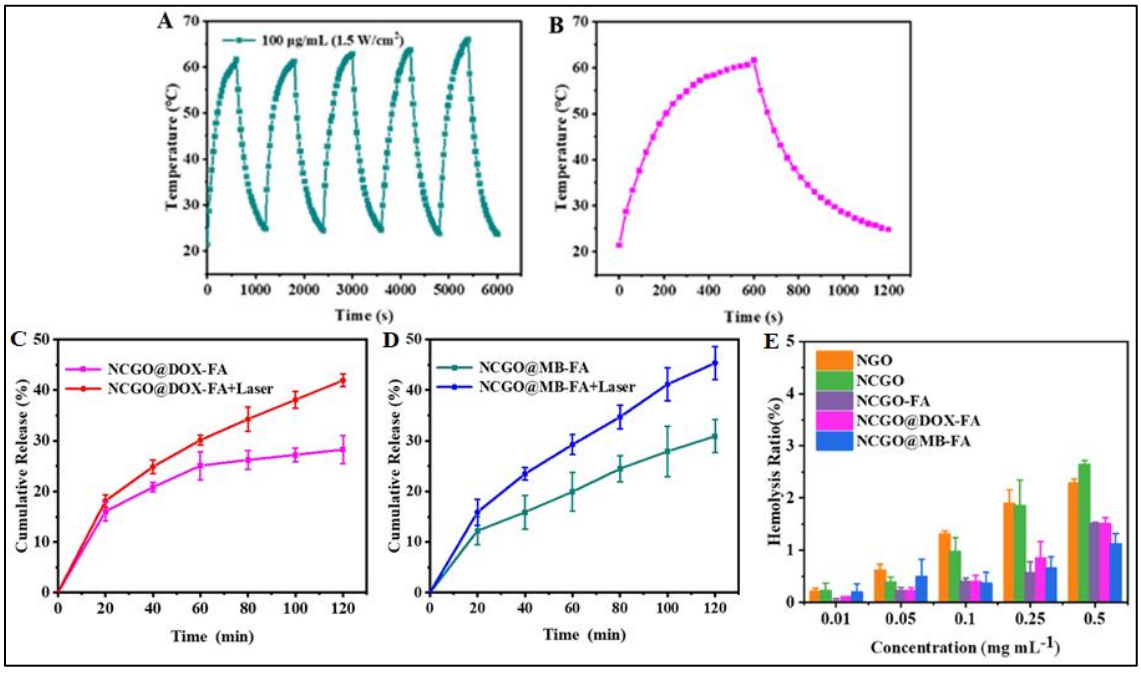

Figure 1-7 A) Photostability of NGGO-FA, B) Phototermal response of NCGO-FA, Drug release profiles of (C) NCGO@DOX-FA & (D) NCGO@MB-FA, and E) Hemolysis assay.[22]

6. Conclusion

In conclusion, the discovery of graphene revolutionized the world by offering new ways to fight cancer. Due to graphene's outstanding properties, the role of these emerging materials in cancer applications has grown rapidly in the last five years. There have been several promising results indicating that graphene-based materials not only have the ability to improve the delivery of drugs thanks to their large surface areas, but they also can enhance therapies thanks to their high electrical and thermal conductivities. Even though there have been several successful studies demonstrating the potential of graphene-based materials in cancer applications, there are still several challenges that need to be addressed before these materials reach clinical human trials. One of the most fundamental challenges graphene-based materials face is the mass-production of high-quality graphene sheets. Another important challenge is their biocompatibility as well as their long-term toxicity. Although several studies have reported that functionalizing G to GO significantly improves biocompatibility, since most of the current investigations are short-term *in-vitro* studies, the potential long-term toxicity of graphene-based materials needs to be explored. Therefore, further *in-vivo* studies including their effect on metabolism needs to be investigated before these can be used for clinical human trials. Nevertheless, as time passes, there are more results strongly supporting the evidence that graphene-based material could play a critical role in the fight against cancer.

7. References

[1]Understanding Cancer https://www.cancer.gov/about-cancer/understanding

[2]Cancer https://www.mayoclinic.org/diseases-conditions/cancer/symptoms-causes/syc-20370588

[3]Holland, K. 12 leading causes of death in the United States https://www.healthline.com/health/leading-causes-of-death

[4]Cancer Facts & Figures 2021 https://www.cancer.org/research/cancer-facts-statistics/all-cancer-facts-figures/cancer-facts-figures-2021.html

[5]U.S. Population Growth Rate 1950-2021 https://www.macrotrends.net/countries/USA/united-states/population-growth-rate

[6]Bohara, R. A.; Thorat, N. D.; Pawar, S. H. Role of Functionalization: Strategies to Explore Potential Nano-Bio Applications of Magnetic Nanoparticles. *RSC Adv.* **2016**, *6* (50), 43989–44012. [7]Geim, A. K., & Novoselov, K. S. (2007). The rise of graphene. *Nature Materials*, 6(3), 183–191.

[8]Michael, B. What is graphene? https://www.nanowerk.com/what_is_graphene.php

[9]Gulfam, S. Graphene's Properties. http://www.jamiamedia.com/2019/08/graphenes-properties/

[10]Liu, J.; Cui, L.; Losic, D. Graphene and Graphene Oxide as New Nanocarriers for Drug Delivery Applications. *Acta Biomater.* **2013**, *9* (12), 9243–9257.

[11]Edwards, R. S.; Coleman, K. S. Graphene Synthesis: Relationship to Applications. *Nanoscale* **2013**, *5* (1), 38–51.

[12]Li, D.; Müller, M. B.; Gilje, S.; Kaner, R. B.; Wallace, G. G. Processable Aqueous Dispersions of Graphene Nanosheets. *Nat. Nanotechnol.* **2008**, *3* (2), 101–105.

[13]Orecchioni, M.; Cabizza, R.; Bianco, A.; Delogu, L. G. Graphene as Cancer Theranostic Tool: Progress and Future Challenges. *Theranostics* **2015**, *5* (7), 710–723.

[14]Dideikin, A. T.; Vul, A. Y. Graphene Oxide and Derivatives: The Place in Graphene Family. *Frontiers in Physics* **2019**, 6.

[15]Tadyszak, K.; Wychowaniec, J. K.; Litowczenko, J. Biomedical Applications of Graphene-Based Structures. *Nanomaterials (Basel)* **2018**, *8* (11), 944.

[16] Zhang, Z.; Li, Q.; Du, X.; Liu, M. Application of Electrochemical Biosensors in Tumor Cell Detection. *Thoracic Cancer* **2020**, *11* (4), 840–850.

[17]Roberts, A.; Tripathi, P. P.; Gandhi, S. Graphene Nanosheets as an Electric Mediator for Ultrafast Sensing of Urokinase Plasminogen Activator Receptor-A Biomarker of Cancer. *Biosensors and Bioelectronics* **2019**, 141, 111398.

[18]www.cancer.gov/about-cancer/treatment/types.

[19]Foroushani, M. S. *et. al*. Folate-Graphene Chelate Manganese Nanoparticles as a Theranostic System for Colon Cancer MR Imaging and Drug Delivery: In-Vivo Examinations. *Journal of Drug Delivery Science and Technology* **2019**, *54*, 101223.

[20]Gai, L.-X.; Wang, W.-Q.; Wu, X.; Su, X.-J.; Yang, F.-C. NIR Absorbing Reduced Graphene Oxide for Photothermal Radiotherapy for Treatment of Esophageal Cancer. *Journal of Photochemistry and Photobiology B: Biology* **2019**, *194*, 188–193.

[21]Savchuk, O., Carvajal, J., Massons, J., Aguiló, M., & Díaz, F. Determination of photothermal conversion efficiency of graphene and graphene oxide through an integrating sphere method. *Carbon* **2016**, 103, 134–141.

[22]Liang, J.; Chen, B.; Hu, J.; Huang, Q.; Zhang, D.; Wan, J.; Hu, Z.; Wang, B. PH and Thermal Dual-Responsive Graphene Oxide Nanocomplexes for Targeted Drug Delivery and Photothermal-Chemo/Photodynamic Synergetic Therapy. *ACS Applied Bio Materials* **2019**, *2* (12), 5859–5871.

Chapter 2 - Surface Modification of Few-Layer Graphene to Achieve Rational Chemical Applications of Graphene

Abstract:

Graphene possesses multiple superior qualities such as electrical and thermal conductivity, mechanical strength, and optical transparency. The discovery of such extraordinary properties led graphene to be considered the wonder material of the 21st century. Despite its easy method of isolation, it has not been possible to take complete advantage of graphene's superior properties because of following reasons: 1) large scale production is neither simple nor economical, 2) graphene, which is pure carbon is chemically very unreactive, and 3) it agglomerates and stacks forming multilayer graphite. For these reasons, we developed a method to oxidize the surface layers of few-layer explosion synthesized graphene by implementing the Fenton oxidation method. This method led to the synthesis of a unique graphene/graphene oxide core/shell particle that consists of an uncompromised graphene core and a highly reactive shell. Furthermore, to the best of our knowledge this is the first turbostratic graphene oxide reported. Additionally, the resulting oxidized surfaces feature predominately COOH groups that can be easily modified according to the requirements of the graphene material being synthesized. This is a potentially transformative discovery, because it permits the integration of virtually intact high-value graphene into multiple new materials.

1. Introduction

Prof. Christopher Sorensen, Kansas State Department of Physics has defined the ultimate challenge in graphene materials chemistry: "Graphene is well known to offer a broad spectrum of remarkable physical properties, yet graphene-based technology has been slow to enter the marketplace where advantage can be taken of its remarkable properties. Attempts to use graphene to augment favorably the physical properties of other materials have invariably resorted to simple "shake and bake" procedures of physical mixing without a rational design for how graphene might in fact yield a product with improved properties. A more rational approach would be to chemically react graphene with the matrix material. This would be done with an eye towards the chemistry of the material in which the graphene is to be mixed. It would also require that the graphene have the correct chemistry to react with a given material. However, pure graphene, is pure carbon which is chemically very unreactive. Thus this "more rational approach" would require chemical modification of the graphene in a manner that does not destroy its many favorable physical properties."[1]

In this chapter, we describe a method to oxidize the surface layers of few layer graphene.[2] The resulting oxidized surfaces feature predominately COOH groups that can be easily modified according to the requirements of the graphene material being synthesized. The interior graphene layers are unaffected by the process of surface oxidation. The result is a core/shell structure that consists of an uncompromised graphene core and a highly reactive shell.

The starting material for the process of graphene oxidation described here is explosion-synthesized graphene that was developed by Sorensen and Nepal.[3] The reaction mixture precursor O/C ratio = 0.3. The physical appearance of explosion-graphene is black, fluffy, very fragile. The material forms 1 - 10mm aerosol gel globules, as shown in Figure 2-1. Explosion-graphene is very rich in carbon (99.2% carbon, 0. 7% oxygen, 0.1% hydrogen), no polycyclic aromatic hydrocarbons were detected by solid state NMR, Fourier transform infrared spectroscopy, or gas chromatography with mass sensitive detection). The thermal stability of explosion-graphene is excellent. No chemical decomposition up to 600°C was detected. The specific surface area (SSA), as detected by recording BET-isotherms[4] was 165 m^2/g.[5] However, the graphene material is both fractal in nature and nano-porous. Therefore, N_2 adsorption is unable to detect the entire surface area.[5] The interplanar d-spacing is 0.352 nm, which again confirms that the material is graphene and not graphite (d-spacing: 0.337 nm).[6] Important parameters from Raman characterization are $I_{2D}/I_G \geq 0.5$, implying bilayer graphene; and $I_D/I_G = 1.1$, implying a graphenic material.[7] Finally, TEM-characterization confirms both, the presence of stacked graphene layers and the fractal nature of explosion-graphene.

Figure 2-1 Explosion-graphene (O/C ratio = 0.3). Photo taken by Justin Wright.

(Note that the discrepancy of the stacking numbers that were obtained by Raman and TEM indicate the turbostratic nature of explosion graphene. The term turbostratic defines a "crystal structure in which basal planes have slipped out of alignment".[8] For the discussion of rational graphene oxidation, an average stacking number of n=5 was chosen as an average of the Raman and TEM results.)

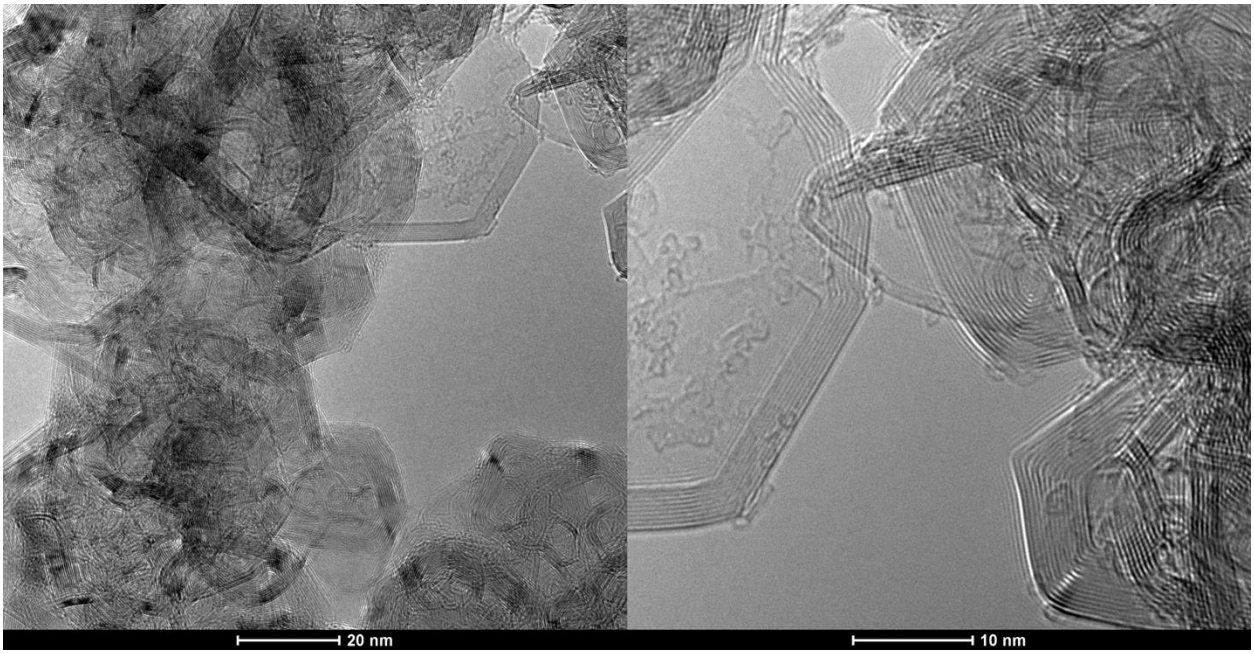

Figure 2-2 TEM graphene (precursor O/C ratio = 0.3.) The stacking numbers of the stacked graphene layers range from 7 to 20. The fractal composition of the material is clearly discernible as well.

1.1. How is Graphene Oxide Conventionally Synthesized?

The classic approaches to graphene oxide (GO) start with graphite (Gr) and use strong oxidizers and harsh chemical reaction conditions. The three basic approaches were developed by Brodie ($KClO_3$ in HNO_3) [9], Staudenmaier ($KClO_3$ in H_2SO_4 or H_2SO_4/HNO_3)[10] or Hummers and Offeman (Hummers Method) ($NaNO_3$ and $KMnO_4$ in H_2SO_4).[11] Numerous modifications exist in the literature.[12-18] They all have in common to start with graphite, which reacts to graphite oxide, which then undergoes exfoliation and further oxidation to graphene oxide. The process of exfoliation is driven by harsh chemical conditions and subsequent heating.[12] Sulfuric acid acts as intercalator between graphite layers, thus extending the layer distance of graphite from 0.335 nm to > 0.6 nm.[17, 18] There is agreement in the literature that the classic syntheses of GO from graphite are all somewhat irreproducible and, therefore, not ideally suited for the applications of GO in materials science and electronics.[12, 19]

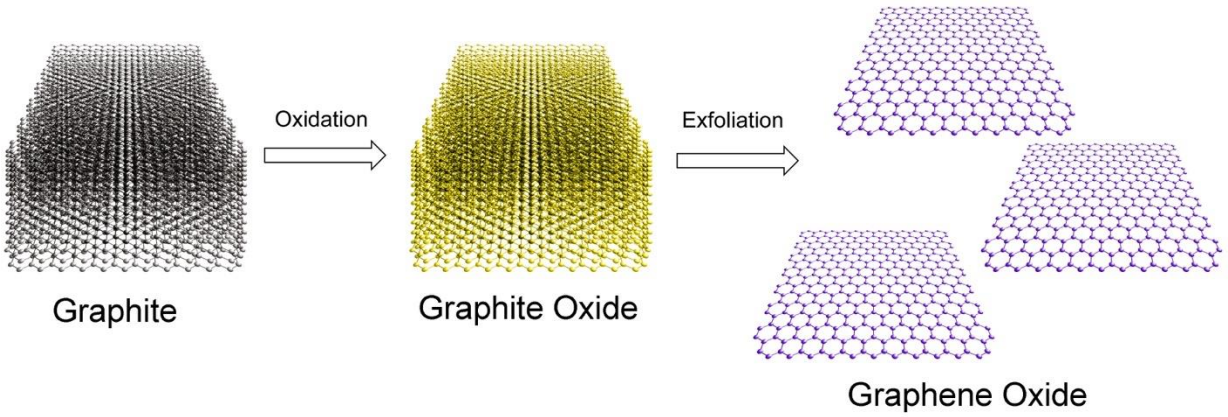

Figure 2-3 The classic synthesis of graphene oxide proceeds via graphite oxidation and exfoliation.

The production of classic GO produces significant amounts of chemical waste and releases toxic gases, such as ClO_3 (very explosive!), NO_2, or N_2O_4.[12] Furthermore, sodium- and potassium-cations are hard to remove from graphene oxide after completion of the oxidation process, leading to impure materials.[12] GO produced by means of chemical oxidation of graphite, followed by exfoliation and further oxidation features carbonyl and carboxylic acid groups at the edges and epoxy and hydroxyl groups in the basal plane; however, a defined chemistry on the surface of classic GO is virtually impossible. Furthermore, classic GO contains remnants from the strongly oxidizing reagents that were used to create it. This may be disadvantageous for any future biosensing, in-vivo, or in-vitro application.

1.2. Other Methods for Synthesizing Graphene Oxide

Tang et al. reported the synthesis of graphene oxide nanosheets (GON) on surfaces by means of hydrothermal polymerization of glucose, followed by thermal annealing at 1300 K on quartz wafers.[20] This method permits the synthesis of tunable monolayer and few-layer (<5) GONs with about 20 μm and 100 μm lateral extent, respectively. Although this appears to be a green

approach to graphene oxide, this method is energy intensive and unable to produce large amounts of GO. Furthermore, the chemical structure of the GON on quartz is not fully characterized to date.

Hossain et al. oxidized epitaxial graphene on SiC(0001) using atomic oxygen in ultra-high vacuum.[19] The chemisorption of oxygen atoms on graphene was verified by means of using scanning tunneling microscopy (STM), high-resolution core-level X-ray photoelectron spectroscopy (XPS), Raman spectroscopy and ultraviolet photoelectron spectroscopy (UPS). Thermal reversibility occurred at 533 K. Again, this approach, albeit interesting for the semiconductor industry, is unable to produce large quantities of chemically stable GO. Electrochemical methods to produce GO from graphite are being developed by several research groups. The state-of-the-art of electrochemical production of GO is described in a recent review by Fang et al.[21] It should be noted that these approaches are capable of producing classic GO significantly faster and "greener". However, these synthetic methods do not generate core/shell graphenic materials where the inner layers are chemically preserved, which is exactly what we have synthesized by oxidizing explosion-synthesized graphene nanosheets (GNs) by implementing the Fenton oxidation method.

1.3. The Fenton Reaction, an Advanced Oxidation Process

The key reaction of the thermal Fenton reaction is between iron(II) and hydrogen peroxide in aqueous solution.[22, 23] The observed reaction kinetics of H_2O_2 consumption shows an exponential dependence on the temperature.[23] Depending on the substrate and possible chelation of iron(II), there are two competing main reactions:[24]

$$Fe^{2+} + H_2O_2 \rightarrow Fe^{3+} + HO^{\bullet} + HO^{-} \quad (1)$$

$$Fe^{2+} + H_2O_2 \rightarrow FeO^{2+} + H_2O \quad (2)$$

In reaction (1), the hydroxyl radical is formed via electron transfer from iron (II) to H_2O_2. In reaction (2), an oxoiron(IV) species is formed.[24] It should be noted that the water molecules that

are participating in these reactions are not shown to permit more clarity. Hydroxyl radicals react either (a) via hydrogen abstraction, which is not likely here due to the low hydrogen content of explosion-synthesized graphene, or (b) under electron transfer from graphene to the hydroxyl radical, or (c) under addition to carbon-carbon double bonds. All three reactions form organic radicals, which then react with oxygen (d) under formation of peroxyl radicals, which further react to eventually form ketones or carboxylic acids.[25]

$$HO^{\bullet} + R-H \rightarrow H_2O + R^{\bullet} \text{ (a)}$$

$$HO^{\bullet} + R-H \rightarrow RH^{\bullet+} + HO^{-} \text{ (b)}$$

$$HO^{\bullet} + C=C \rightarrow HO-C-C^{\bullet} \text{ (c)}$$

$$R^{\bullet} + O_2 \rightarrow R-O-O^{\bullet} \rightarrow\rightarrow\rightarrow R-COOH \text{ and other products (d)}$$

The oxoiron(IV) species can live up to several seconds in aqueous solutions.[26] It reacts by means of electron transfer with organic matter (e).

$$FeO^{2+} + R-H \rightarrow R^{\bullet} + Fe^{3+} + HO^{-} \text{ (e)}$$

This reaction is followed by addition of oxygen (d) and formation of carboylic acids, ketones, and other oxidation products via peroxoradical chemistry.[25, 27] In conclusion, both principal reaction pathways lead to the oxidation of graphene. Oxoiron (IV) is more effective than the hydroxyl radical, because the latter can recombine to hydrogen peroxide.[28, 29]

$$2\,HO^{\bullet} \rightarrow H_2O_2 \text{ (f)}$$

In addition to reacting with graphene, both reactive intermediates of the Fenton reaction are capable of reacting with H_2O_2 forming hydroperoxyl radicals ($HO_2^{\cdot}$).[28, 29] The hydroperoxyl radical is a powerful oxidant which can react with organic matter, such as graphene, under hydrogen abstraction, electron transfer, and addition to formerly formed radicals.

$$HO^{\bullet} + H_2O_2 \rightarrow H_2O + HO_2^{\bullet} \text{ (g)}$$

$$FeO^{2+} + H_2O_2 \rightarrow Fe^{3+} + HO^{-} + HO_2^{\bullet} \text{ (h)}$$

Lastly, iron (III) is recycled via reaction with superoxide ($O_2^{\cdot -}$), the conjugate base of the hydroperoxyl radical ($HO_2^{\cdot}$) (pK_a ($HO_2^{\cdot}/O_2^{\cdot -}$) = 4.88[30]) (Haber-Weiss reaction[30, 31]). This step concludes the catalytic cycle of the Fenton reaction.

$$Fe^{3+} + O_2^{\bullet -} \rightarrow Fe^{2+} + O_2 \text{ (i)}$$

2. Methodology

2.1. Optimal Experimental Design Methodology (OEDM)

Unfortunately, the intrinsic problem with complex reaction networks, such as Fenton reaction, is that it is virtually impossible to predict the kinetics of graphene to graphene/graphene oxide. Therefore, we have applied Optimal Experimental Design Methodology to optimize the Fenton oxidation reaction conditions of explosion-synthesized graphene to graphene/graphene oxide (G/GO) core/shell particles. OEDM was used because it allows for statistically significant modeling and prediction of optimized variables.[44-50] In this case, we chose the Doehlert matrix because it provides a straightforward approach to optimize process parameters. Basically, OEDM was used to design an experimental matrix, shown in Fig. 2-4, to analyze the effects of two main process variables on oxygen content: 1) concentration of iron (II) sulfate (mg/100 mL aqueous H2O2 solution, pH=3.0) and 2) reaction temperature (°C). (A detailed explanation of OEDM modeling is shown in Appendix A). Experimental results indicated that the optimal conditions were 125 mg $FeSO_4$ x H_2O and 60 °C (demonstrated as well by OEDM in Fig A.2.).

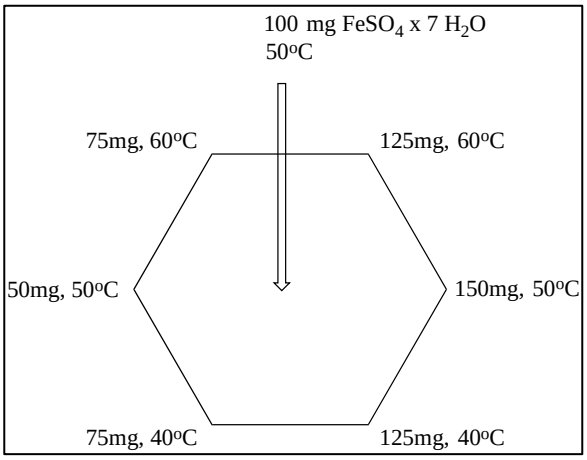

Figure 2-4 Doehlert matrix of the Fenton oxidation of graphene.

2.2. Fenton Oxidation of Explosion-Graphene

The oxidation and optimization experiments reported here were performed in a 250 mL flask equipped with a motor-driven overhead stirrer and an electronic thermometer with a stainless-steel probe. The flask was immersed into a water bath that was kept at a precisely selected temperature (see Table 2-1). The flask was filled with 90.0 ml aqueous solution of pH=3.0 (sulfuric acid, Fisher Chemical) and allowed to stir until the temperature inside the flask reached the temperature of the external water bath (permitted $\Delta T = 2K$). Then, 10.0 mL of 30% H_2O_2 (Acros Organics) were added to the flask and the mixture stirred for 5 min, followed by addition of 1.0g of explosion-synthesized graphene[3], which was obtained from the Sorensen research group at Kansas State. The resulting suspension was stirred until a dispersion was formed (approx. 10 min.). At this point, a defined amount of $FeSO_4$ x 7 H_2O (Table 2-1) was added at once as a solid. The Fenton oxidation system was continuously stirred at the selected bath temperature for 24h. Then, the oxidation product (graphene/graphene oxide core/shell particles (G/GO)) was removed by means of filtration using either a Corning 3606060M glass filter (pore size 10 to 15 μm) or a GE Healthcare 1001030 (medium pore size) filter paper. Alternatively, the formed G/GO can be centrifuged off at 7000 RPM, 5 min. The obtained G/GO was resuspended in 100 mL of H_2O and filtered off (or centrifuged off) again. This procedure was repeated until the pH of the supernatant was > 6.0 (here: five times). The G/GO was stored in a vacuum desiccator for 24h over P_2O_5. After that time, it can be stored in polyethylene or polypropylene containers at RT.

3. Results and Discussion

3.1. Characterization of the Reaction Products

Elemental (CHO) Analysis and Zeta Potential Measurements

Table 2-1 summarizes the elemental (CHO) analysis and zeta potential of the reaction products. Elemental (CHO) analysis indicates the oxidation of the graphene starting material. The extent of oxidation depends on the chosen process conditions (Table 2-1). Whereas other reports describe the synthesis of graphene oxide via classic Hummers method with a C/O ratio of down to 1:1[12, 13, 15, 32], the C/O ratio reported here does not fall below 10:1. This finding is consistent with outer shell oxidation around the graphene particle, resulting in a graphene / graphene oxide core/shell nanoparticle. Similarly, the zeta potential measurements[42] clearly indicate the chemical changes at the surface of Fenton oxidized graphene. Whereas the zeta potential of pristine explosion-synthesized graphene in H_2O (pH = 7.0) is + 60 mV (Table 2-1), it decreases to + 17.7 to - 8.2 mV for Fenton oxidized graphene oxide, depending on the actual oxidation conditions. In comparison with graphene oxide synthesized using Hummers method, which has a zeta potential of approx. - 40 mV in water (pH = 7.0)[42], the data obtained for the oxidation method discussed here is distinctly different, which is indicative of a different oxidized structure that is obtained via Fenton-oxidation of graphene. Less negative zeta potentials found in graphene oxide are in agreement with the explanation that graphene is not undergoing exfoliation during oxidation. Therefore, graphene sheets cannot become oxidized from both sides, resulting in lesser content of carboxylic acids in graphene oxide. The paradigm of graphene / graphene oxide core shell particles also fits this experimental observation best.

Table 2-1 Fenton reaction conditions, CHO Analysis and Zeta Potentials, First Round of Optimization Experiments.

Graphene[3]	T / °C	mg $FeSO_4$ x 7 H_2O added	CHO Analysis**	Zeta Potential (mV)
O/C = 0.3*	/	/	99.2% C, 0.1% H, 0.7% O	+ 60
O/C = 0.3	40	75	94.3% C, 1.1% H, 4.6% O	+ 10.4
O/C = 0.3	40	125	93.5% C, 1.4% H, 5.1% O	+ 9.6
O/C = 0.3	50	50	96.3% C, 1.6% H, 2.1% O	+ 17.7
O/C = 0.3	50	100	94.7% C, 1.2% H, 4.1% O	+11.9
O/C = 0.3	50	150	95.4% C, 1.8% H, 3.9% O	+ 14.5
O/C = 0.3	60	75	95.1% C, 1.5% H, 3.4% O	+ 13.1
O/C = 0.3	60	125	90.1% C, 1.7% H, 8.2% O	- 8.2
O/C = 0.3	60	175	92.2% C, 1.6% H, 6.2% O	- 5.8
O/C = 0.3	70	100	92.4% C, 1.8% H, 5.8% O	- 1.4
O/C = 0.3	70	150	90.6% C, 1.9% H, 7.5% O	- 5.8
* precursor O/C ratio for explosion graphene synthesis= 0.3[3] ** performed by ALS Environmental, Tucson, AZ.				

X-Ray Powder Diffraction (XRD)

XRD is a physical method that is frequently used in materials science.[33] XRD is able to probe, whether a material is (partially) crystalline or not. X-ray diffraction is based on constructive interference of monochromatic X-rays and a crystalline sample. The interaction of the incident X-rays with the sample generates constructive interference (and a diffracted ray) when conditions satisfy Bragg's Law.[33]

$$n\lambda = 2d \sin\theta$$

n: diffraction order; λ: X-ray wavelength, *d*: d-spacing (grating constant), θ: angle of constructive interference. Strong intensities (Bragg peaks) are observed at angles where the scattering angles satisfy the Bragg condition. Quite obviously, this is only possible in crystalline materials. The

combined XRD spectra of all graphene oxide samples are summarized in Figure 2-5. The measurements were performed by Shusil Sigdel, who is a graduate student in the group of Dr. Sorensen in Kansas State Physics. The X-ray powder diffraction data were collected with a Bruker AXS D8 Advance Diffractometer (X-rays of 0.15406 nm) operating at 40 kV and 40 mA. Measurements of each sample were performed in the scattering angle, 2θ range from 5° to 60° with a step of 0.05° and a step time of 1.6 sec/step. The results shown in Figure 2-5 indicate that all investigated graphene oxide samples that were synthesized by means of Fenton oxidation were crystalline.

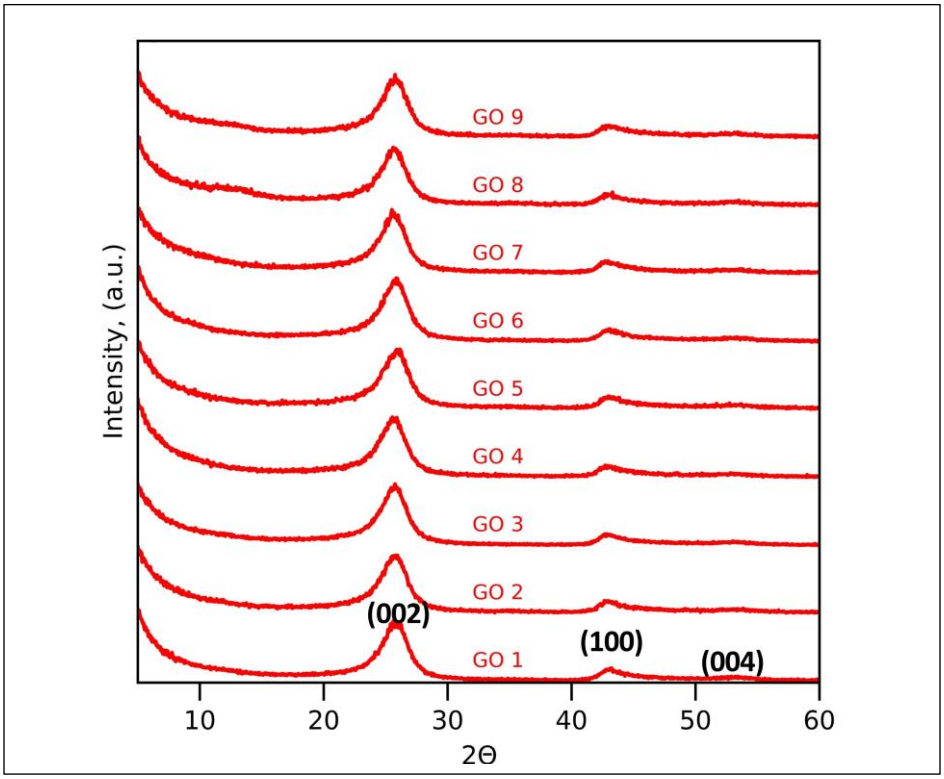

Figure 2-5 Combined XRD spectra of nine graphene oxide samples (see Table 2-1). All graphs are scaled to have same (002) peak intensity.

Furthermore, Figure 2-6 shows the XRD comparison of all nine synthesized graphene oxide samples with 0.3 explosion-graphene, as well as graphite. It becomes immediately clear that the XRD spectra of both 0.3 explosion-graphene and all nine graphene oxides that were

synthesized by Fenton oxidation are strikingly similar. All ten samples differ remarkably from the XRD spectrum of graphite, proving that the Fenton oxidation method utilized here preserves the graphene-cores of the material. The (002) peak of all GO samples is slightly shifted to right in comparison to the 0.3 explosion graphene sample (summarized in Table 2-2). This indicates a somewhat more graphitic behavior. However, this does not indicate that the material itself belongs to the group of graphite materials!

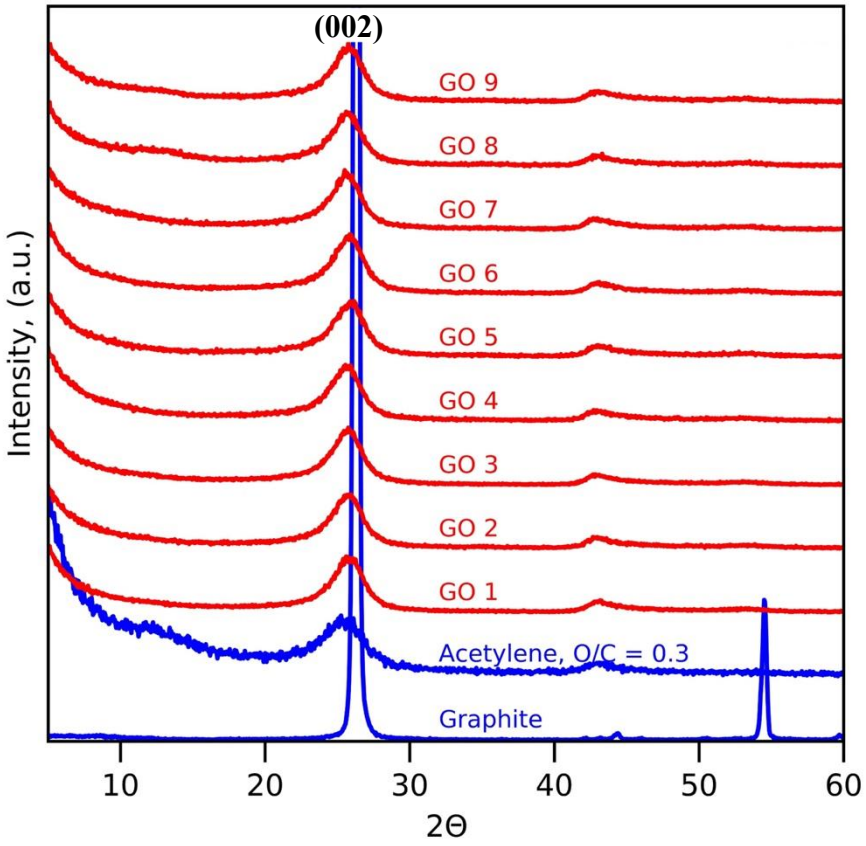

Figure 2-6 Combined XRD spectra of nine graphene oxide samples (see Table 2-1) in comparison with explosion-graphene (from acetylene/oxygen mixture, O/C = 0.3), and graphite. All graphs are scaled to have same (002) peak intensity. (Acetylene, O/C = 0.3 denotes for 0.3 explosion-graphene). All critical data are summarized in Table 2-2.

As shown in Figures 2-5, 2-6, and summarized Table 2-2, the position of the (002) and (100) lines are virtually the same for graphene and Fenton-oxidized graphene oxide. Our paradigm is that there is no significant change in d-spacing between graphene layers in graphene

and oxidized graphene. Graphene oxide that has been synthesized via oxidation of graphite[12, 13, 15, 16] or explosion-synthesized graphene[3] by means if Hummers method [32] is known to feature larger d-spacing due to intercalation of sulfuric acid between graphene layers and subsequent oxidation, leading to a discernible left shift of the position of the peak with highest intensity. Since this effect is not observed, our conclusion is that no intercalation occurs during the synthesis. Based on the comparison of XRD spectra of graphene and oxidized graphene, our novel material possesses virtually intact graphene cores, only the outer layers are affected by the oxidation process.

Table 2-2 Summary of XRD Results (Peak Positions and d-Spacing) for Nine Graphene Oxide Samples Synthesized via Fenton-Oxidation in Comparison to 0.3 Explosion-Graphene and Graphite.

Sample	1st peak loc (θ)	Plane	1st peak d-spacing (nm)	2nd peak loc (θ)	Plane	3rd peak loc (θ)	Plane
Graphite	26.4	(002)	0.337	44.4	(101)	54.5	(004)
0.3 Graphene	25.3	(002)	0.352	43.1	(100)	n/a	n/a
GO 1	25.8	(002)	0.345	43.1	(100)	53.2	(004)
GO 2	25.8	(002)	0.345	42.7	(100)	53.2	(004)
GO 3	25.8	(002)	0.345	42.8	(100)	53.2	(004)
GO 4	25.7	(002)	0.346	42.8	(100)	53	(004)
GO 5	25.9	(002)	0.344	43	(100)	53.4	(004)
GO 6	25.8	(002)	0.345	43	(100)	53.2	(004)
GO 7	25.6	(002)	0.348	42.9	(100)	53.5	(004)
GO 8	25.7	(002)	0.346	42.9	(100)	53.4	(004)
GO 9	25.8	(002)	0.345	43	(100)	53.3	(004)

Raman Characterization of Graphene Oxide Synthesized by Means of a Fenton Process

Raman spectroscopy is among the most important characterization methods of carbon materials. This is especially valid for graphene and graphene oxide, because the global community of graphene and graphene manufacturers is in dire need of international standards.[34] Raman measurements have been performed by Shusil Sigdel and Archana Sekar utilizing the Thermo Fischer DXR microRaman Spectrometer in the research laboratories of Prof. Dr. Jun Li, Chemistry Department at Kansas State University. The most important result is that the Raman spectra of 0.3 G and the nine GO samples are very similar. This finding is corroborating the results from XRD. All Raman spectra, except for graphite, show signature features for graphene and graphene-derived materials. The D, G and 2D peaks are centered at 1339 cm^{-1}, 1570 cm^{-1} and 2673 cm^{-1}, respectively (summarized in Table 2-3). The I_D/I_G ratios for the graphene oxide materials are smaller than for graphene (0.90 ± 0.10 vs. 1.14); whereas the I_{2D}/I_G ratios are enhanced (0.62 ± 0.03 vs. 0.54). In general, higher I_D/I_G ratios indicate higher degrees of disorder. For instance, graphite crystals are well-ordered and show, therefore, $I_D/I_G = 0.20$.[35, 36] The conclusion from these measurements is that Fenton oxidation increases order in Fenton-oxidation synthesized graphene oxide! Our working paradigm is that the number of stacked graphene layers is reduced by n=2 due to the oxidation of the outer layers. At the same time, all high-energy impurities will be removed by oxidation as well. These two effects result in increased order of the few layer graphene oxide, as indicated by higher I_D/I_G ratios. Enhanced I_{2D}/I_G ratios of graphene oxide compared to the explosion-graphene from which they have originated indicate paradoxically a higher number of stacked graphene layers. An intensity ratio of $I_{2D}/I_G > 0.5$ is consistent with bilayer graphene.[37] $I_{2D}/I_G >> 0.5$ is consistent with more than two stacked graphene layers. Without overinterpreting this data, they clearly indicate that Fenton

oxidation synthesized graphene oxide contains several stacked intact layers of graphene.[37] This is in stark contrast to conventionally synthesized graphene oxide, in which the layers are oxidatively disrupted and essentially no stacking of intact layers can be observed by either Raman, TEM or XRD.[38]

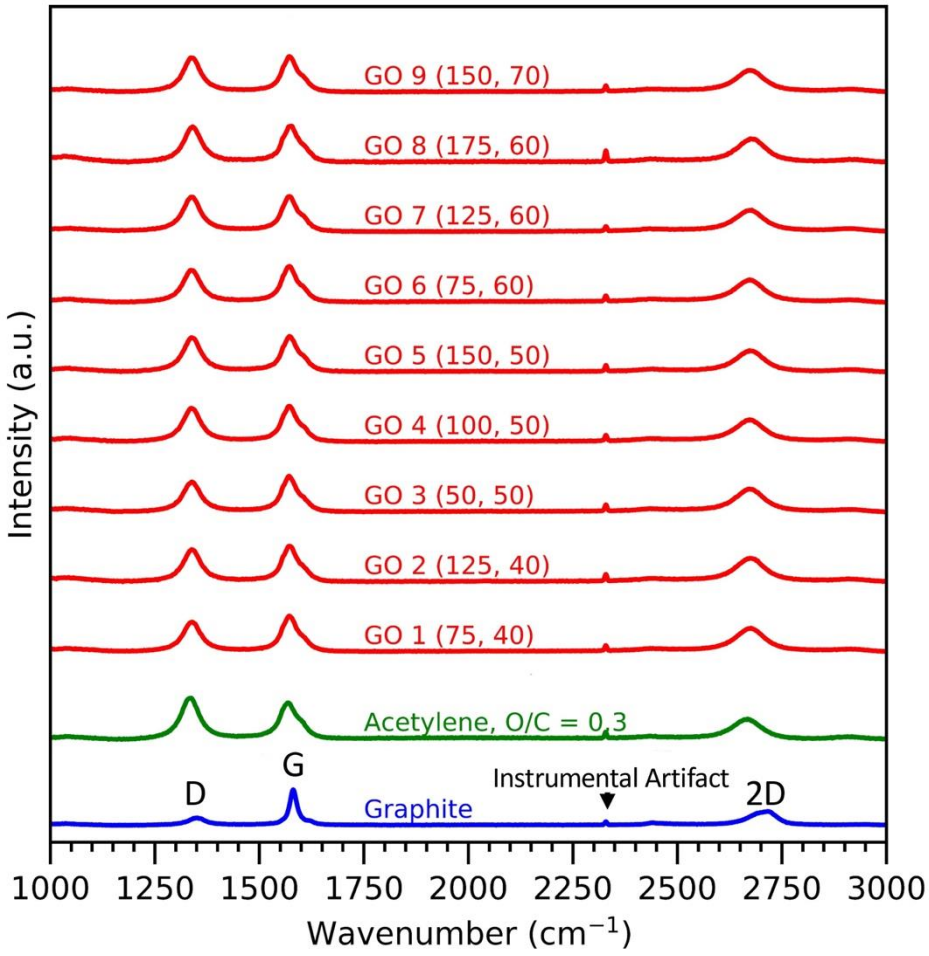

Figure 2-7 Raman spectra of nine graphene oxide samples (see Table 2-1) in comparison with explosion-graphene (from acetylene/oxygen mixture, O/C = 0.3), and graphite. Laser wavelength: 532 nm; laser power: 10 mW; 50 μM slit aperture; data range: 0-3000 cm-1; magnification factor: 10; exposure time: 9s; sample exposures: 10, background exposures: 11. The D peak of 0.3 graphene and all nine graphene oxide samples lies at wavenumber 1339 ± 3 cm^{-1}, the G peak lies at wavenumber 1570 ± 2 cm^{-1}, and the 2D peak lies at wavenumber 2673 ± 2 cm^{-1}. All spectra are normalized to have the same G peak intensity.

Table 2-3 Comprehensive Raman Data of 0.3 Graphene and Nine Graphene Oxide Materials, as well as Graphite (Table 2-1) Obtained at 532nm Laser Wavelength.

Sample Name	**Peak Position**			**Intensity Ratio**	
	I_D	I_G	I_{2D}	I_D/I_G	I_{2D}/I_G
Graphite	1350	1580	2716	0.20	0.38
0.3 Graphene	1337	1568	2668	1.14	0.54
GO 1	1340	1572	2676	0.83	0.65
GO 2	1339	1572	2674	0.90	0.65
GO 3	1339	1571	2672	0.84	0.64
GO 4	1338	1572	2672	0.95	0.61
GO 5	1338	1572	2672	0.96	0.59
GO 6	1337	1572	2672	0.89	0.62
GO 7	1337	1572	2674	0.98	0.60
GO 8	1341	1576	2675	1.00	0.65
GO 9	1336	1572	2672	0.96	0.61

0.3 Explosion Graphene and Derived Graphene Oxide are Turbostratic

Adjunct Research Prof. Dr. Ranjith Divigalpitiya, Chemistry Department, Western University, London, Ontario, Canada has performed an investigation of 0.3 explosion-graphene and graphene oxide (90.1% C, 1.7% H, 8.2% O) using a high-performance Raman device (Renishaw InVia Raman Spectrometer; λ_{ex} = 514 nm; 10% power, exposure time: 60s) at the surface science laboratory located at his university. A 50x objective was used to focus the laser onto the surface. The spot size analyzed was approx. 1 μm in diameter. The results obtained for both, graphene and graphene-oxide are summarized in Figure 2-8. As anticipated from the Raman results at λ=532 nm, there is a noticeable gradual blue shift in the GO spectrum, but Fenton oxidation did not significantly alter the Raman spectrum. Using I_D/I_G ratio, the crystallite size of the graphene flakes was estimated to L_a = 21.8 +/- 2.2 nm. For GO, the crystallite size

was virtually unchanged L_a = 21.9 +/- 0.5 nm. This finding is further confirmation that the Fenton oxidation process only oxidizes the outer layers and potentially high-energy sites at the layer edges of few layer graphene. The observed crystallite size correlates well with our TEM findings that are shown on Figure 2-2 for 0.3 explosion-graphene and Figure 2-10 for GO (90.1% C, 1.7% H, 8.2% O) (L_a ~20 nm for both).

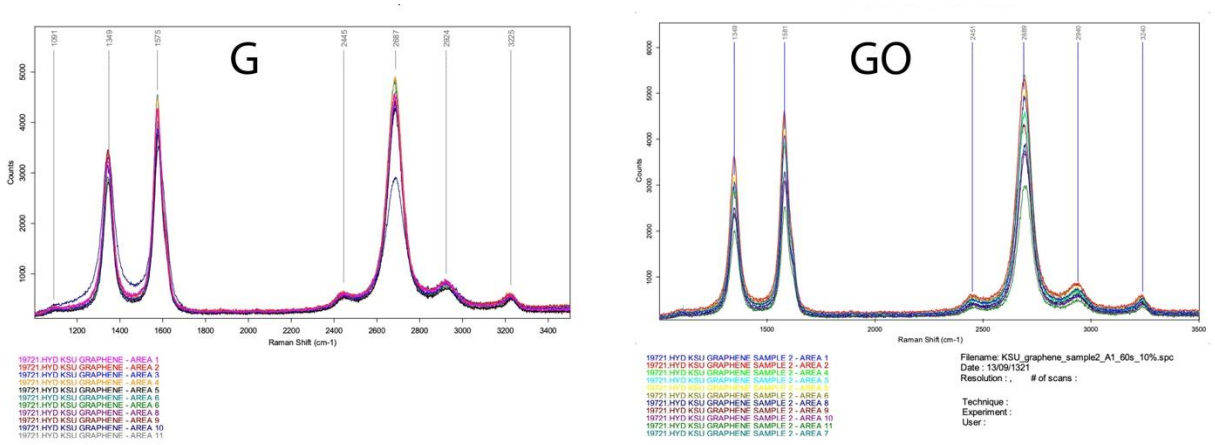

Figure 2-8 High-resolution Raman spectra of surface spots (approx. 1 μm in diameter) of 0.3 explosion-graphene and Fenton oxidation synthesized graphene oxide (90.1% C, 1.7% H, 8.2% O). The Raman experiment was repeated 11 times. As anticipated, signal bleaching upon photoexcitation is observed.

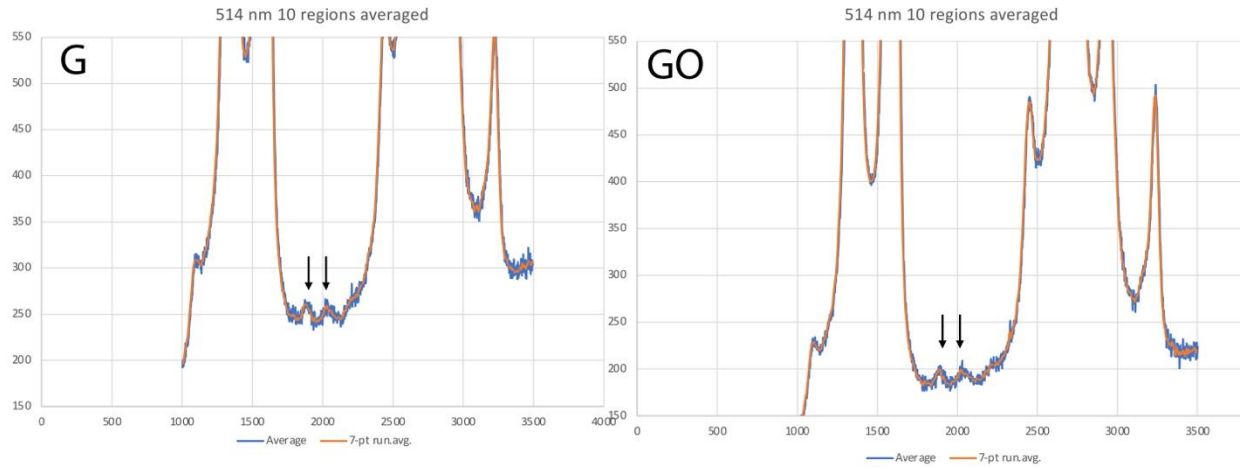

Figure 2-9 High-resolution Raman spectra of surface spots (approx. 1 μm in diameter) of 0.3 explosion-graphene and Fenton oxidation synthesized graphene oxide (90.1% C, 1.7% H, 8.2% O). The signal for 10 respective regions was averaged.

Turbostratic graphene displays two small signature Raman peaks between wavenumbers 1800-2200 cm^{-1}; both are approx. 30-times smaller than the G peak.[39] Therefore, high-resolution Raman was required to be able to detect the presence of the turbostratic peaks. As shown in Figure 2-9, both signature turbostratic Raman peaks are present in the spectra of both, graphene (G) and graphene oxide (GO). This is the ultimate proof that the physical properties of explosion graphene are preserved in Fenton oxidation synthesized graphene oxide (GO). Furthermore, to the best of our knowledge, this is the first reported turbostratic graphene oxide! As discussed in the introduction section, this is a potentially transformative discovery, because it permits the integration of virtually intact high-value graphene into multiple new materials.

Electron Microscopy

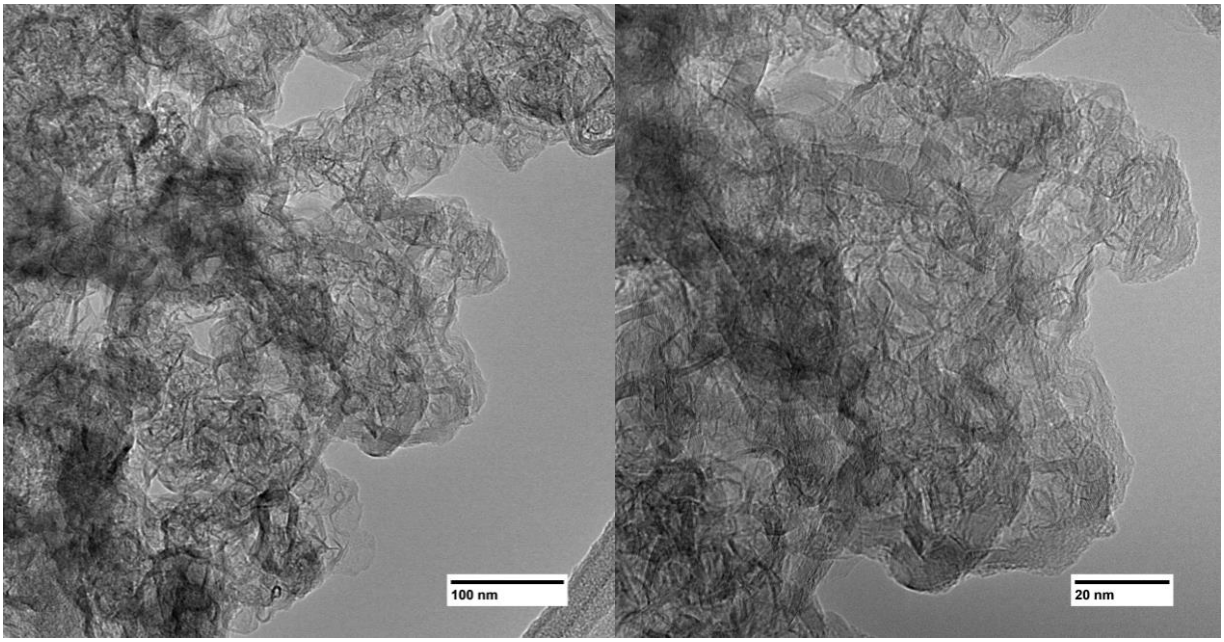

Figure 2-10 TEM of Graphene Oxide (90.1% C, 1.7% H, 8.2% O).

The TEM characterization of graphene and graphene oxide has been performed at the Microscopy and Analytical Imaging Research Resource Core Laboratory (MAI) at the

University of Kansas, Lawrence Campus, by Dr. Prem Thapa. The measurements were performed on a Hitachi H-8100 Transmission Electron Microscopy (200 kEV) on copper grids. As discussed above, there is a very good agreement of the findings by TEM and the Raman data of graphene and Fenton oxidation synthesized graphene oxide:

1) Both G and GO show layer stacking and a general fractal structure.
2) The morphology of G does not change during Fenton oxidation to GO.
3) The particle sizes for G and GO calculated using Raman data and imaged by means of TEM are essentially the same.

From combined Raman and TEM results we conclude that only the outer layers of G will be oxidized during Fenton oxidation. The next question is, what do we find on the surface of the resulting GO/G core/shell structures?

Fourier Transform Infrared Spectroscopy (FTIR)

FTIR is ideal for detecting the presence of functional groups with permanent dipole moment in a material.[40] FTIR spectra were collected in an Agilent Cary 630 FTIR spectrometer over a range of 400 – 4000 cm^{-1} using the attenuated total reflectance (ATR) sampling accessory. In short, the sample was loaded into the diamond sampling window. Next, the sample press tip was lowered so that there was contact made between the sample and infrared energy emitting from the diamond window. As shown in Figure 2-11, there are significant differences between the powder FTIR spectra of explosion-synthesized graphene (99.2% C, 0.1% H, 0.7% O) and Fenton-oxidized graphene (90.1% C, 1.7% H, 8.2% O). The high-energy FTIR window of the Fenton-oxidized graphene is dominated by the signal of the -COOH group (3500-2500 cm^{-1}), which is completely absent in graphene. In the low-energy FTIR window, a broad C=O

absorption band (1800-1680 cm^{-1}) and a shoulder around 1330 cm^{-1}, indicating the presence of C-O-H functions, are discernible for Fenton-oxidized graphene, but not for graphene before oxidation. From the FTIR data, we have concluded that Fenton-oxidation produces carboxylic acid groups and virtually no other oxidation products (e.g., alcohols, aldehydes/ketones, and alcohols) at the outside of the graphene particles. This finding corroborates the paradigm of the formation of graphene/ graphene oxide core/shell particles during Fenton-oxidation of graphene: Only the exterior layers and potentially high-energy locations at the edges of the stacked graphene layers are being oxidized. Carboxylic acids are the major product (> 95% according to FTIR) of the Fenton oxidation process.

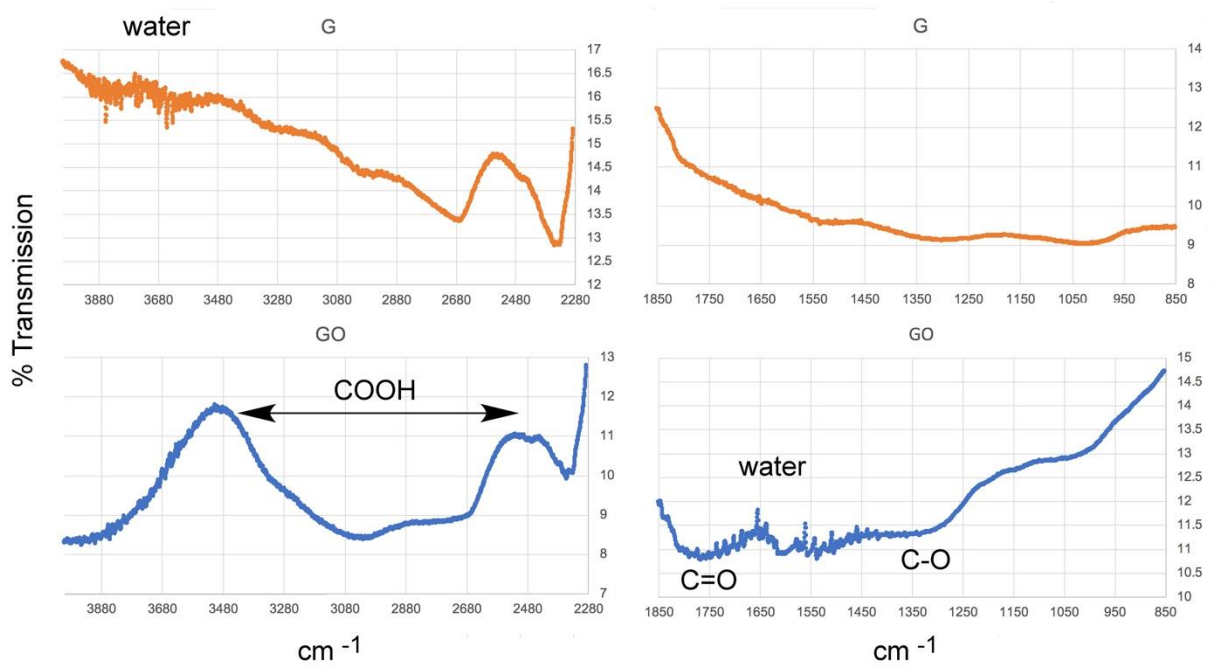

Figure 2-11 Comparison of FTIR transmission spectra of pristine explosion-synthesized graphene (99.2% C, 0.1% H, 0.7% O, Table 1, orange spectra) and Fenton-oxidized graphene (90.1% C, 1.7% H, 8.2% O, Table 2-1, blue spectra).

Thermogravimetry Analysis (TGA)

The thermal (and mechanical) stability of graphene-derivatives is of very high importance with respect to their use in novel materials. The higher the thermal (and mechanical) stability of graphene oxides, the more suitable these materials are for composite materials. Graphene is known to exhibit excellent thermostability up to 900°C. [3, 14, 15, 32], whereas classically synthesized graphene oxide[3, 12, 13, 15, 19] undergoes decomposition between 200°C and 400°C, depending on the extent of oxidation. The mass of graphene oxide that was synthesized via Fenton oxidation decreases only between 3.5% by weight (shown below) and 5% (other oxidation conditions, not shown in Figure 2-12) when heated to 600°C. Most importantly, this process starts at 550°C, which is significantly higher than for other graphene oxides. It must be noted that below 100°C a variable mass loss (up to 7% by weight) is observed for Fenton-oxidized graphene oxide, which was attributed to physisorbed water and low molecular weight oxidation products. Therefore, all of the results discussed above are in agreement with the formation of graphene / graphene oxide core/shell particles. Its principal structure is depicted in Figure 2-13.

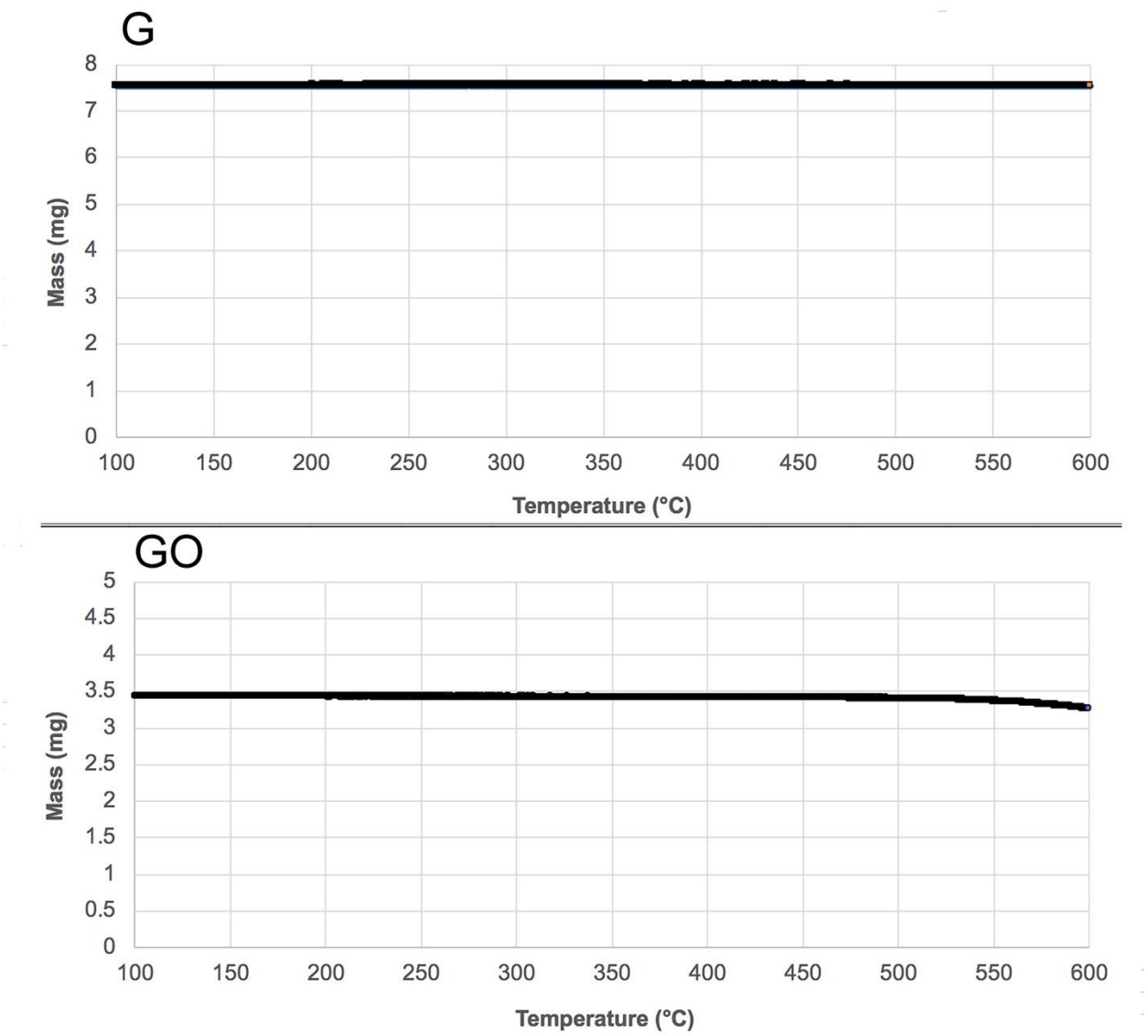

Figure 2-12 Thermogravimetric behavior of graphene (G: 99.2% C, 0.1% H, 0.7% O, Table 2-1) and Fenton-oxidized graphene oxide (GO: 90.1% C, 1.7% H, 8.2% O, Table 1). Whereas a slight increase of weight can be discerned for graphene, due to minor oxidation at higher temperatures, Fenton-oxidized graphene oxide is thermally stable up to 550 ^{o}C. At 600 ^{o}C, a weight loss of 3.5 % is observed**.**

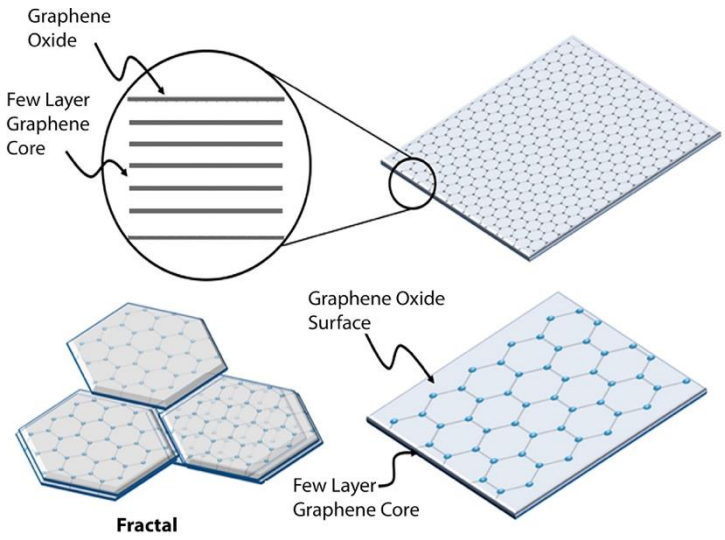

Figure 2-13 Graphene / graphene oxide core/shell particles comprise a chemically intact graphene core and a top and a bottom layer of graphene oxidation products (carboxylic acids). Potentially, carboxylic acids can be found at the edges of the intact core few layer graphene as well.

3.2. Chemical Reactions of Fenton Oxidation-Derived Graphene Oxide

This section describes a successful approach to tailor the surface properties of Fenton oxidation derived graphene oxide (GO). Following the concept of rational chemistry design of our turbostratic graphene oxide, the carboxylic acid groups located at the outer layers of the stacked few-layer graphene assembly can be further reacted or functionalized depending upon the desired use, to create a wide variety of new materials (GO derivatives). For example, reaction of the graphene oxide surface layer with methanol in the presence of thionyl chloride yields GO methyl esters (mGO). The methyl groups can be substituted by ammonia (NH_3). GO reacts with ethylene glycol in a similar manner than methanol using thionyl chloride ($SOCl_2$) as reagent.

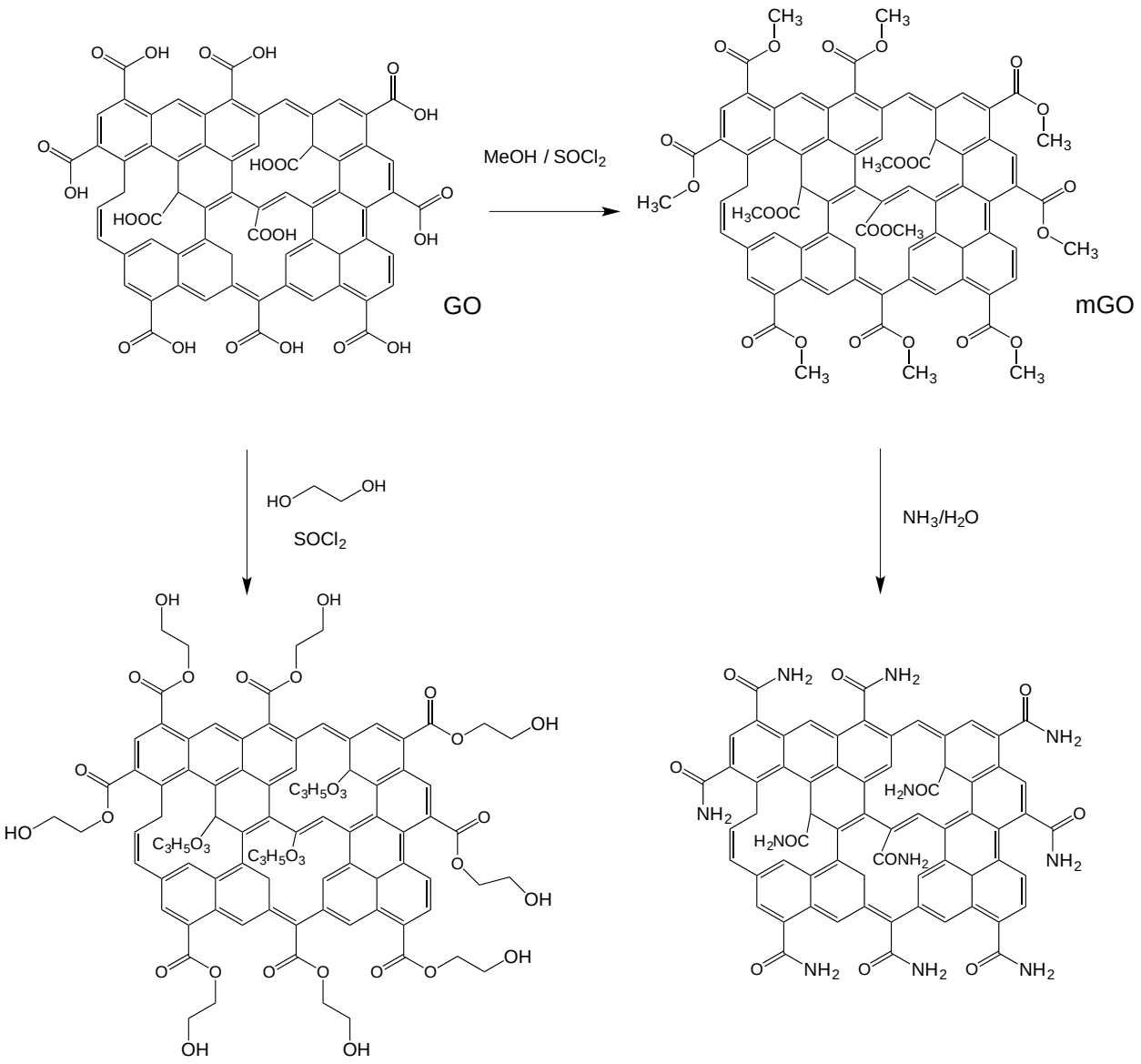

Figure 2-14 Schematic representation for general reactions of graphene oxide and graphene oxide methyl ester.

Graphene Oxide Methyl Ester (mGO)

500 mg of GO were suspended via sonication in 25 mL methanol in a 150 mL round bottom flask equipped with a magnetic stirring bar and reflux condenser. Then, the GO suspension was cooled down to 0° C in an ice bath and 1.25 mL of thionyl chloride was added slowly (1.25 mL $SOCl_2$ is 5% by volume of the amount of methanol). After the addition of $SOCl_2$ was complete, the reaction was stirred at room temperature for 24 hours. After 24 hours, the reaction was refluxed

for 1 hour and then allowed to cool down to room temperature. Finally, mGO was collected via centrifugation (10 min @ 7,000 rpm) and washed 5 times with distilled water and then lyophilized to dryness overnight.

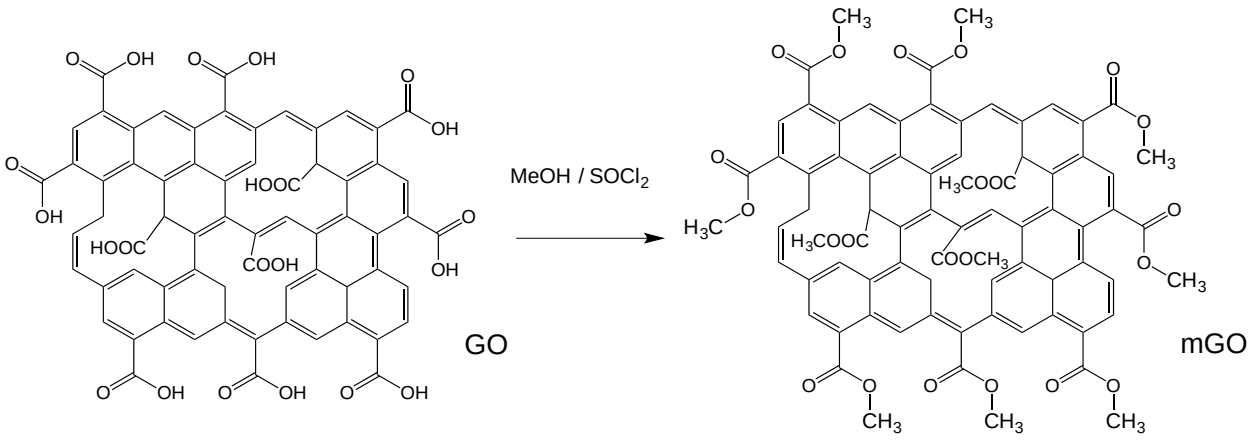

Figure 2-15 Thionyl chloride-mediated esterification of GO to mGO.
Yield: 472mg (94%), zeta potential: ξ = - 15.34 mV. CHNO of GO: 88.37% C, 2.36% H, 0% N, 9.27% O; CHNO of mGO: 88.29% C, 3.40% H, 0% N, 8.31% O

The graphene oxide-derived material is virtually thermostable up to 600 ^{o}C. Whereas the loss of mass of graphene oxide is approx. 3.5% in the temperature interval from 550 to 600 ^{o}C, the loss of mass of the GO methyl ester is less than 1.0 %. Furthermore, the loss of adsorbed water between room temperature and 100 ^{o}C is not observed as well, as shown in Figure 2-16. Additionally, the FTIR spectrum shows the CH-stretch, C=O and C-O IR bands that are consistent with the formation of methyl esters. The OH-band arises most likely from adsorbed methanol (Fig. 2-17). Furthermore, the loss of surface carboxylic acid groups is clearly discernible when compared with the FTIR spectrum of GO.

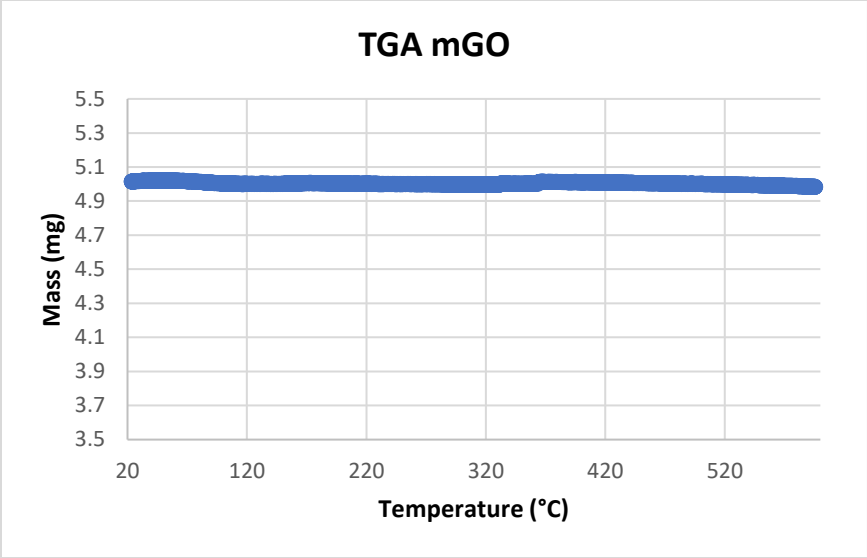

Figure 2-16 Differential Thermogravimetry (TGA) of Graphene Oxide Methyl Ester (mGO)) prepared via thionyl chloride-mediated esterification reaction.

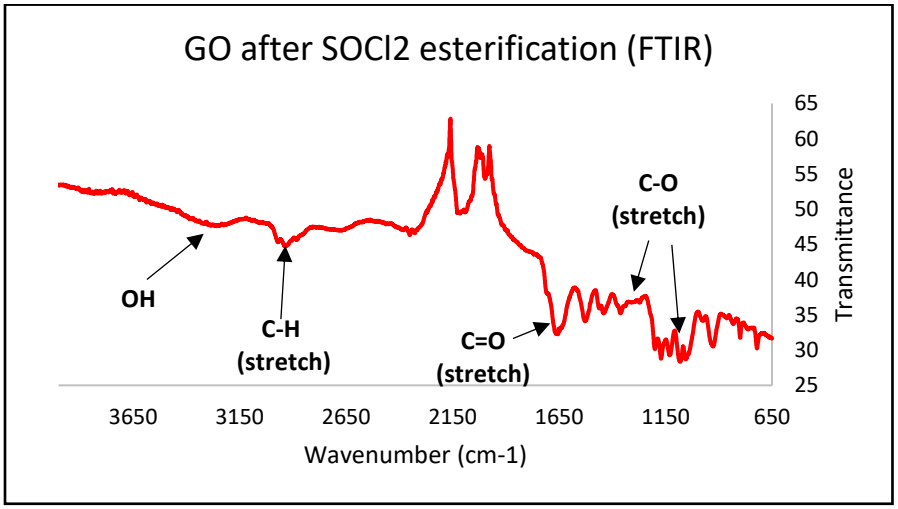

Figure 2-17 FTIR of mGO (ATR detection).

Graphene Oxide Diethylene Glycol Ester (degGO)

200 mg of GO were suspended in 20 mL ethylene glycol via sonication in a 150 mL round bottom flask equipped with a magnetic stir bar and a reflux condenser. The suspension was stirred at room temperature for 24 hours, followed by reflux at 197-198^{o}C for 1 hour. Then, the degGO suspension was cooled down to room temperature and collected via centrifugation

(10 min @ 7,000 rpm) and washed 5 times with distilled water and then lyophilized to dryness overnight. The results showed degGO material was thermostable up to 600 ^{o}C (Fig. 2-19). There was an initial drop of weight attributed to the loss of adsorbed ethylene glycol. Furthermore, the CHNO elemental analysis showed an increase in H and N for degGO compared to starting material GO which was attributed to the incorporation of ethylene glycol (Fig. 2-18).

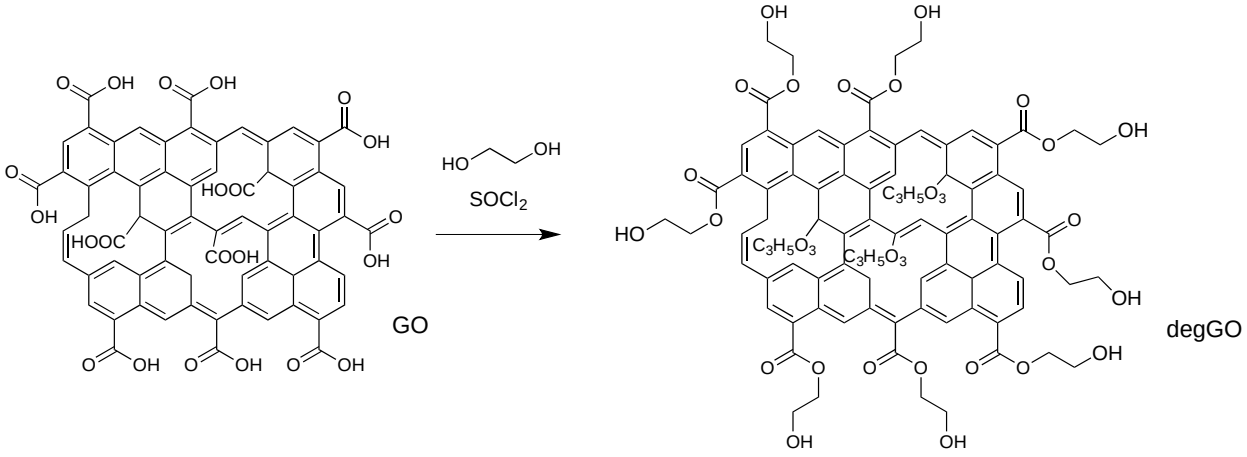

Figure 2-18 Thionyl chloride-mediated esterification of graphene oxide (GO) to Graphene Oxide Diethylene Glycol Ester (degGO).
Yield: 188mg (94%), zeta potential: ξ = - 12.9 mV. CHNO of GO: 88.37% C, 2.36% H, 0% N, 9.27% O; CHNO of degGO: 86.48% C, 3.78% H, 0% N, 9.74% O.

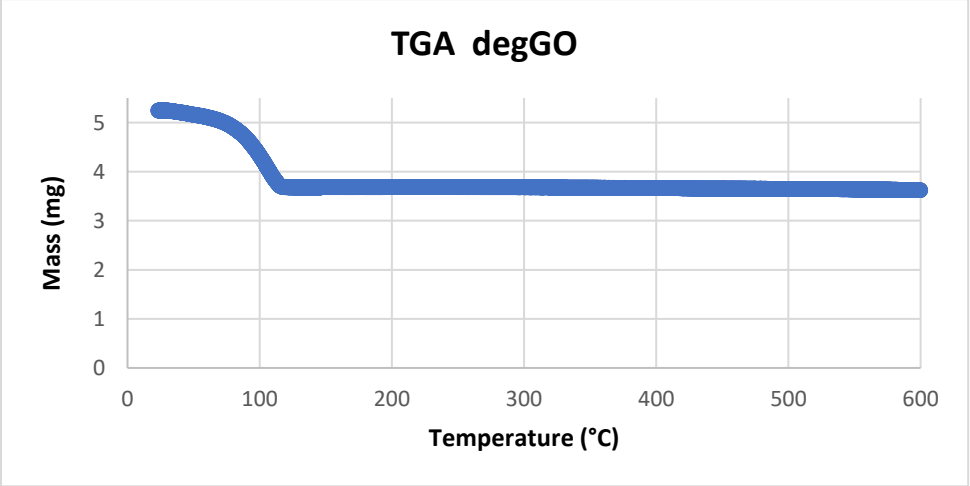

Figure 2-19 Differential Thermogravimetry (TGA) of Graphene Oxide Diethylene Glycol Ester (degGO)) prepared via thionyl chloride-mediated esterification reaction.

Graphene Oxide Amide (aGO)

50 mg of mGO were suspended in 25 mL of ammonium hydroxide (30% NH_3 by weight in H_2O) via sonication in a 150 mL round bottom flask equipped with a magnetic stirrer and reflux condenser. The suspension was refluxed for 1 hour and then allowed to cool down to room temperature. Then, amidated GO was collected via centrifugation (10 min @ 7,000 rpm) and washed 5 times with distilled water and then lyophilized to dryness overnight. Similarly, the aminated GO (aGO) showed to be thermostable up to 600 ^oC (Fig. 2-22). Furthermore, the CHNO elemental analysis showed the incorporation of N and the reduction of both H and O content, which was attributed to the amide group conjugation (Fig. 2-20). Unfortunately, the FTIR spectrum was inconclusive. However, the loss of surface carboxylic acid groups was clearly discernible when compared with the FTIR spectrum of GO (Fig. 2-21).

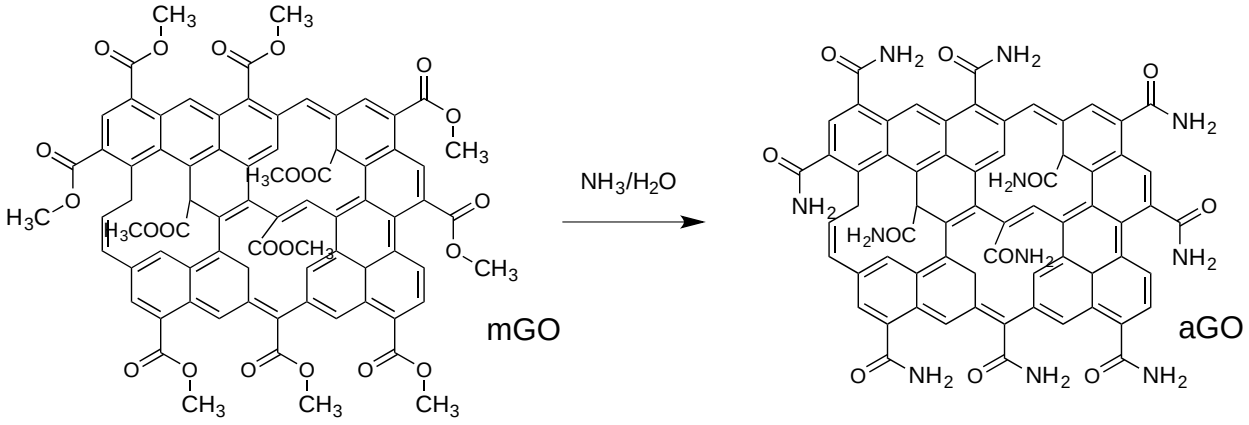

Figure 2-20 Synthesis of Graphene Oxide Amide (aGO) from Graphene Oxide Methyl Ester (mGO). YIELD: 34 mg (68%), zeta potential: ξ = - 27.6 mV. CHNO of mGO: 88.29% C, 3.40% H, 0% N, 8.31% O; CHNO of aGO: 88.17% C, 3.05% H, 4.05% N, 4.73% O**.**

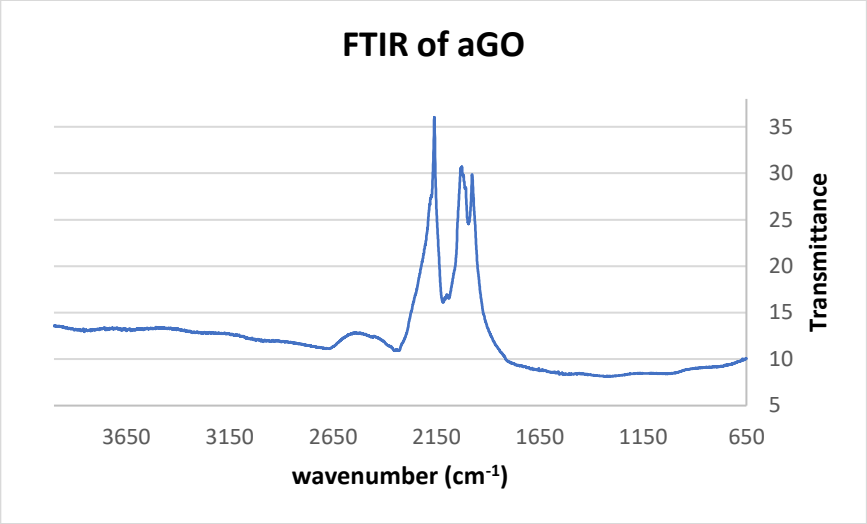

Figure 2-21 FTIR of aGO (ATR detection).

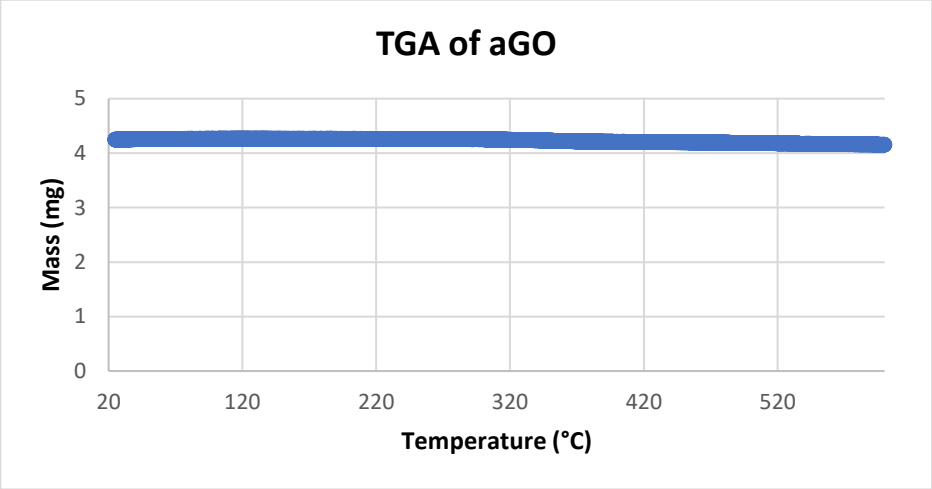

Figure 2-22 Differential Thermogravimetry (TGA) of Graphene Oxide Amide (aGO)).

4. Conclusion

The application of Fenton oxidation chemistry to synthesize the first known turbostratic core/shell graphene oxide is a powerful example of a rational chemical application, which is designed to incorporate the unique physical and materials properties of graphene into numerous materials. The experiments described in this chapter demonstrate that the general few-layer graphene structure does not change during Fenton oxidation. The functional groups that are being

formed at the outer graphene layers are predominantly carboxylic acids. This will permit the use of well-established carboxylic acid chemistry to incorporate these graphene oxide nanostructures into multiple materials and attach them at the molecular level. Furthermore, it should be noted the exemplary advantages of using rationally designed graphene oxide in comparison with current graphene oxide technologies are as follows: 1) We use explosion-derived graphene as starting materials, not expensive materials, such as mined graphite. Depending on the C to O ratio during detonation synthesis, graphene can be synthesized in multiple sizes and shapes.[5] It forms fractal aggregates. The surface of these aggregates can be oxidized, whereas their fractal structures can be preserved. 2) Detonation-derived graphene can be produced in large quantities in excellent purities. Therefore, the bulk-synthesis of tailored graphene / graphene oxide particles is possible. 3) By using Optimal Experimental Design Methodology, we have quantitatively understood the process conditions required for varying the surface oxygen content (CHO) and surface charge (zeta potential). Chemical derivatization of the resulting carboxyl group creates chemical labels in varying densities on the surface of few layer graphene assemblies. 3) Graphene oxide derivatives with appropriate surface modifications can be used in a variety of technologies for biochemical or biosensing applications, including electrical impedance or voltammetry measurements of biologically active surfaces. 4) Graphene oxide derivatives with surface modification have excellent thermostability, with a broad UV/Vis absorption spectrum, which can be used in hyperthermic applications, such as therapeutic or theranostic technologies.

5. References

[1]Sorensen, C. M., Private Communication. **2021**.

[2]Solis-Fernandez, P.; Bissett, M.; Ago, H., Synthesis, structure and applications of graphene-based 2D heterostructures. *Chem. Soc. Rev.* **2017,** *46* (15), 4572-4613.

[3]Nepal, A.; Singh, G. P.; Flanders, B. N.; Sorensen, C. M., One-step synthesis of graphene via catalyst-free gas-phase hydrocarbon detonation. *Nanotechnology* **2013,** *24* (24), 245602, 7 pp.

[4]Dollimore, D.; Spooner, P.; Turner, A., The BET method of analysis of gas adsorption data and its relevance to the calculation of surface areas. *Surf. Technol.* **1976,** *4* (2), 121-60.

[5]Wright, J. P.; Sigdel, S.; Corkill, S.; Covarrubias, J.; LeBan, L.; Nepal, A.; Li, J.; Bossmann, S. H.; Sorensen, C. M., Synthesis of nanoscale graphene via chamber detonation of oxygen/acetylene mixtures. *Materials Chemistry and Physics* **2021,** *submitted*.

[6]Tuz Johra, F.; Lee, J.; Jung, W.-G., Facile and safe graphene preparation on solution based platform. *Journal of Industrial and Engineering Chemistry* **2014,** *20*, 2883–2887.

[7]Paillet, M.; Parret, R.; Sauvajol, J.-L.; Colomban, P., Graphene and related 2D materials: An overview of the Raman studies. *J. Raman Spectrosc.* **2018,** *49* (1), 8-12.

[8]Ruz, P.; Banerjee, S.; Pandey, M.; Sudarsan, V.; Sastry, P. U.; Kshirsagar, R. J., Structural evolution of turbostratic carbon: Implications in H2 storage. *Solid State Sci.* **2016,** *62*, 105-111.

[9]Brodie, B. C., XIII. On the atomic weight of graphite. *Philosophical Transactions of the Royal Society of London* **1859,** (149), 249-259.

[10]Staudenmaier, L., Verfahren zur Darstellung der Graphitsäure. Ber Dtsch Chem Ges 31: 1481–1487. 1898.

[11]Hummers Jr, W. S.; Offeman, R. E., Preparation of graphitic oxide. *Journal of the american chemical society* **1958,** *80* (6), 1339-1339.

[12]Kondratowicz, I.; Zelechowska, K.; Sadowski, W., Optimization of Graphene Oxide Synthesis and Its Reduction. *Springer Proc. Phys.* **2015,** *167* (Nanoplasmonics, Nano-Optics, Nanocomposites, and Surface Studies), 467-484.

[13]Dreyer, D. R.; Park, S.; Bielawski, C. W.; Ruoff, R. S., The chemistry of graphene oxide. *Chemical society reviews* **2010,** *39* (1), 228-240.

[14]Park, S.; Ruoff, R. S., Synthesis and characterization of chemically modified graphenes. *Current opinion in colloid & interface science* **2015,** *20* (5-6), 322-328.

[15]Zhu, Y.; Murali, S.; Cai, W.; Li, X.; Suk, J. W.; Potts, J. R.; Ruoff, R. S., Graphene and graphene oxide: synthesis, properties, and applications. *Advanced materials* **2010,** *22* (35), 3906-3924.

[16]Dong, L.; Yang, J.; Chhowalla, M.; Loh, K. P., Synthesis and reduction of large sized graphene oxide sheets. *Chem. Soc. Rev.* **2017,** *46* (23), 7306-7316.

[17]Park, S.; Ruoff, R. S., Chemical methods for the production of graphenes. *Nat. Nanotechnol.* **2009,** *4* (4), 217-224.

[18]Park, S.; Ruoff, R. S., Chemical methods for the production of graphenes. [Erratum to document cited in CA151:014005]. *Nat. Nanotechnol.* **2010,** *5* (4), 309.

[19]Hossain, M. Z.; Johns, J. E.; Bevan, K. H.; Karmel, H. J.; Liang, Y. T.; Yoshimoto, S.; Mukai, K.; Koitaya, T.; Yoshinobu, J.; Kawai, M.; Lear, A. M.; Kesmodel, L. L.; Tait, S. L.; Hersam, M. C., Chemically homogeneous and thermally reversible oxidation of epitaxial graphene. *Nat. Chem.* **2012,** *4* (4), 305-309.

[20]Tang, L.; Li, X.; Ji, R.; Teng, K. S.; Tai, G.; Ye, J.; Wei, C.; Lau, S. P., Bottom-up synthesis of large-scale graphene oxide nanosheets. *J. Mater. Chem.* **2012,** *22* (12), 5676-5683.

[21]Fang, S.; Lin, Y.; Hu, Y. H., Recent Advances in Green, Safe, and Fast Production of Graphene Oxide via Electrochemical Approaches. *ACS Sustainable Chem. Eng.* **2019,** *7* (15), 12671-12681.

[22]Fenton, H., LXXIII.—Oxidation of tartaric acid in presence of iron. *Journal of the Chemical Society, Transactions* **1894,** *65*, 899-910.

[23]Walling, C., Fenton's reagent revisited. *Accounts of chemical research* **1975,** *8* (4), 125-131.

[24]Bossmann, S. H.; Oliveros, E.; Goeb, S.; Siegwart, S.; Dahlen, E. P.; Payawan, L., Jr.; Straub, M.; Woerner, M.; Braun, A. M., New Evidence against Hydroxyl Radicals as Reactive Intermediates in the Thermal and Photochemically Enhanced Fenton Reactions. *J. Phys. Chem. A* **1998,** *102* (28), 5542-5550.

[25]Legrini, O.; Oliveros, E.; Braun, A., Photochemical processes for water treatment. *Chemical reviews* **1993,** *93* (2), 671-698.

[26]Luzzatto, E.; Cohen, H.; Stocheim, C.; Wieghardt, K.; Meyerstein, D., Reactions of low valent transition metal complexes with hydrogen peroxide. Are they "Fenton-like" or not? 4. The case of Fe(II), L = EDTA; HEDTA and TCMA. *Free Radical Res.* **1995,** *23* (5), 453-63.

[27]Bossmann, S. H.; Oliveros, E.; Kantor, M.; Niebler, S.; Bonfill, A.; Shahin, N.; Woerner, M.; Braun, A. M., New insights into the mechanisms of the thermal Fenton reactions occurring using different iron(II)-complexes. *Water Sci. Technol.* **2004,** *49* (4, Oxidation Technologies for Water and Wastewater Treatment III), 75-80.

[28]Gob, S.; Oliveros, E.; Bossmann, S. H.; Braun, A. M.; Guardani, R.; Nascimento, C. A. O., Modeling the kinetics of a photochemical water treatment process by means of artificial neural networks. *Chem. Eng. Process.* **1999,** *38* (4-6), 373-382.

[29]Gob, S.; Oliveros, E.; Bossmann, S. H.; Braun, A. M.; Nascimento, C. A. O.; Guardani, R., Optimal experimental design and artificial neural networks applied to the photochemically enhanced Fenton reaction. *Water Sci. Technol.* **2001,** *44* (5, Oxidation Technologies for Water and Wastewater Treatment II), 339-345.

[30]Koppenol, W. H., The Haber-Weiss cycle - 70 years later. *Redox Rep.* **2001,** *6* (4), 229-234.

[31]Haber, F.; Weiss, J. J., Über die Katalyse des Hydroperoxydes (On the catalysis of hydroperoxide). *Naturwissenschaften* **1932,** *20* (51), 948-950.

[32]Nepal, A.; Chiu, G.; Xie, J.; Singh, G. P.; Ploscariu, N.; Klankowski, S.; Sung, T.; Li, J.; Flanders, B. N.; Hohn, K. L.; Sorensen, C. M., Highly oxidized graphene nanosheets via the oxidization of detonation carbon. *Appl. Phys. A: Mater. Sci. Process.* **2015,** *120* (2), 543-549.

[33]Klung, H. P.; Alexander, L. E., *The X-Ray Diffraction Procedures for Polycrystalline and Amorphous Materials. 2nd Ed*. Wiley: 1974; p 966 pp.

[34]Clifford, C. A.; Martins Ferreira, E. H.; Fujimoto, T.; Herrmann, J.; Hight Walker, A. R.; Koltsov, D.; Punckt, C.; Ren, L.; Smallwood, G. J.; Pollard, A. J., The importance of international standards for the graphene community. *Nature Reviews Physics* **2021,** *3* (4), 233-235.

[35]Tuinstra, F.; Koenig, J. L., Raman spectrum of graphite. *J. Chem. Phys.* **1970,** *53* (3), 1126-30.

[36]Kawashima, Y.; Katagiri, G., Fundamentals, overtones, and combinations in the Raman spectrum of graphite. *Phys. Rev. B: Condens. Matter* **1995,** *52* (14), 10053-9.

[37]Hao, Y.; Wang, Y.; Wang, L.; Ni, Z.; Wang, Z.; Wang, R.; Koo, C. K.; Shen, Z.; Thong, J. T. L., Probing Layer Number and Stacking Order of Few-Layer Graphene by Raman Spectroscopy. *Small* **2010,** *6* (2), 195-200.

[38]Kornilov, D. Y.; Gubin, S. P., Graphene Oxide: Structure, Properties, Synthesis, and Reduction (A Review). *Russ. J. Inorg. Chem.* **2020,** *65* (13), 1965-1976.

[39]Luong, D. X.; Bets, K. V.; Algozeeb, W. A.; Stanford, M. G.; Kittrell, C.; Chen, W.; Salvatierra, R. V.; Ren, M.; McHugh, E. A.; Advincula, P. A.; Wang, Z.; Bhatt, M.; Guo, H.; Mancevski, V.; Shahsavari, R.; Yakobson, B. I.; Tour, J. M., Gram-scale bottom-up flash graphene synthesis. *Nature (London, U. K.)* **2020,** *577* (7792), 647-651.

[40]Baibarac, M.; Baltog, I.; Szunerits, S. In *Raman and FTIR spectroscopy as valuable tools for the characterization of graphene-based materials*, CRC Press: 2016; pp 235-253.

[41]Watanabe, S.; Ishikura, T.; Hayashi, N.; Uchida, Y.; Duck-Chool, L.; Dykes, D.; Touchard, G.; Ieda, M. In *Potential energy in the electrical double layer and slipping plane potential*, ICDL'96. 12th International Conference on Conduction and Breakdown in Dielectric Liquids, 15-19 July 1996; 1996; pp 61-64.

[42]Sabzevari, M.; Cree, D. E.; Wilson, L. D., Graphene Oxide-Chitosan Composite Material for Treatment of a Model Dye Effluent. *ACS Omega* **2018,** *3* (10), 13045-13054.

[43]Kelly, K. F.; Billups, W. E., Synthesis of Soluble Graphite and Graphene. *Acc. Chem. Res.* **2013,** *46* (1), 4-13.

[44]Lundstedt, T.; Seifert, E.; Abramo, L.; Thelin, B.; Nyström, Å.; Pettersen, J.; Bergman, R., Experimental design and optimization. *Chemometrics and intelligent laboratory systems* **1998,** *42* (1-2), 3-40.

[45]Oliveros, E.; Gob, S.; Bossmann, S. H.; Braun, A. M.; Nascimento, C. A. O.; Guardani, R. In *Waste water treatment by the photochemically enhanced fenton reaction: modeling and optimization using experimental design and artificial neural networks*, World Scientific Publishing Co. Pte. Ltd.: 2001; pp 577-581.

[46]Amat, A. M.; Arques, A.; Bossmann, S. H.; Braun, A. M.; Goeb, S.; Miranda, M. A.; Oliveros, E., Oxidative degradation of 2,4-xylidine by photosensitization with 2,4,6-triphenylpyrylium: homogeneous and heterogeneous catalysis. *Chemosphere* **2004,** *57* (9), 1123-1130.

[47]Rios-Enriquez, M.; Shahin, N.; Duran-De-Bazua, C.; Lang, J.; Oliveros, E.; Bossmann, S. H.; Braun, A. M., Optimization of the heterogeneous Fenton-oxidation of the model pollutant 2,4-xylidine using the optimal experimental design methodology. *Sol. Energy* **2004,** *77* (5), 491-501.

[48]Silvares, A. F. M.; Nascimento, C. A. O.; Oliveros, E.; Bossmann, S. H.; Braun, A. M., Optimization of the photochemically initiated polymerization of methyl methacrylate. *Chem. Eng. Process.* **2006,** *45* (11), 1001-1010.

[49]Silvares, A. F. M.; do Nascimento, C. A. O.; Oliveros, E.; Bossmann, S. H.; Braun, A. M., Pulsed XeCl Excimer Radiation for Optimizing the Polydispersity of Methyl Methacrylate Pre-Polymers. *Ind. Eng. Chem. Res.* **2007,** *46* (23), 7436-7447.

[50]Wendel, S. O.; Perera, A. S.; Pfromm, P. H.; Czermak, P.; Bossmann, S. H., Fermentation optimization of Mycobacterium smegmatis using experimental design. *Br. J. Appl. Sci. Technol.* **2014,** *4* (10), 1472-1484, 13.

[51]https://shop.statease.com/dx11.html.

[52]Smith, A. M.; Mancini, M. C.; Nie, S., Bioimaging: second window for in vivo imaging. *Nat Nanotechnol* **2009,** *4* (11), 710-711.

Chapter 3 - Upscale Synthesis Graphene/Graphene Oxide Core/Shell Particles from Detonation Synthesized Graphene

Abstract:

Throughout the last decade, graphene has become one of the latest sensation materials of research due to its remarkable physical and chemical properties that are suitable for an infinite number of applications. However, taking complete advantage of graphene has been difficult since large-scale production methods are neither simple nor economical. Hence, we have developed a novel, simple, economical, and up-scalable method for the preparation of graphene/graphene (G/GO) oxide core/shell particles from explosion-synthesized graphene to overcome the issue of agglomeration and restacking of graphene sheets. Herein, graphene/graphene oxide particles were synthesized in large-scale quantities from high-quality explosion-synthesized graphene by means of Fenton oxidation. CHO elemental analysis, TGA, FTIR, Raman, XRD, and TEM analyses confirmed that G/GO particles produced at large-scale had the same quality as that obtained from small-scale synthesis. Thus, this strategy showed a promising approach to overcoming one of the greatest challenges in mass-producing high-quality material in a reproducible way at low cost.

1. Introduction

Graphene is two-dimensional, one atom-thick, honeycomb sheet of sp^2 hybridized carbon atoms, and it is the building block for other materials (e.g. graphite, carbon nanotubes, and fullerene).[1] Since its discovery in 2004, graphene has been considered to be the wonder material of the 21st century due to its remarkable properties including excellent electrical and thermal conductivity, high carrier mobility, mechanical strength, and optical transparency.[2-3] Thus, making graphene a suitable material for the development of next-generation technologies such as sensors, nanoelectronics, energy harvesting and storage, multifunctional composites and coatings, as well as in biomedical applications. [2-6] Unfortunately, taking complete advantage of graphene's exceptional properties has been difficult since large-scale production methods are neither simple nor economical. Albeit the biggest problem remains in preventing the irreversible agglomeration and restacking of graphene sheets which leads to the formation of graphite through strong $\pi-\pi$ stacking and van der Waals interaction.[7]

Since most of the unique properties are associated only with mono- and few-layer graphene (2-10 layers), it is crucial to prevent agglomeration of graphene sheets. For this purpose, numerous attempts to create processable graphene oxide (GO) have been explored. In general, GO is chemically synthesized by some variation of either the Brodie, Hummers, or Staudenmaier methods; Hummer's being the most popular. Staudenmaier and Brodie methods use a combination of potassium chlorate with nitric and/or sulfuric strong acids, whereas Hummer's method uses a combination of potassium permanganate, sulfuric acid, and sodium nitrate.[8-10] They all have in common to start with some source of graphite precursor, which gets oxidized and then undergoes exfoliation to yield GO. Unfortunately, these methods have several major drawbacks including generation of toxic waste, slow process, low yield, imperfect

structure, difficult purification, and most important irreproducible results thus making these methods not suitable for scale-up synthesis.[8-10]

Many researchers have implemented several modifications to the Hummers method to overcome these challenges and improve the product yield while reducing the cost.[11-13] Although, there have been significant advances in creating more efficient ways to synthesize GO, the challenge remains in the development of an economical large-scale method with reproducible high quality material production. Recently, Ranjan *et al*. reported an inexpensive route for synthesizing GO via modifications to Hummer's method.[14] They claimed their method not only produced high yields of great quality GO from graphite, but also eliminated the explosive nature of the underlying reactions by adding a pre-cooling protocol and changing the reaction time and temperature. Similarly, Benzait *et al*. reported the enhanced synthesis of GO by further improving the established "improved Hummer's method" by adding a pre-treatment step using piranha solution which allows the chemical expansion of graphite before oxidation.[15] They claimed the addition of this simple step helped improve the oxidation reaction which led to the production of GO with a higher degree of oxidation, larger sheets, better structural integrity, and a higher yield of monolayers. Furthermore, Costa *et al*. demonstrated an accelerated synthesis of GO obtained directly from the oxidation of graphene using an environmentally friendly modified Hummers method.[16] Their results showed their GO could be rapidly produced (5 min of oxidation) with a controllable degree oxidation due to the higher surface area of unstacked graphene sheets, which are quickly and more homogeneously oxidized since the flakes are exposed at the same extension to the chemical agents. The biggest advantage is the use of high-quality graphene as the starting material because the use of intercalant agents is not required. However, access to high-quality graphene is expensive thus making upscale production not

suitable. All three groups (Ranjan *et al*.; Benzait *et al*. & Costa *et al*.)[14,15,16] reported their processes to be promising methods for the mass-production of GO, but still, none of them has reported any successes in doing up-scale synthesis. Besides, all three required the use of dangerous reagents during their synthesis, rely heavily in graphite precursor or high-quality graphene, and struggled to make GO with consistent properties.

In this work, we report the progress made in controlling the upscale synthesis of graphene/graphene oxide (G/GO) core/shell particles from high-quality explosion-synthesized graphene by means of Fenton oxidation. The reaction was easily scaled up from a small scale of 1.0 g per batch to a large scale 200 g per batch. More importantly, the quality of the G/GO core/shell particles prepared from both small scale (1 g) and large scale (200 g) were nearly the same.

2. Materials and Methods

2.1. Chemicals and Instrumentation

All chemicals used in the synthesis process were purchased from ThermoFisher Scientific and were used without further purification. Chemicals used were hydrogen peroxide (H_2O_2) (30%), ferrous sulfate heptahydrate ($FeSO_4$ x 7 H_2O), and concentrated sulfuric acid (H_2SO_4). Detonation-synthesized graphene nanosheets (GNs), a pristine graphene material, were obtained from our collaborators in the Sorensen Research Laboratories, Physics Department at Kansas State University.

The zeta potential of the G/GO particles were measured on a ZetaPALS zeta potential analyzer (Brookhaven Instruments Corporation) by hydrodynamic light scattering and laser Doppler electrophoresis. Thermogravimetric analysis (TGA) of graphene nanosheets and graphene oxide synthesized via Fenton oxidation was performed on a Shimadzu TGA-50 Analyzer.

Approximately 5 mg of each sample was heated under a stream of nitrogen gas flow (10 mL/min) from 25 to 600 °C at a rate of 10 °C/ min. X-ray powder diffraction (XRD) analysis was performed using a Bruker AXS D8 Advance diffractometer operating at 40 kV and 40 mA. Measurements of each sample were performed in the scattering angle, 2θ range from 5° to 60° with a step of 0.05° and step time of 1.6 sec/step. Raman spectroscopy analysis was performed in a DXR Raman microscope at 532 nm (2.33 eV) with a resolution of 0.1 cm^{-1}. CHO elemental analysis was performed in the core chemical laboratory of the University of Kansas Medical Center. FTIR spectra were collected in an Agilent Cary 630 FTIR spectrometer over a range of 650 – 4000 cm^{-1}. The morphology of the G/GO core/shell particles was characterized by transmission electron microscopy (TEM). The TEM characterization of graphene oxide has been performed at the Microscopy and Analytical Imaging Research Resource Core Laboratory (MAI) at the University of Kansas. The measurements were performed on a Hitachi H-8100 Transmission Electron Microscopy (200 kEV) on copper grids. Graphene oxide deposition on the grids was achieved via MeOH dispersion, followed by evaporation in high vacuum.

2.2. Upscale Synthesis of Graphene/Graphene Oxide Core/Shell Nanoparticles

Graphene nanosheets (GNs) were prepared from the catalyst-free, controlled detonation of acetylene gas in the presence of oxygen in a 16.61 cylindrical aluminum chamber.[17] For this study, GNs prepared with a pre-detonation molar ratio of O_2/C_2H_2=O/C of 0.3 were used. After performing an optimal experimental design methodology (OEDM) to find the optimize Fenton oxidation conditions for the preparation of Graphene/Graphene Oxide (G/GO) core/shell nanoparticles, we discovered the optimized parameters to oxidize 1.0 g of GN in 100 mL of 10 vol% H_2O_2 in water (pH=3, sulfuric acid) required the use of 125 mg of $FeSO_4$ X 7 H_2O and a temperature of 60 °C for 24 hours of constant stirring. From this, the first upscale reaction was

performed by increasing the small-scale reaction by a factor of 10. In short, 10.0 g of graphene were added to 1000 ml aqueous reactant (10 vol% H_2O_2 in water (pH=3, sulfuric acid)) in a 3000 ml flask. The sample was stirred with a mechanical stirrer for 1h. During this time, the graphene was dispersed in the aqueous reactant and began to react. After 30 min, the temperature reached 80 ± 5 °C. Substantial foaming was observed. The reactor was continuously stirred until the temperature decreased to 60 °C. Afterwards, 1.25 g of solid FeSO4 x 7 H2O was added at once. The temperature increased to 95 ± 5 °C within 15 min. and then slowly decreased. The mixture was then stirred for 24 hours at 60 °C. Fenton oxidized GO was collected via centrifugation (10 min @ 7000 rpm) and washed 5-7 times with water. Finally, GO was lyophilized to dryness overnight for characterization. The reaction was repeated twice to verify if reaction was reproducible.

After successful results were obtained from both upscale reactions performed with 10 g of GNs in 1000 mL of H_2O_2, the next step was to optimize the maximum amount of graphene that could be oxidized in 100 mL of H_2O_2. For the optimization experiments, all reaction conditions were kept constant (100 mL H_2O_2, 125 mg FeSO4 x 7 H2O, and 60 °C) the only variable that was changed was the amount of graphene where it was increased by a factor of x3, x6, and x10. The reactions were labeled and are referenced herein as following: 1:1, 1:3, 1:6, and 1:10.

Ultimately, after finding optimized conditions for maximum amount of graphene oxidized in 100 mL H_2O_2, the next goal was to upscale the reaction by a factor of 10. In short, 100 g of GNs were added to 1000 mL (10 vol% H_2O_2 in water (pH=3, sulfuric acid)) in a 5000 mL flask. Next, the sample was stirred at 60 °C with 1.25 g of $FeSO_4$ x 7 H2O for 24 hours. After 24 hours, GO was collected via centrifugation (10 min @ 7000 rpm) and washed 5 times

with water. Lastly, GO was dried at 40 °C for 48-72 hours for characterization. After confirming that a constant 60 °C temperature could be maintained and that our method was broadly scalable, the next step was to increase the reaction by a factor of 2. In short, 200 g of GNs were added to 2000 mL (10 vol% H_2O_2 in water (pH=3, sulfuric acid)) in a 5000 mL flask. Briefly, 200 g of GNs were added to 2000 ml aqueous reactant (10 vol% H_2O_2 in water (pH=3, sulfuric acid)) in a 5000 ml flask, along with 2.50 g of solid $FeSO_4$ x 7 H_2O.

2.3. Titration of Graphene/Graphene Oxide Core/Shell Nanoparticles

100 mg of Fenton-oxidized GO were suspended in 10 mL of 0.100 M NaOH. After stirring the suspension for 5 min at 300K, 0.100 M HCl solution was added in incremental steps. At each step, the pH of the solution was recorded using a pH meter after making sure equilibrium had been reached (1-5 min.), before the next amount of HCl. The same procedure was used with the same volume of NaOH but without the addition of GO. The difference in the volumes of HCl in the two titration curves for the same value of pH of ~7.00 directly corresponds to the concentration of the ionized groups (hydroxyl and carboxyl groups) per weight increment of GO.[18] The titration procedure was performed for both Fenton-oxidized small-scale (1:1) and large-scale (200 g) reactions.

3. Results and Discussion

Table 3-1 summarizes the CHO elemental analysis which is used to indicate the oxidation of the explosion-synthesized graphene starting material. Results showed the C/O ratio changed from 11:1 for small scale GO reaction to 9.5:1 for large-scale GO. Also, the zeta potentials for the samples were measured in DMF for graphene and water for both GO samples. The zeta potential is a useful way to characterize the stability of colloidal dispersions, where particles with

zeta potentials in the range -30 mV to +30 mV are generally considered stable due to electrostatic repulsion. [19] Our results showed that zeta potentials changed from +60 mV for graphene, to -8.20 ± 0.78 mV for small scale GO and -8.62 mV ± 0.76 for large-scale GO. The negative zeta potential values are because of the presence of ionizable -COOH functional groups formed after oxidizing GNs.[20] Similar zeta potentials were obtained for the first two large-scale reactions performed using 10 g GNs in 1 L H_2O_2 and the first large-scale using 100 g GNs in 1 L H_2O_2 (Appendix B). Therefore, these findings provide evidence that the quality of G/GO particles produced from large-scale reaction is nearly the same as the one from small scale reaction.

Table 3-1 CHO elemental analysis and zeta potentials of graphene, small scale GO, and large-scale GO.

Sample	CHO Analysis	Zeta Potential (mv)
Graphene 0.3	99.8% C, 0.15% H, 0.05% O	+ 60
Small scale (1.0 g)	90.1% C, 1.7% H, 8.2% O	- 8.20
Large-scale (200.0 g)	88.37% C, 2.36% H, 9.27% O	- 8.62

Graphene is known to have an excellent thermal stability which is one of its unique properties. It was reported that the thermal stability of graphene is related to its layering and the interaction of it in air atmosphere, and it is also dependent on the annealing time, atmosphere, and preparation method.[21] Graphene can be heated up to 800 °C with limited damage but starts to suffer major damage when heated to 1000 °C.[21] The high thermal stability of graphene materials is very crucial because the higher the thermal stability is for such materials, the more suitable they are for composite materials. For this reason, the thermal decomposition behavior of GO and GNs was investigated by thermogravimetric analysis. As shown in Figure 3-1, GNs are very stable when heated up to 600 °C, similarly both GO small scale and GO large-scale are stable up

to 550 °C. Both GOs have a mass decrease of 3.5 – 5% by weight when heated to 600 °C. This process starts at 550 °C, which is a very different behavior than for other graphene oxides. Typically, synthesized graphene oxides, via some type of variation from Hummer's method, undergo serious decomposition between 200 °C and 475 °C.[22-25] The weight loss of GO can be explained based on their decomposition temperatures: <100 °C is attributed to the removal of adsorbed water, between 100 – 360 °C is due to the decomposition of labile oxygen containing functional groups, and in the range of 400 – 800 °C is due to the removal of more stable oxygen functional groups.[23,25-26] Similar results were observed for the first two large-scale reactions performed using 10 g GNs in 1 L H_2O_2 and the first large-scale using 100 g GNs in 1 L H_2O_2 (Appendix B). Thus, results demonstrated our large-scale GO is reproducible in larger scales without affecting the excellent thermal stability of our original product. These results are in agreement with the formation of graphene/graphene oxide core/shell particles even at large scales, which maintain an intact graphene core allowing it to retain its excellent thermal stability.

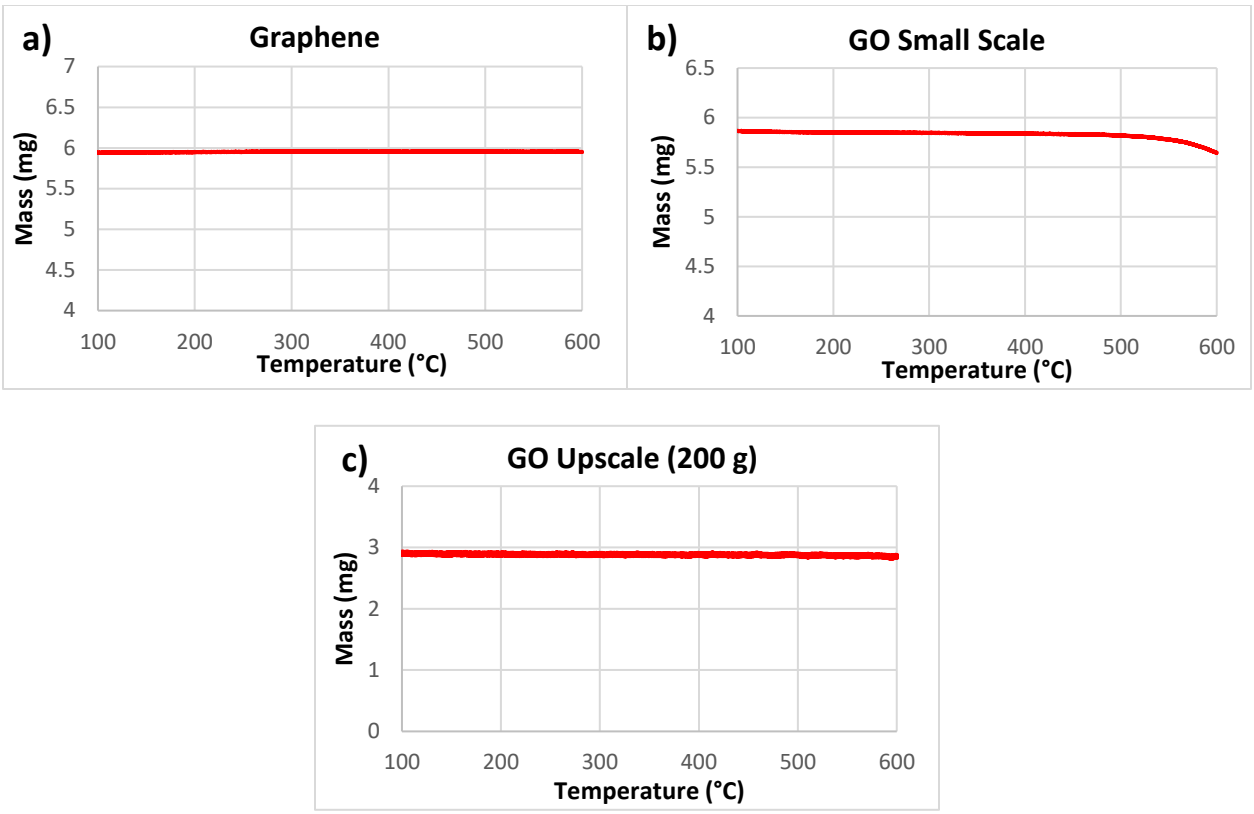

Figure 3-1 TGA analysis of a) GNs, b) small scale GO, and c) large-scale GO.

FTIR spectroscopy analysis is a simple but effective way to identify the presence of unique chemical functional groups introduced by oxidation to graphene oxide and its derivatives. Figure 3-2 shows the FTIR spectra obtained for a) starting material detonation-synthesized GNs, b) small-scale synthesized GO, and c) large-scale synthesized GO. The spectrum of GNs do not show any presence of functional groups attached on the surface, thus suggesting its pristine nature.[17] In comparison, both GO spectra (small- and large-scale) showed broad peaks in the wavenumber range of 3500 – 2500 cm^{-1} attributed to the stretching mode of the –OH groups. It is worth mentioning that the presence of residual water molecules and the shifts in the frequency of vibration of the O-H bonds (bonded at different locations ranging from center of the sheet to its borders) contribute to the broadening of the O–H band.[14] Similarly, the absorption bands at 1800 – 1680 cm^{-1} (both small & large spectra) are attributed to the stretching vibration of C=O bonds

in carboxyl/carbonyl groups, and the bands at ~1280 cm^{-1} are due to the stretching vibrations of the C–OH group. The same results were observed for all of the optimization reactions (1:1, 1:3, 1:6, and 1:10) as well as the first large-scale reactions (10 g in 1 L & 100 g in 1 L) shown in Appendix B. The absorption peaks observed for all of our GO samples are similar to those mentioned in previous literature.[14, 27-29] More importantly, our FTIR results suggested that oxidation of GNs in both small and large-scale synthesis gave identical results confirming that our reaction is reproducible at large-scales.

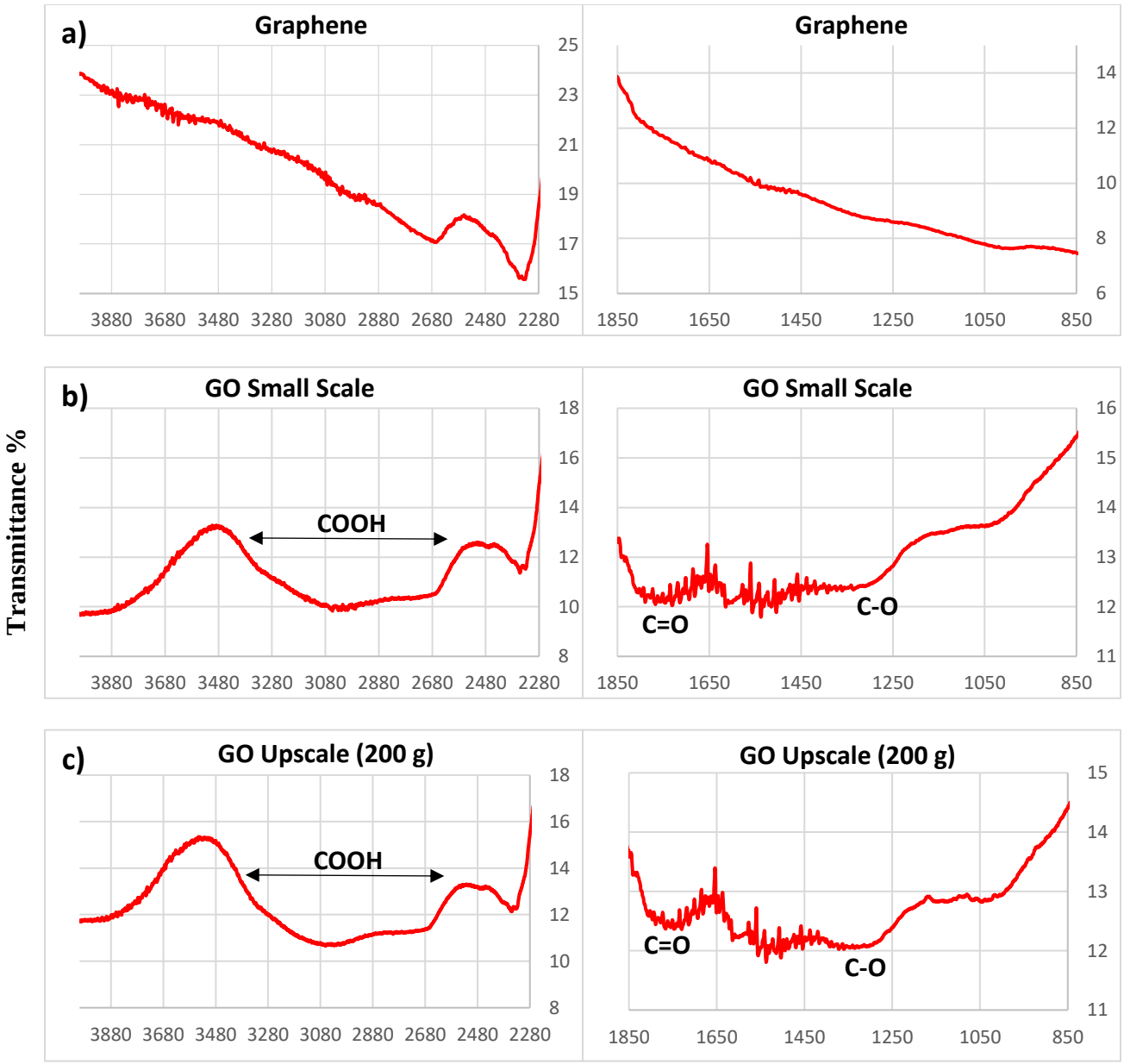

Figure 3-2 FTIR spectra of a) GNs, b) GO small scale, and c) GO large-scale.

Figure 3-3 shows the XRD spectra of the GNs prepared by detonation at O_2/C_2H_2 = 0.3 molar ratio and the two GOs from small and large-scale synthesis. The GN sample showed a strong peak at 2θ ~ 25.3° corresponding to the (002) planes of stacked graphene layers, similarly both GOs (small and large-scale) showed the same strong peak at 2θ ~ 25.6°. Additionally, a weak peak at 2θ ~ 43° corresponding to the (100) plane was found in all three samples which is

an indication of the turbostratic band of disordered carbon materials.[30,31] Also, the interplanar spacing (d) indicated by XRD spectra was shifted from 0.352 nm for GN to 0.348 nm for both GO samples. The (002) peak and the interplanar spacing for both GO samples remained almost unchanged compared to the starting GN material suggesting that intercalation of oxygen did not take place after Fenton oxidizing GNs. In most GO samples, the intercalation of oxygen functional groups such as hydroxyl and carboxylic groups typically leads to an increase of interlayer d-spacing between graphene layers as well as a unique peak shift to $2\theta \sim 10.7°$.[26,28-31] Therefore, the results obtained in the XRD patterns corroborated that Fenton oxidation only oxidizes the outside layer of the GNs creating a GO outer shell.

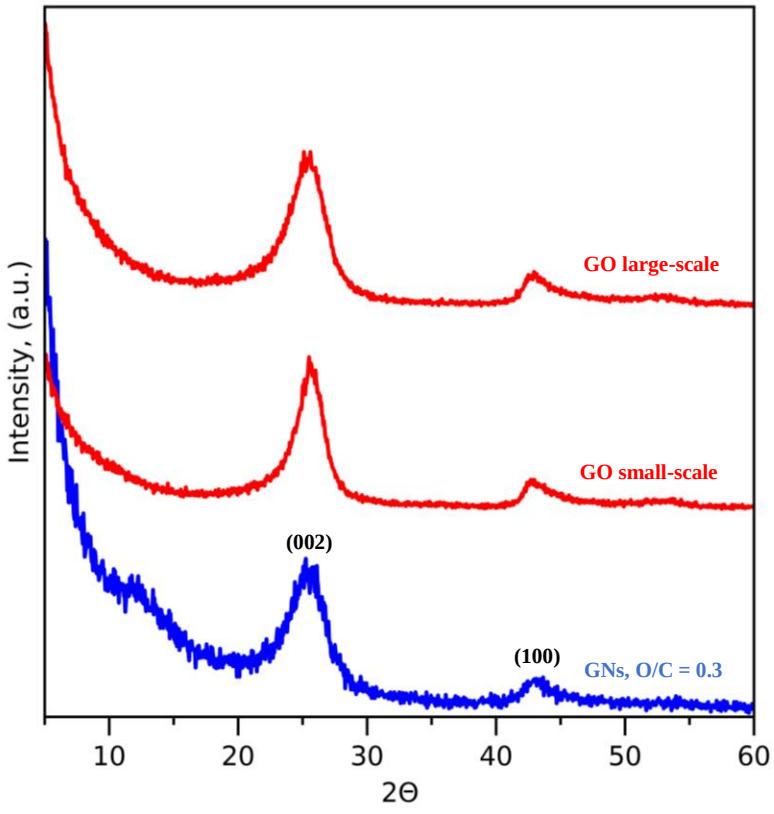

Figure 3-3 XRD patterns of GN (O/C = 0.3), GO small-scale, and GO large-scale. (All graphs scaled to have same (002) peak intensity)

Raman spectroscopy was performed to investigate the oxidation of the GNs. Figure 3-4 shows the Raman spectra of pristine GNs and both GO (small and large-scale) samples. The three significant peaks on GNs spectrum at 1337, 1568, and 2668 cm^{-1} correspond to D, G, and 2D bands, respectively. The G band is an in-plane vibrational mode involving the sp^2 hybridized carbon atoms; the D band is the defect band and represents the defect or partially disordered structure of the sp^2 domains, and the 2D band is the second order of the D band, sometimes referred as an overtone of the D band.[33] Similarly, GO small-scale showed the three peaks at 1337 (D), 1572 (G), and 2674 (2D) and GO large-scale at 1337 (D), 1571 (G), and 2670 (2D). Typically, the oxidation of graphene or graphite to produce GO induces several disorders in sp^2 hybridized carbon sheets which leads to a higher intensity of the D band and a broader G band.[16,29,31] Additionally, the I_D/I_G ratio observed for GNs ($I_D/I_G \sim 1.14$) is slightly reduced after oxidation in both GO small-scale ($I_D/I_G \sim 0.98$) and GO large-scale ($I_D/I_G \sim 1.09$), thus indicating a lower level of disorder.[30] In this case, results demonstrated that oxidation did not cause any major shifts in any of the D, G, and 2D peaks compared to those from the starting GNs material, rather the reduction of I_D/I_G ratio indicated that the level of disorder was decreased. Again, the results provide evidence that Fenton oxidation only oxidizes the outside layer, leaving the graphene inner core intact. More importantly, the large-scale GO showed similar Raman results compared to small-scale GO confirming that the quality of GO produced at large scale reactions remained unchanged.

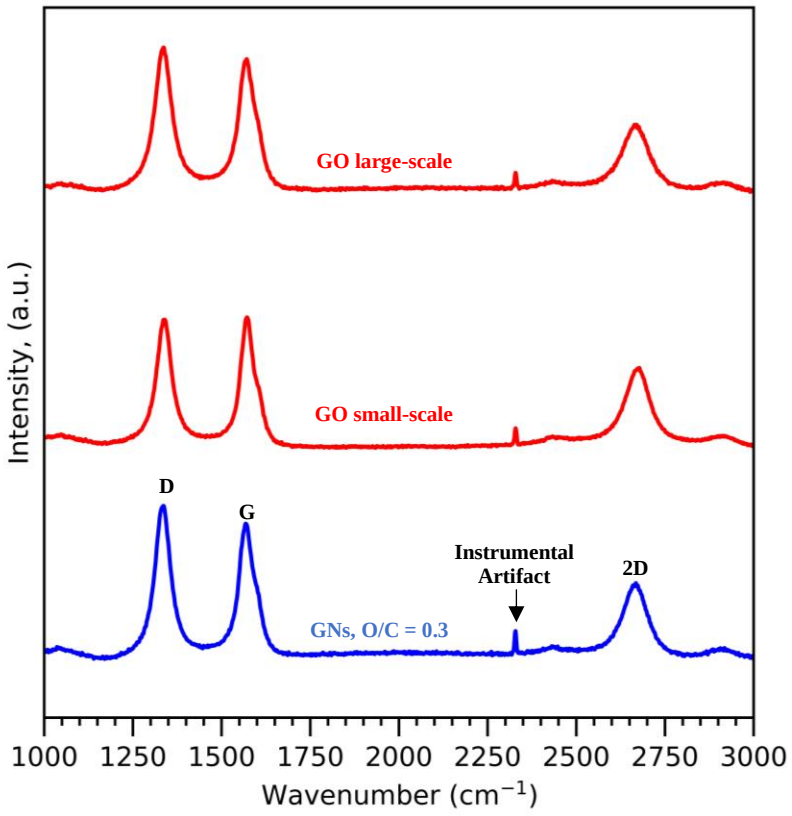

Figure 3-4 Raman spectra of GNs (O/C=0.3), GO small-scale, and GO large-scale. (All Raman graphs are scaled to have same G peak intensity)

Figure 3-5 shows the titration results for both small- and large-scale GO. The Δvolume at pH ~7 was 245 uL for the GO small scale reaction and 225 uL for upscale GO. This is equivalent to 2.45 x 10^{-5} moles acidic groups per 100 mg GO or 2.45 x 10^{-4} moles/g GO for small scale, and 2.25 x 10^{-5} moles acidic groups per 100 mg GO or 2.25 x 10^{-4} moles/g GO for upscale. Furthermore, from the shape of the titration curve we conclude that the acidic group is predominantly (> 95%) -COOH, since -OH will be (re)protonated at high pH where both the GO and reference titration curved are almost identical. More remarkably, large-scale synthesis showed a similar number of acidic groups as the small-scale reaction, thus demonstrating the oxidation of GNs can be performed at a large-scale with reproducible results.

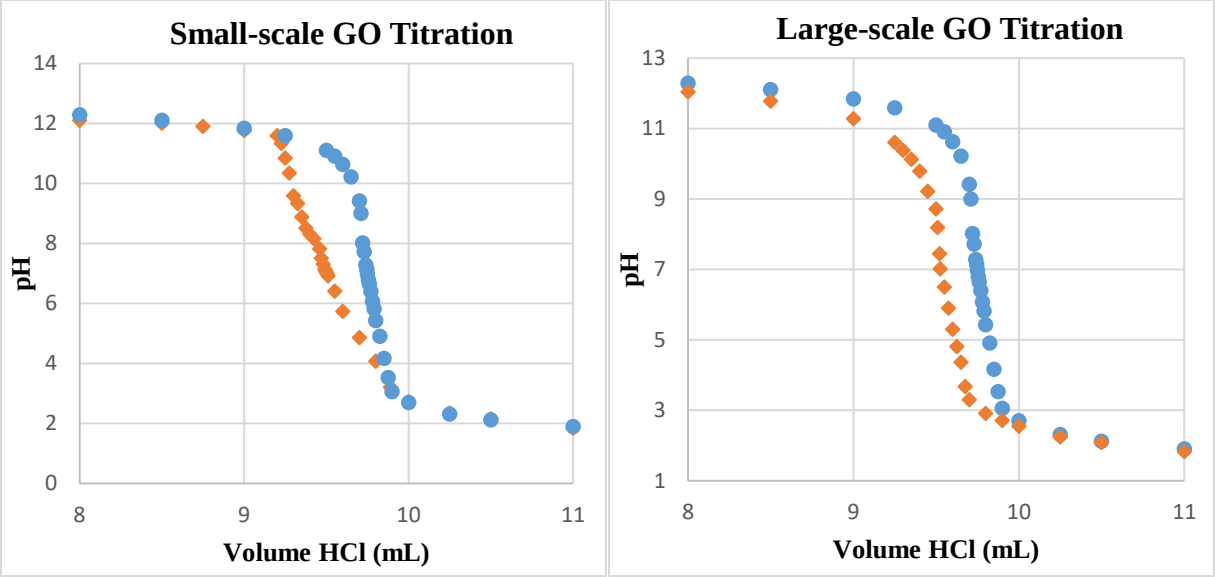

Figure 3-5 Titration curves (pH vs volume 0.10 M HCl) for both small- and large-scale GO. (Blue circles: reference curve; Orange diamonds: titration of GO. *100 mg of sample was used for both small and large)

Figure 3-6 shows the comparison TEM images of graphene, small scale GO, and large-scale GO. The results clearly showed that the morphology of graphene does not change during Fenton oxidation for both samples small and large-scale GO. Thus, once again, the results demonstrated that oxidation of GNs can be performed at a large scale without affecting the remarkable properties of graphene because only the outer layers get oxidized leaving the interior graphene layers intact.

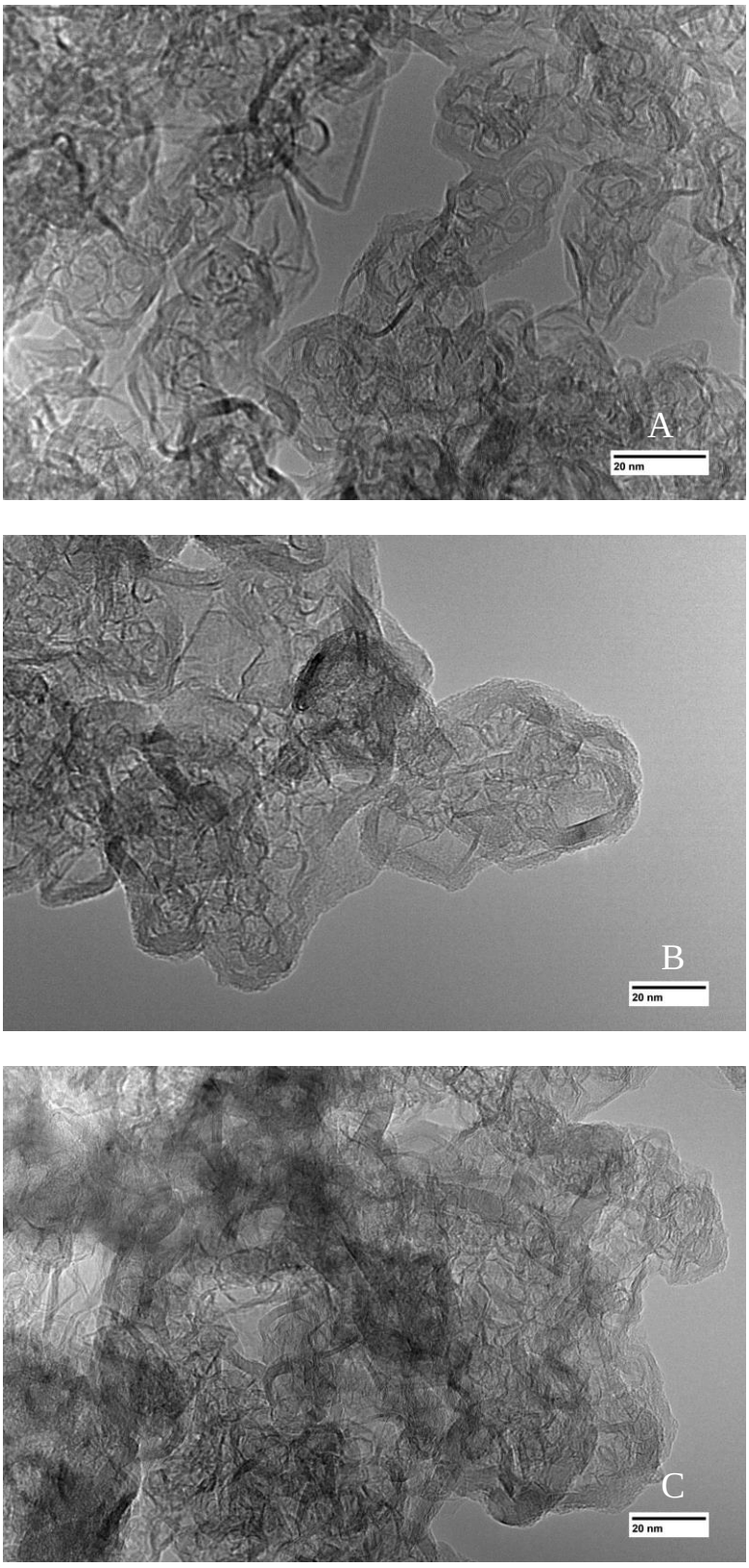

Figure 3-6 TEM images of a) graphene (O/C ratio = 0.3), b) small-scale GO, and c) large-scale GO.

4. Conclusion

We have demonstrated that explosion-synthesized GNs can be successfully oxidized at a large-scale to produce G/GO particles which retain graphene's remarkable properties. Zeta potential, CHO elemental analysis, and FTIR proved that we had successfully oxidized GNs at a large-scale. Similarly, TGA results indicated our G/GO has excellent thermal stability, while Raman and XRD results showed that oxidation occurs only on the outside layers of GNs which means that intercalation of oxygen functional groups does not take place. Most importantly, our research study demonstrated a novel and unique approach for large scale production of G/GO particles with unique remarkably properties suitable for a large number of applications in a variety of areas.

5. References

[1]Geim, A. K.; Novoselov, K. S. The Rise of Graphene. *Nat. Mater.* **2007**, *6* (3), 183–191.

[2]Michael, Berger. (2019). What is graphene? https://www.nanowerk.com/what_is_graphene.php

[3]Graphene Synthesis, Properties, And Applications https://www.cheaptubes.com/graphene-synthesis-properties-and-applications/

[4]Liu, J.; Cui, L.; Losic, D. Graphene and Graphene Oxide as New Nanocarriers for Drug Delivery Applications. *Acta Biomater.* **2013**, *9* (12), 9243–9257.

[5]Roberts, A.; Tripathi, P. P.; Gandhi, S. Graphene Nanosheets as an Electric Mediator for Ultrafast Sensing of Urokinase Plasminogen Activator Receptor-A Biomarker of Cancer. *Biosensors and Bioelectronics* **2019**, 141, 111398.

[6]Foroushani, M. S. *et. al*. Folate-Graphene Chelate Manganese Nanoparticles as a Theranostic System for Colon Cancer MR Imaging and Drug Delivery: In-Vivo Examinations. *Journal of Drug Delivery Science and Technology* **2019**, *54*, 101223.

[7]Li, D.; Müller, M. B.; Gilje, S.; Kaner, R. B.; Wallace, G. G. Processable Aqueous Dispersions of Graphene Nanosheets. *Nat. Nanotechnol.* **2008**, *3* (2), 101–105.

[8]Brodie, B. C. XIII. On the Atomic Weight of Graphite. Philos. Trans. R. Soc. Lond. **1859**, 149 (0), 249–259.

[9]Staudenmaier, L. Verfahren zur Darstellung der Graphitsäure. *Ber. Dtsch. Chem. Ges.* **1898**, *31* (2), 1481–1487.

[10]Hummers, W. S., Jr; Offeman, R. E. Preparation of Graphitic Oxide. J. Am. Chem. Soc. **1958**, 80 (6), 1339–1339.

[11]Luo, D.; Zhang, F.; Ren, Z.; Ren, W.; Yu, L.; Jiang, L.; Ren, B.; Wang, L.; Wang, Z.; Yu, Y.; Zhang, Q.; Ren, Z. An Improved Method to Synthesize Nanoscale Graphene Oxide Using Much Less Acid. *Mater. Today Phys.* **2019**, *9* (100097), 100097.

[12]Yu, H.; Zhang, B.; Bulin, C.; Li, R.; Xing, R. High-Efficient Synthesis of Graphene Oxide Based on Improved Hummers Method. *Sci. Rep.* **2016**, *6* (1), 1–7.

[13]Chen, J.; Yao, B.; Li, C.; Shi, G. An Improved Hummers Method for Eco-Friendly Synthesis of Graphene Oxide. *Carbon N. Y.* **2013**, *64*, 225–229.

[14]Ranjan, P.; Agrawal, S.; Sinha, A.; Rao, T. R.; Balakrishnan, J.; Thakur, A. D. Author Correction: A Low-Cost Non-Explosive Synthesis of Graphene Oxide for Scalable Applications. *Sci. Rep.* **2018**, *8* (1), 14593.

[15] Benzait, Z.; Chen, P.; Trabzon, L. Enhanced Synthesis Method of Graphene Oxide. *Nanoscale adv.* **2021**.

[16]Costa, M. C. F.; Marangoni, V. S.; Ng, P. R.; Nguyen, H. T. L.; Carvalho, A.; Castro Neto, A. H. Accelerated Synthesis of Graphene Oxide from Graphene. *Nanomaterials (Basel)* **2021**, *11* (2), 551.

[17]Nepal, A.; Singh, G. P.; Flanders, B. N.; Sorensen, C. M. One-Step Synthesis of Graphene via Catalyst-Free Gas-Phase Hydrocarbon Detonation. *Nanotechnology* **2013**, *24* (24), 245602.

[18]Konkena, B.; Vasudevan, S. Understanding Aqueous Dispersibility of Graphene Oxide and Reduced Graphene Oxide through PKa Measurements. *J. Phys. Chem. Lett.* **2012**, *3* (7), 867–872.

[19]Kashyap, S.; Mishra, S.; Behera, S. K. Aqueous Colloidal Stability of Graphene Oxide and Chemically Converted Graphene. *J. Nanoparticles* **2014**, *2014*, 1–6.

[20]Krishnamoorthy, K.; Veerapandian, M.; Yun, K.; Kim, S.-J. The Chemical and Structural Analysis of Graphene Oxide with Different Degrees of Oxidation. *Carbon N. Y.* **2013**, *53*, 38–49

[21]Liu, F.; Wang, M.; Chen, Y.; Gao, J. Thermal Stability of Graphene in Inert Atmosphere at High Temperature. *J. Solid State Chem.* **2019**, *276*, 100–103.

[22]Najafi, F.; Rajabi, M. Thermal Gravity Analysis for the Study of Stability of Graphene Oxide–Glycine Nanocomposites. *Int. Nano Lett.* **2015**, *5* (4), 187–190.

[23]Chen, J.; Li, Y.; Huang, L.; Li, C.; Shi, G. High-Yield Preparation of Graphene Oxide from Small Graphite Flakes via an Improved Hummers Method with a Simple Purification Process. *Carbon N. Y.* **2015**, *81*, 826–834.

[24]Lavin-Lopez, M. del P.; Romero, A.; Garrido, J.; Sanchez-Silva, L.; Valverde, J. L. Influence of Different Improved Hummers Method Modifications on the Characteristics of Graphite Oxide in Order to Make a More Easily Scalable Method. *Ind. Eng. Chem. Res.* **2016**, *55* (50), 12836–12847.

[25]Shen, J.; Hu, Y.; Shi, M.; Lu, X.; Qin, C.; Li, C.; Ye, M. Fast and Facile Preparation of Graphene Oxide and Reduced Graphene Oxide Nanoplatelets. *Chem. Mater.* **2009**, *21* (15), 3514–3520.

[26]Farivar, F.; Lay Yap, P.; Karunagaran, R. U.; Losic, D. Thermogravimetric Analysis (TGA) of Graphene Materials: Effect of Particle Size of Graphene, Graphene Oxide and Graphite on Thermal Parameters. *C* **2021**, *7* (2), 41.

[27]Lee, X. J.; Hiew, B. Y. Z.; Lai, K. C.; Lee, L. Y.; Gan, S.; Thangalazhy-Gopakumar, S.; Rigby, S. Review on Graphene and Its Derivatives: Synthesis Methods and Potential Industrial Implementation. *J. Taiwan Inst. Chem. Eng.* **2018**, *98*, 163–180.

[28]Ikram, R.; Jan, B. M.; Ahmad, W. An Overview of Industrial Scalable Production of Graphene Oxide and Analytical Approaches for Synthesis and Characterization. *J. Mater. Res. Technol.* **2020**, *9* (5), 11587–11610.

[29]Nepal, A.; Chiu, G.; Xie, J.; Singh, G. P.; Ploscariu, N.; Klankowski, S.; Sung, T.; Li, J.; Flanders, B. N.; Hohn, K. L.; Sorensen, C. M. Highly Oxidized Graphene Nanosheets via the Oxidization of Detonation Carbon. *Appl. Phys. A Mater. Sci. Process.* **2015**, *120* (2), 543–549.

[30]Yap, P. L.; Kabiri, S.; Auyoong, Y. L.; Tran, D. N. H.; Losic, D. Tuning the Multifunctional Surface Chemistry of Reduced Graphene Oxide via Combined Elemental Doping and Chemical Modifications. *ACS Omega* **2019**, *4* (22), 19787–19798.

[31]Dave, K.; Park, K. H.; Dhayal, M. Two-Step Process for Programmable Removal of Oxygen Functionalities of Graphene Oxide: Functional, Structural and Electrical Characteristics. *RSC Adv.* **2015**, *5* (116), 95657–95665.

[32]Nishina, Y.; Eigler, S. Chemical and Electrochemical Synthesis of Graphene Oxide - a Generalized View. *Nanoscale* **2020**, *12* (24), 12731–12740.

[33]Wall, M. The Raman Spectroscopy of Graphene and the Determination of Layer Thickness https://tools.thermofisher.com/content/sfs/brochures/AN52252_E%201111%20LayerThkns_H_1.pdf.

Chapter 4 - Development of detonation-graphene based nano-biosensor for lung cancer detection

Abstract

Lung cancer causes a higher number of deaths than any other type of cancer in the United States, making up almost 25% of all cancer deaths. For this reason, there has been a great effort in trying to find ways to detect it sooner because the survival rate increases when it is detected at an early stage. Therefore, the goal of this research is to develop a graphene-based nanobiosensor for clinical diagnostics, which can measure cancer-related biomarkers, such as proteases in biospecimens. The nanobiosensor consists of a graphene-based nanoplatform coated with polyethylenimine (PEI) and labeled with fluorescent dyes and porphyrins via consensus peptide sequences. Advantageously, the graphene-based nanoplatform acts as a quencher for the detectable fluorophore, thus there is no need for a co-attached quencher. Once the protease cleaves the consensus sequence, the attached fluorophore is released, escaping the quenching by graphene which results in a measurable increase in fluorescence. Based on the results from GNB-MMP1 prototype, the nanosensor was able to detect biomarkers down to the sub-femtomolar level after 1 hour of incubation utilizing a conventional plate reader.

1. Introduction

Lung cancer is the second most common cancer in both men and women, not including skin cancer. However, lung cancer is the one that causes the highest number of deaths among all types of cancers in the United States, making up almost 25% of all cancer deaths.[1] The American Cancer Society estimated that for 2021 there will be approximately 235,760 new cases of lung cancer and about 131,880 deaths in the United States alone.[2] Overall, there is a chance in men that about 1 in 15 will develop lung cancer in his lifetime, whereas the risk for woman is about 1 in 17. Generally, lung cancers are categorized into two main groups called small cell lung cancer (SCLC) and non-small cell lung cancer (NSCLC), which are treated very differently. The three main subtypes of NSCLC are adenocarcinoma (cells that secrete substances such as mucus), squamous cell carcinoma (flat cells that line the inside of the airways in the lungs), and large cell carcinoma which can appear in any part of the lung; however, the treatment and prognoses are frequently similar for these subtypes which is why they are grouped together as NSCLC.[2] Approximately 80 – 85% of lung cancers correspond to NSCLC, while the other 10 – 15% is attributed to SCLC which tends to grow and spread faster than NSCLC.[2] Furthermore, the 5-year relative survival rate for NSCLC is 63% in localized stage (cancer has not spread), 35% in regional stage (cancer has spread to nearby tissues), and 7% in distant stage (cancer has spread to distant body parts). But for SCLC, the 5-year relative survival rate is 27% in localized, 16% regional, and 3% in distant stage.[2] Unfortunately, the lung cancers that are diagnosed at a localized stage only represents 17% of all lung cancers.[3] For this reason, there is an urgent need for the development of an early detection technique for lung cancers to improve survival outcomes.

1.1. Cancer Biomarkers

To date, there is no precise way to prevent lung cancer; however, there are known factors that can be controlled to help reduce the risk, such as quitting smoking. For this reason, researchers have devoted their efforts towards developing new ways that can help find lung cancers at an earlier stage by evaluating the critical role biomarkers play at different stages of the disease. A biomarker is a biological molecule that can be found in body fluids or tissues and can help identify a condition or disease. There is a large number of biomarkers which include enzymes, nucleic acids, antibodies, and peptides.[4] Proteases are enzymes that degrade proteins, regulate signaling and are known to play a critical role in cancer progression and spread.[4-5] There are over 500 human proteases which regulate numerous processes, and it is well known that these processes are dysregulated and functionally distinct in tumors. In particular, proteases, such as matrix metalloproteinase (MMP), cathepsin (CTS), and urokinase plasminogen activator (uPA), are either over- or under expressed in cancers, and this unusual protease function contributes to numerous hallmarks of cancer in a complex manner.[5,8] These proteases contribute to cancer progression by regulating the following pathways: 1) cell growth: they disrupt balance between growth and antigrowth signals in tumor environment, and 2) angiogenesis: they initiate angiogenesis by generating proangiogenic fragments and enabling the breakdown of the extracellular matrix (ECM) thus promoting spread of cancer to distant organs.[6-8] Therefore, as proteases play a critical role in cancer progression, the measurements of their activity can serve as suitable biomarkers for cancer detection.

1.2. Nanobiosensors for protease detection

As the understanding of the critical role of proteases in cancer expanded, new approaches have been explored to identify proteases as candidate biomarkers or therapeutic targets. More

specifically, a wide variety of nanoparticles ranging from inorganic nanoparticles to silica and polymeric based particles have been used to create biosensing devices. Typically, nanoparticle – enzyme sensors consist of conjugating the nanoparticles to biological specific substrates labeled with fluorogenic molecules in which the active enzyme induces a change which results in a detectable fluorescence signal.[8] Several nanosensors have been developed using proteases as markers for the detection of colorectal, breast, prostate, pancreatic and lung cancers via noninvasive protocols.[7-11]

Since 2007, the Bossmann group has been extensively working in the development of ultra-sensitive protease detection technologies that are capable of detecting protease activities over a wide range down to sub-femtomolar limits of detection (LODs).[12-17] These nanoplatforms consist of dopamine-covered iron/iron oxide core/shell nanoparticles conjugated with tetrakis (4-carboxyphenyl) porphyrin (TCPP) via a protease-cleavable consensus peptide sequence and a second dye cyanine 5.5 which is permanently linked to the dopamine layer and acts as a quencher for TCPP. Upon cleavage of the consensus sequence in the presence of the correct protease, TCPP is released, and the fluorescence signal is increased thus creating a "light switch effect" which enables highly sensitive detection of protease activity which is quantified utilizing a plate reader. Despite the great successful results obtained, there are still some limitations with the iron/iron oxide nanobiosensor technology. These limitations include that the iron/iron oxide nanoparticles are expensive and not long-term stable; additionally, there is a requirement of using two fluorescent dyes, one for Förster Resonance Energy Transfer (FRET) quenching and one for sensing. For this same reason, we have developed a highly water/buffer – dispersible graphene – based nanobiosensor (shown in Figure 4-1) that is long – term stable thus overcoming the drawbacks presented in the iron/iron oxide nano-biosensor. Furthermore, we

have overcome the issue of having to use two dyes by using a graphene – based nanoplatform and taking advantage of graphene's optical absorption property which allows graphene to behave as a very efficient quencher for fluorescent molecules, as it has been reported in previous studies.[18] This project is still in progress and in collaboration with Hawkeye Bio, a new medical technology company focused on cancer detection.

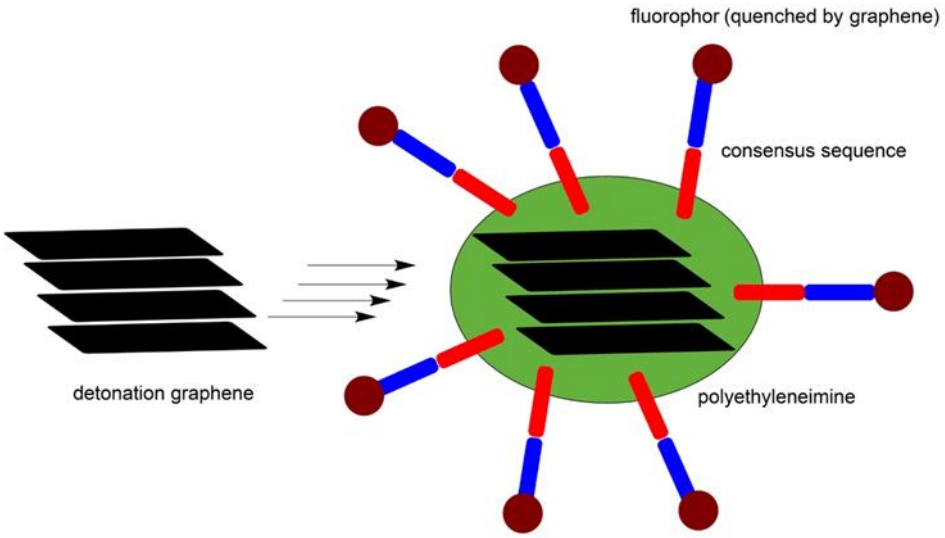

Figure 4-1 Graphene-based nanobiosensor for protease detection.

2. Methodology

2.1. Synthesis of Carboxygraphene (CG)

Approximately 2.0 g of detonation-synthesized graphene nanosheets 0.3 (O/C ratio) were suspended in 40 mL DMF at room temperature in a 250mL three-necked round bottom flask equipped with a magnetic stir bar. Next, temperature was increased to 40 °C and 1.0 g of 5-bromovaleric acid (0.0055 mol) were added to the graphene suspension, followed by the addition of 0.36 g sodium azide crystals (NaN_3) (0.0055 mol). After NaN_3 was dissolved, the suspension was slowly heated up to 80 °C (about 1^oC/min.) and stirred for 1 hour. After 1 hour, the suspension was cooled down to room temperature, and the carboxygraphene was collected via

centrifugation (5 min @ 7,000 rpm) and washed five times with DMF and then three times with anhydrous diethyl ether. Finally, resulting CG was dried for characterization and then stored under argon. The synthesis of "carboxygraphene" is shown in Figure 4-2.

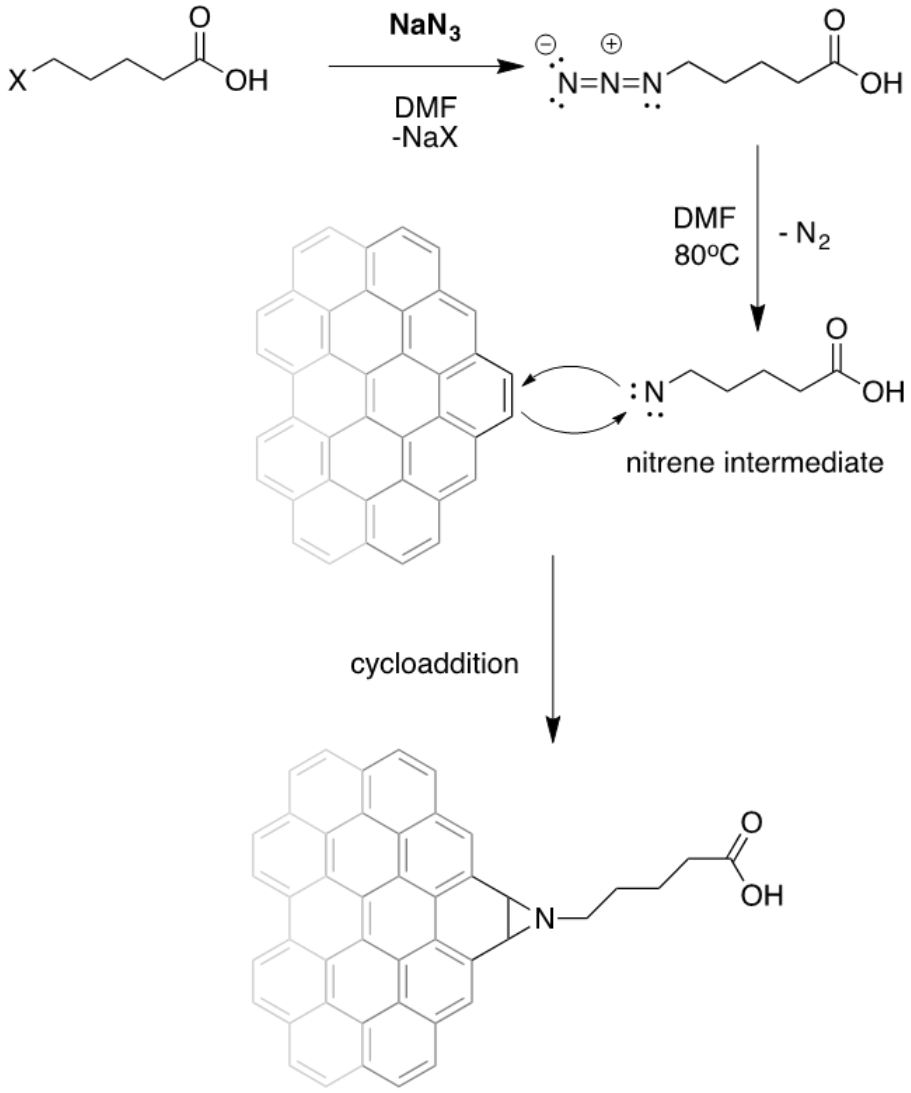

Figure 4-2 Scheme of the synthesis of carboxygraphene from detonation graphene in one-pot reaction.

2.1.1. Mechanism for synthesis of Carboxygraphene:

Between 40 °C and 50 °C, a nucleophilic substitution reaction (S_N) occurs, in which an organic azide and DMF-soluble sodium halide are formed. Next, the organic azide releases dinitrogen (N_2) and forms a nitrene intermediate at temperatures above 50 °C. Nitrenes have 6

instead of 8 electrons in the outer shell of nitrogen. This reactive intermediate undergoes a cycloaddition with a pi-pi double bond at the surface of graphene to form a stable azirane anchor (three-membered C-N-C ring). The azirane cycloaddition offers the opportunity to add a tailored amount of carboxylic acids to the surface of graphene without compromising the optical and electrical properties of graphene.

2.2. Titration of Carboxygraphene (CG)

Approximately 100 mg of carboxygraphene (CG) were suspended in 20 mL of 0.100 M NaOH. After stirring the suspension for 5 minutes at room temperature, 0.100 M HCl solution was added in incremental steps. At each step, the pH of the solution was recorded using a pH meter after making sure equilibrium had been reached (1-5 min.), before addition of next amount of HCl. The same procedure was used with the same volume of NaOH but without the addition of Carboxygraphene. The titration was performed to determine the number of -COOH groups present in carboxygraphene.

2.3. Synthesis of Carboxygraphene – polyethylenimine (G-PEI)

1.0 g of synthesized carboxygraphene was suspended in 30 mL anhydrous DMF in a 100 mL round bottom flask equipped with a magnetic stir bar at room temperature. Next, 500 mg of polyethylenimine, branched, molecular weight 10,000 (PEI), 250 mg of 1-Ethyl-3-(3-dimethylaminopropyl) carbodiimide (EDC), and 250 mg of 4-Dimethylaminopyridine **(**DMAP) were added to the graphene solution. The reaction was stirred at room temperature overnight. Afterwards, synthesized carboxygraphene-polyethylenimine (G-PEI) was collected via centrifugation (5 min @ 7000 rpm) and washed twice with DMF and three times with diethyl ether. Collection of the material was achieved by means of centrifugation in each step. Finally,

resulting G-PEI is dried for characterization and further use under argon. The structure of carboxygraphene – polyethylenimine for a single sheet is shown in Figure 4-3.

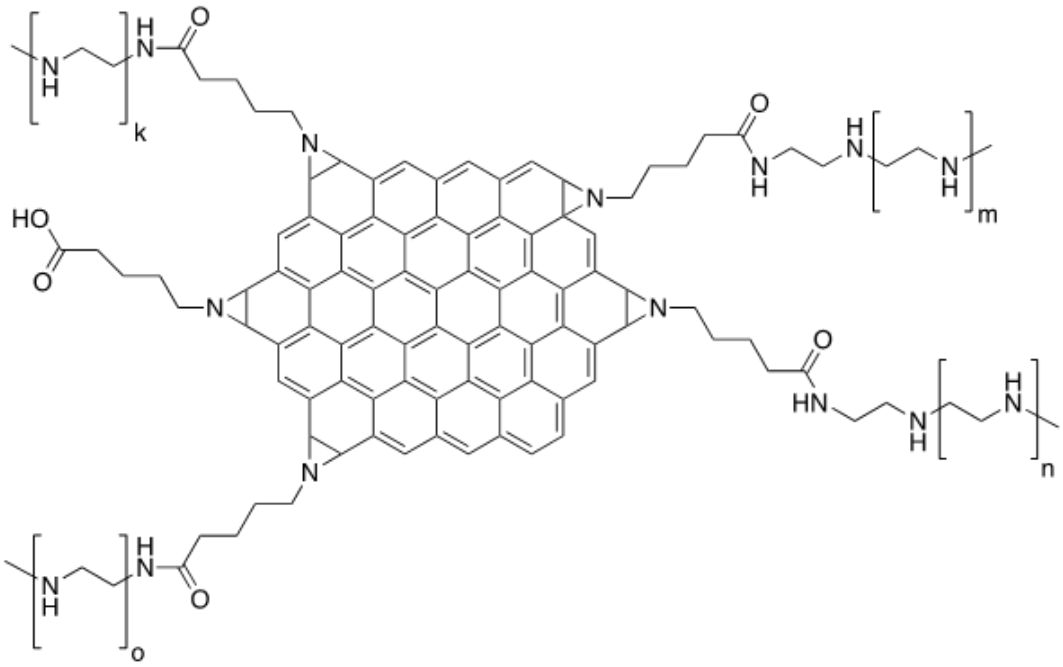

Figure 4-3 Structure of carboxygraphene-polyethylenimine (only a single sheet is shown for reference).

2.4. Solid Phase Peptide Synthesis and TCPP Labeling

All consensus peptide sequences implemented for this project were synthesized via standard solid phase peptide synthesis (SPPS) (scheme shown in Figure 4-4).[19] Briefly, a resin containing the first Fmoc-protected amino acid of the peptide is deprotected and activated in order to couple the next protected amino acid. This cycle of deprotection-activation-coupling is repeated until all amino acids on the peptide sequence are added. By taking advantage of this approach, TCPP is conjugated to the N-terminal of the last amino acid of the peptide sequences.[12] Finally, the TCPP-labeled peptide sequence is cleaved off from the resin and dried under argon for characterization.

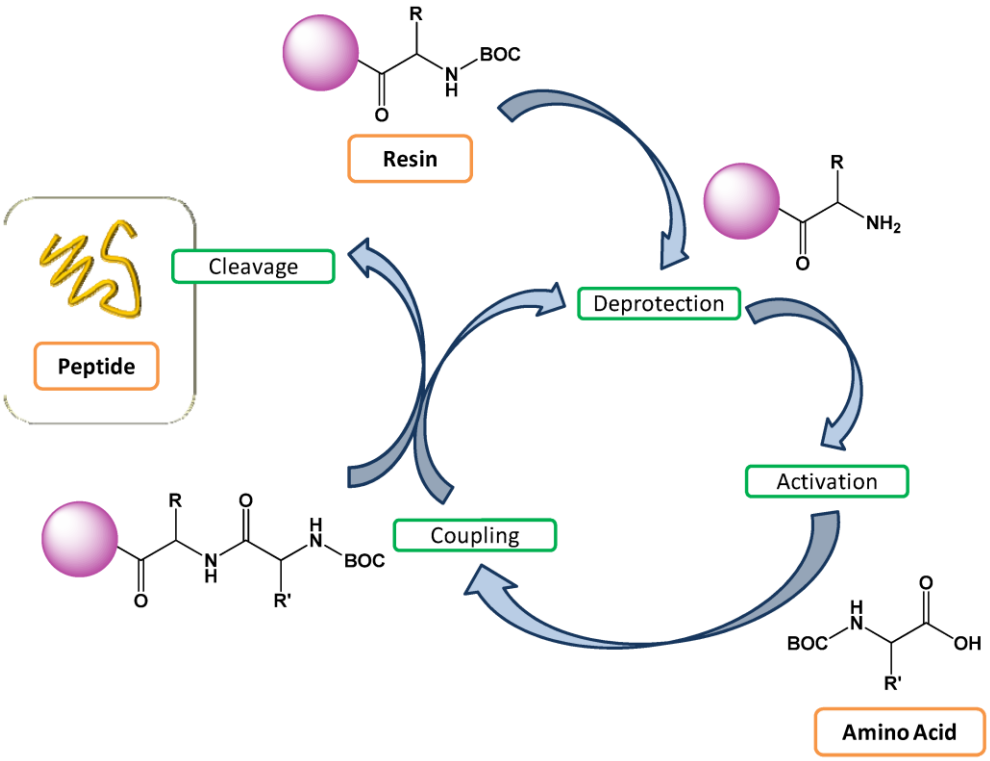

Figure 4-4 Schematic representation of Merrifield solid-phase peptide synthesis (SPPS).[19]

2.5. Synthesis of Detonation – Based Nanobiosensors

50 mg of carboxygraphene-PEI was suspended in ~8.1 mL DMF in a small glass vial, and solution was then sonicated for one min. Next, ~5 mg DMAP and ~5 mg EDC were added to the vial followed by ~3.5 mg of TCPP pre-conjugated with a peptide cleavage sequence for MMP-1 (GAG**VPMS – MRGG**AG). The sample solution was sonicated for about five minutes to ensure full suspension of all components in DMF. The reaction was then stirred overnight at room temperature. The next day, the nanobiosensor was collected via centrifugation (10 min @ 7000 rpm) and washed three times with DMF and three times with diethyl ether. After the last washing with diethyl ether, nanobiosensor was dried with argon. The structure of carboxygraphene – polyethylenimine-based nanobiosensor, or graphene-based nanobiosensor (GNBs) is shown in Figure 4-5.

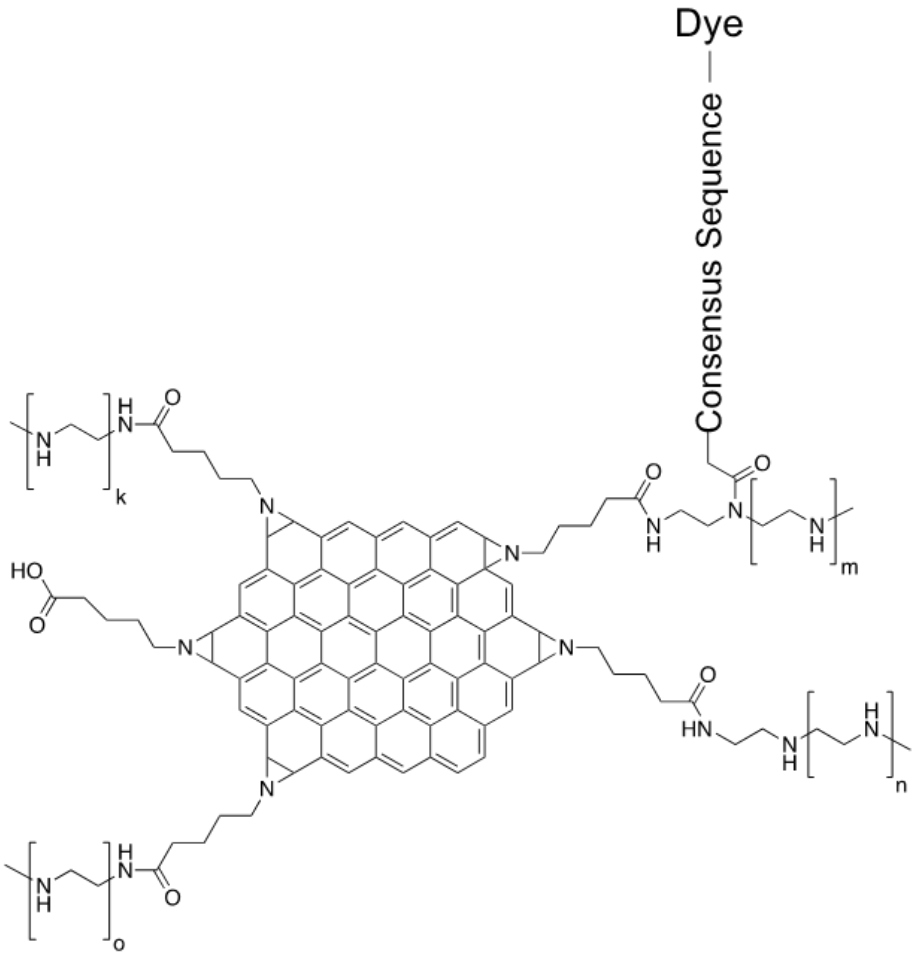

Figure 4-5 Structure of carboxygraphene-polyethylenimine-based nanobiosensor (only a single sheet is shown for reference).

3. Results and Discussion

3.1. Characterization of Graphene-based Nanobiosensors (GNBs)

3.1.1. Elemental (CHNO) and Thermogravimetric Analyses of Carboxygraphene and Carboxygraphene-PEI

Table 4-1 summarizes the CHNO elemental analysis for the starting material graphene, carboxygraphene, and carboxygraphene-PEI. Results demonstrated that the incorporation of N in carboxygraphene is an indication of the formation of the azirane anchor (three member C-N-C ring) thus suggesting that the cycloaddition reaction to conjugate carboxylic acids to the surface

of graphene was successful. Similarly, the significant increase in N content for carboxygraphene – PEI indicates that addition reaction for tethering polyethylenimine to carboxygraphene was successful. Furthermore, based on the N-content for carboxygraphene – PEI we estimated the amount of PEI to be 27 ± 2%.

Table 4-1 CHON elemental analysis of graphene, carboxygraphene, and carboxygraphene-PEI.

Elementary Analysis (CHNO)				
Graphene (0.3)	99.80% C	0.15% H	0.05% O	
Carboxygraphene	94.22% C	1.79% H	2.82% O	1.17% N
Carboxygraphene-PEI	82.58% C	4.65% H	2.12% O	10.65% N

The thermal decomposition of carboxygraphene and carboxygraphene – PEI was studied by thermogravimetric analysis (TGA). For this experiment, the samples were heated up to 600 °C at a heating rate of 10 °C/minute under nitrogen atmosphere. As illustrated by Figure 4-6, there is an initial mass loss of 28 ± 2% by weight in carboxygraphene before reaching 100 °C. At temperatures beyond 100 °C, the material was very stable, as stated in chapters 2 and 3 this behavior can be expected from graphene. On the other side, carboxygraphene – PEI showed an initial mass loss of 9 ± 1% by weight below 100 °C, and a mass loss of 11.5 ± 1% by weight when heated beyond 150 °C and extending through the entire temperature range. The initial weight loss observed in both samples arise from the partial loss of attached valeric acid units in the outer shell of carboxygraphene as well as the removal of adsorbed water; however, the weight loss from carboxygraphene – PEI when heated from 150 to 600 °C arises from the decomposition of PEI.[20,21]

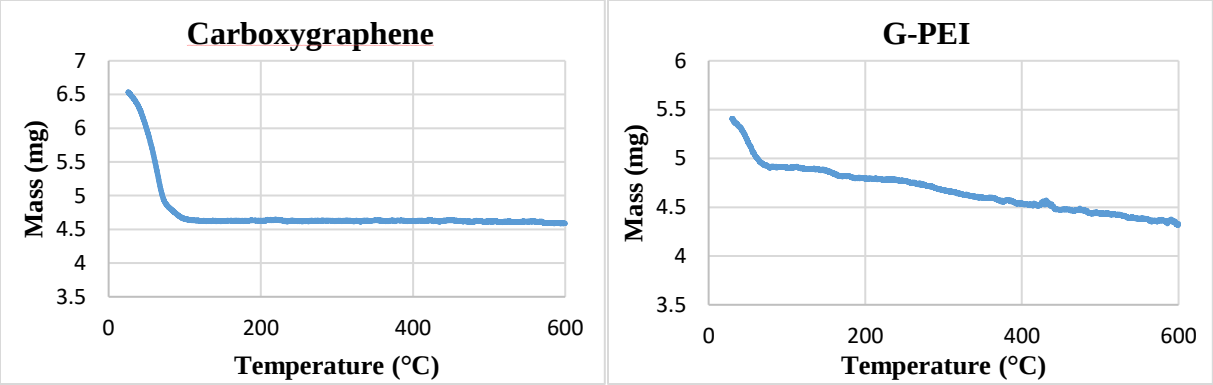

Figure 4-6 TGA Analysis of Carboxygraphene and Carboxygraphene - PEI.

3.1.2. Titration Curve and FTIR Characterization of Carboxygraphene

Direct titration was performed in carboxygraphene in order to quantify the acidic functional group content. The difference in the volumes of HCl in the two titration curves for the same value of pH of ~7.00 gives the concentration of the ionized groups (carboxyl groups) per weight increment of carboxygraphene, as illustrated in Figure 4-7. Based on the titration curve, the results indicated that we have a $6.1*10^{-4}$ mol/g of acidic groups (-COOH) (i.e., surface density of 4 -COOH groups per nm^2). For comparison, this is 4 times higher compared to our Fenton-oxidized graphene oxide (described in chapters 2 and 3) which possesses 1.7*10-4 mol/g (i.e., surface density of 1 -COOH group per nm^2). This density of -COOH groups at the surface of carboxygraphene corresponds to an average space per -COOH group of 0.27 nm^2 in the synthesized carboxygraphene. This corresponds to a very high labeling density with surface -COOH groups, contributing to a much higher water dispersibility for these carboxygraphene nanosheet particulates. It will be appreciated that the synthesis of carboxygraphene is even further simplified as compared to Fenton-oxidized graphene oxide, with faster reaction times. The process also does not involve addition of an iron salt, which would somewhat interfere with the photophysical properties of the attached fluorophore(s) in biosensors described herein.

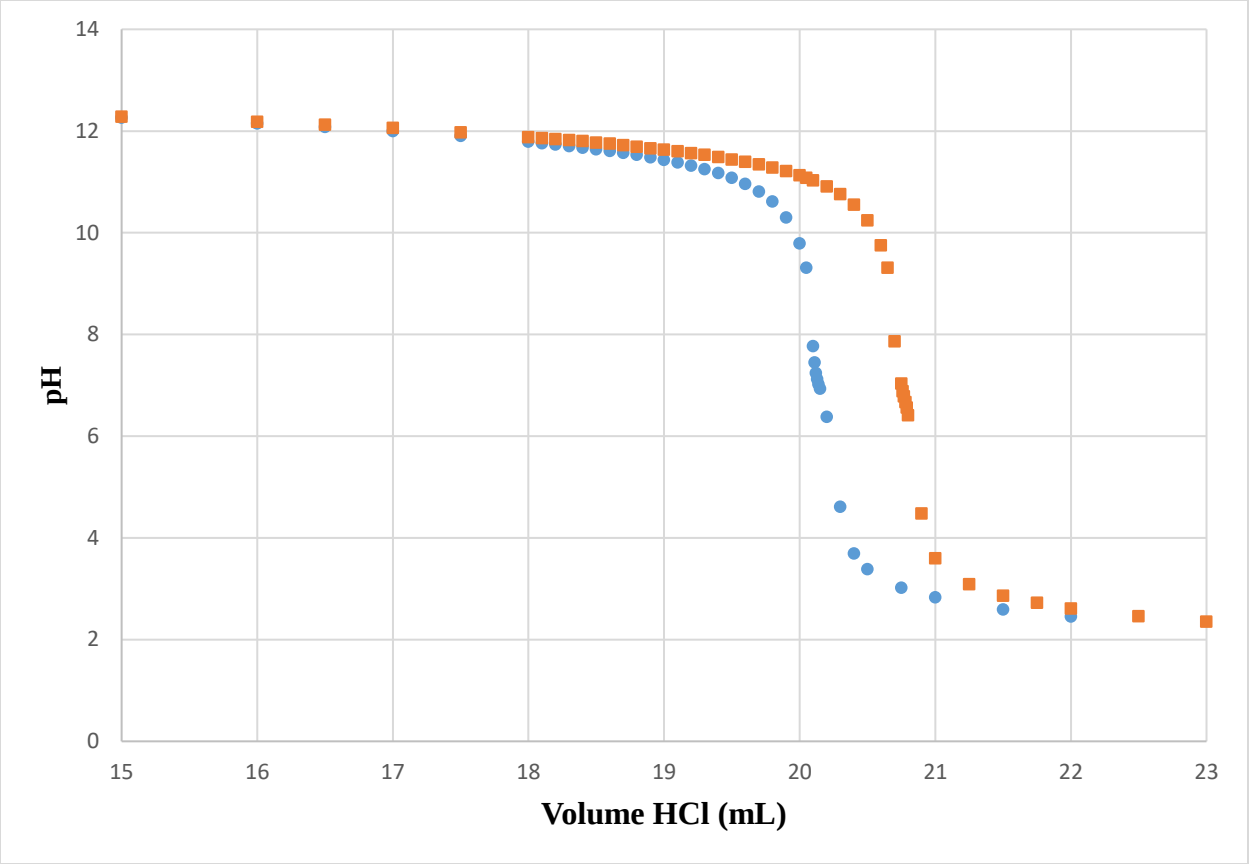

Figure 4-7 Titration curves (pH vs volume 0.10 M HCl) for carboxygraphene. (Blue circles: carboxygraphene; Orange squares: reference curve)

FTIR analysis was performed to identify the presence of functional groups with permanent dipole moments at the surface of carboxygraphene. As shown in Figure 4-8, the results demonstrated the clear signal for the presence of -COOH groups (3400 – 3000 cm^{-1}). Similarly, the absorption band at 2875 cm^{-1} was attributed to the C-H stretching vibrations, the band at 1630 cm^{-1} was due to the stretching vibration of C=O bonds, and the bands at ~1250 and ~1070 cm^{-1} were due to the stretching vibrations of C-O bonds. The FTIR results confirmed that the surface of graphene had been successfully decorated with carboxylic acids thus forming carboxygraphene.

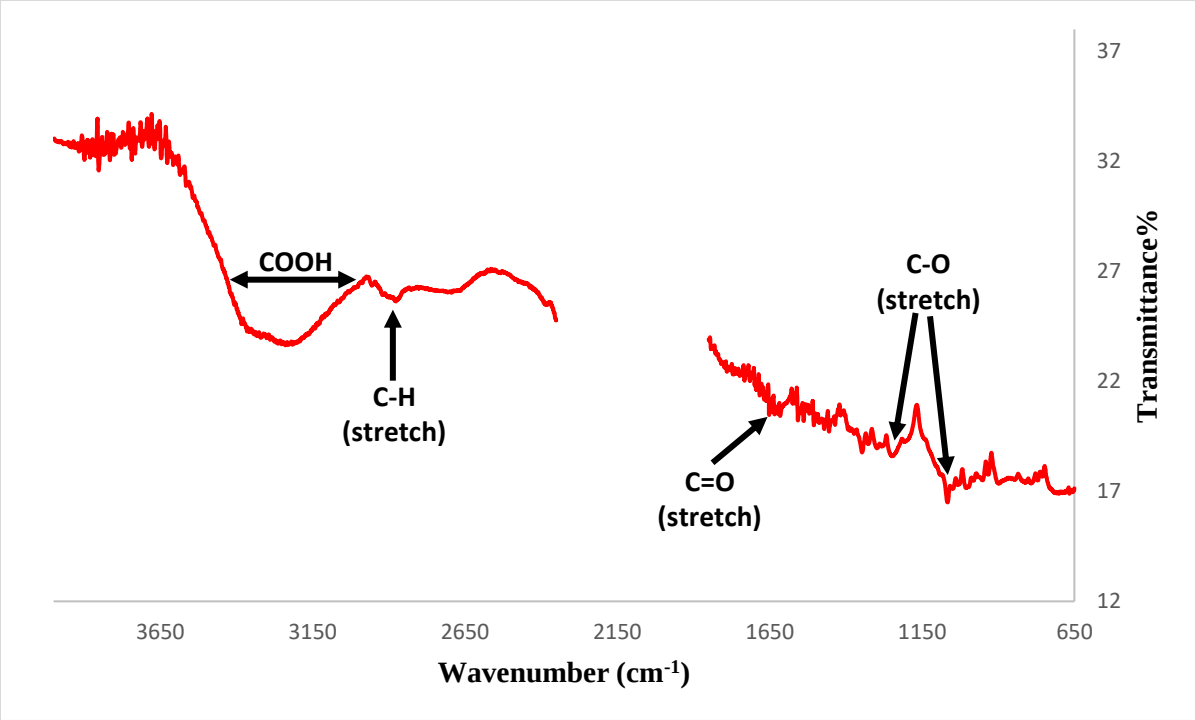

Figure 4-8 FTIR spectra of carboxygraphene.

3.1.3. Water Dispersibility of Graphene, CG, G-PEI and GO

The water dispersibility for all samples (graphene, CG, G-PEI, and GO) was performed by suspending 3.0 mg of sample in 3.0 mL of water. After adding the 3.0 mL of water, the samples were then sonicated for 30 seconds, and images were captured 5 minutes as well as 48 hours after sonication. It can be seen in Figure 4-9 that all samples, except graphene, were well dispersed in water following the 30 seconds of sonication. Similar results were observed after the 5 minutes and the 48 hours of sonication in which all samples were still suspended in water, but graphene had precipitated out, clustering at the top and bottom of the vial. Interestingly, the G-PEI sample showed the least amount of material agglomerated on the walls, even less than GO, thus suggesting that PEI modification not only acts as a linker for loading peptides but also enhances water dispersibility of the graphene nanosensor. The results showed that after each

modification, starting from graphene → CG → G-PEI, water dispersibility was enhanced, thus suggesting that the conjugation of PEI to CG was successful.

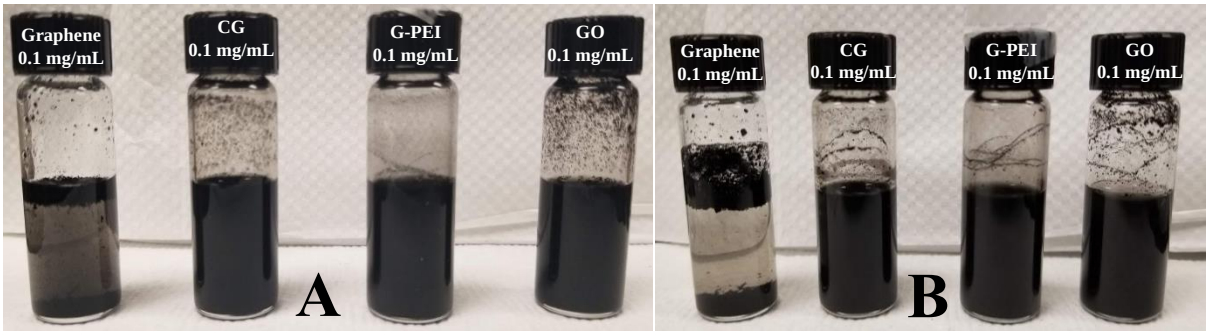

Figure 4-9 Water dispersibility of graphene, CG, G-PEI, and GO. (A: 5 minutes after sonication; B: 48 hours after 30 seconds sonication)

3.1.4. Dynamic Light Scattering, Zeta-Potential, UV-Vis Spectroscopy, and TEM Images of CG, G-PEI, and GNB-MMP1

The hydrodynamic size and zeta potential of the CG, G-PEI, and GNB-MMP1 were measured in water using a ZetaPALS instrument. The results are reported on Table 4-2, it is worth mentioning, that in all samples possible agglomeration occurs based on the results. For all samples, there are two sizes reported, one from individual population and other from the average size (taking in account possible clusters formed). Based on the results, carboxygraphene has an individual hydrodynamic diameter of 147.98 nm, after coating CG with PEI to form G-PEI the size increased to 241.53 nm, and after labeling G-PEI with MMP1-consensus peptide the size increased to 434.81 nm. The increase in sizes suggested that CG was successfully coated with PEI and subsequently labeled with MMP1-TCPP peptide. Similarly, the zeta potential of CG is +22.1 mV, and it increases to +31.9 mV after coating it with PEI, lastly after labeling with MMP1 the zeta potential is almost neutral +1.23 mV. Again, the increase in charge from CG to G-PEI suggested that PEI was successfully conjugated to CG. Similarly, the decrease in charge

from G-PEI after labeling with MMP1 suggested successful labeling because MMP1 is close to neutral charge.

Table 4-2 DLS and Zeta Potential of CG, G-PEI, and GNB-MMP1.

Sample	DLS (nm) Individual Population	DLS (nm) Average	Zeta Potential (mV)
Carboxygraphene	147.98	839.54	+ 22.1
Carboxygraphene-PEI	241.53	362.32	+ 31.9
GNB-MMP1	434.81	587.04	+ 1.23

The synthesized materials were analyzed via UV-Vis spectroscopy. As shown in Figure 4-10, the UV-Vis spectra of CG, G-PEI, and GNB-MMP1 in water were analyzed. The Soret band of the TCPP detectable label was clearly discernible at ~420 nm. Thus, results suggested that TCPP was successfully bound to the polyethylenimine layer via the peptide containing the consensus sequence for MMP-1. Based on an estimated absorption coefficient of 135,000 M^{-1} cm^{-1}, the TCPP concentration was 1.63 x 10^{-5} moles per gram of carboxygraphene. Furthermore, the results showed that carboxygraphene is capable of working in a broad optical region because the absorption spectrum changes only very little between UV and near-IR regions.

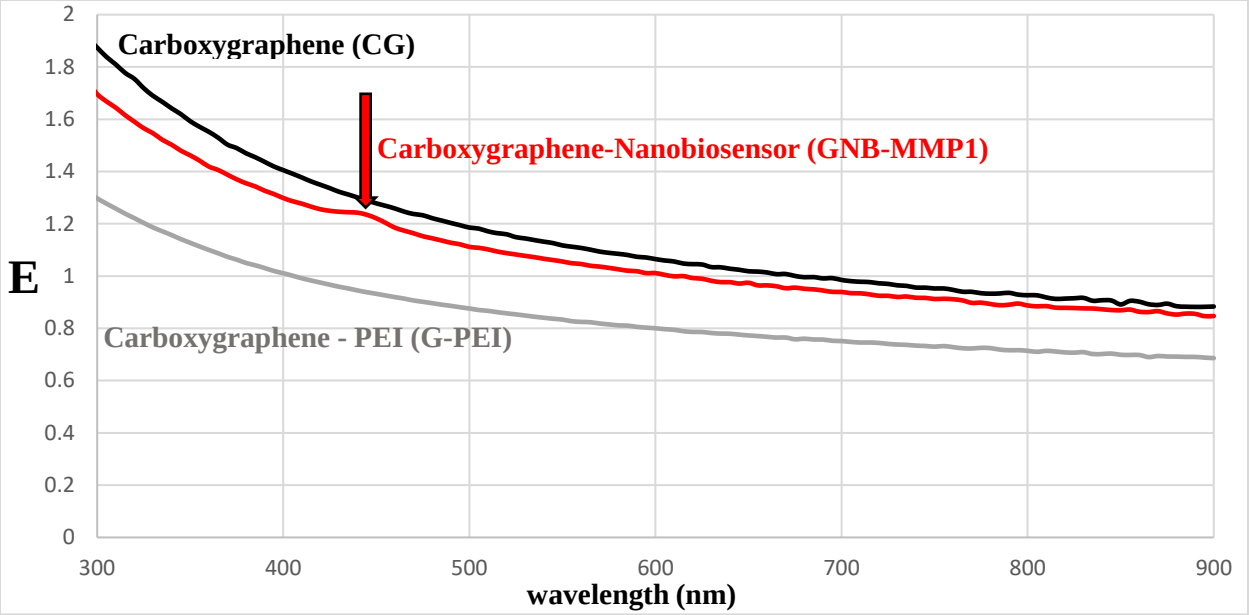

Figure 4-10 UV-Vis spectra of CG (Black), G-PEI (Grey), and the GNB-MMP1 (Red) in water.

The TEM images of graphene, CG, G-PEI, and GNB-MMP1 were collected at the MAI Research Resource Core Laboratory at the University of Kansas, by Dr. Prem Thapa, on a Hitachi H-8100 Transmission Electron Microscopy (200 kEV) to study the morphology of the samples. The samples were dispersed in MeOH and loaded on copper grids, followed by evaporation in high vacuum. The TEM images for all four samples are shown in Figure 4-11. The TEM results showed that the morphology of the samples remained unchanged after all the derivatizations. Similarly, the same results were observed when GNs were oxidized by means of Fenton Oxidation in which only the outside layers get oxidized. Therefore, both derivatization procedures (Fenton Oxidation and Carboxygraphene) showed that the graphenic inner core in both materials is preserved.

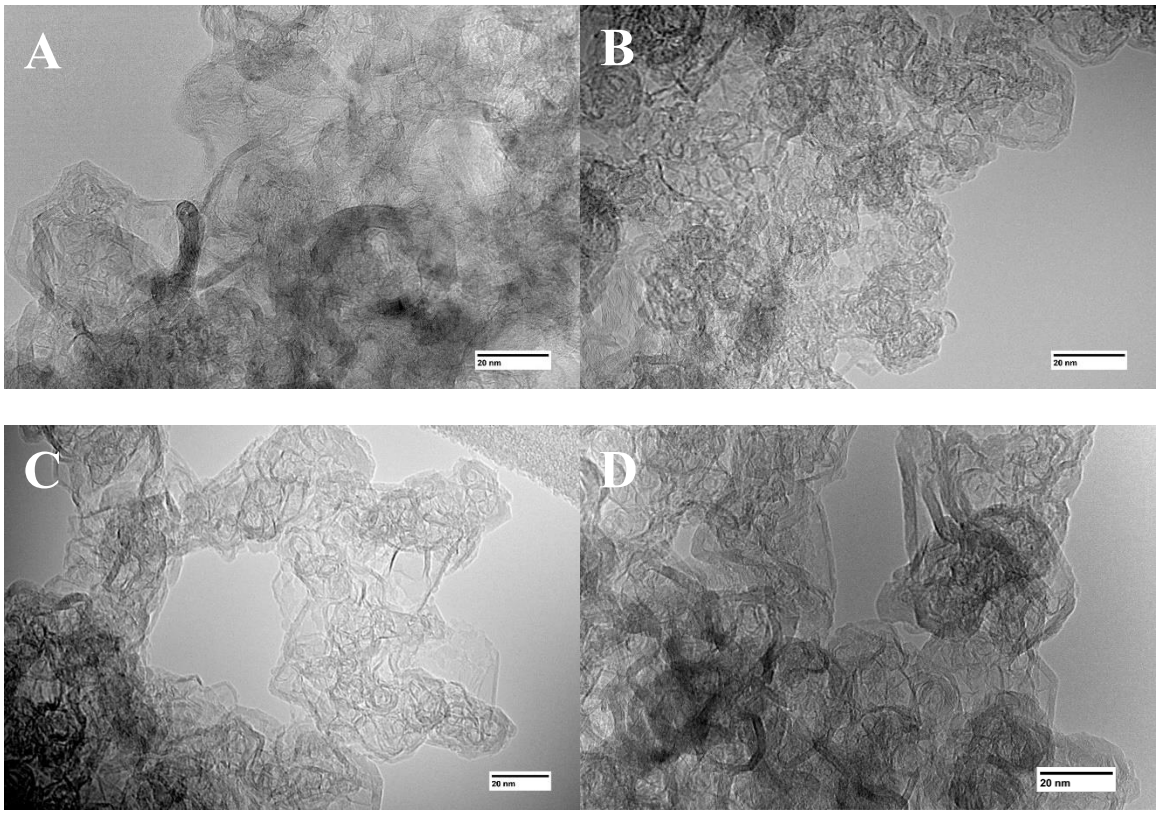

Figure 4-11 TEM of A)GNs, B) CG, C) G-PEI, and D) GNB-MMP1.

3.2. Optimization Parameters for GNB Labeled with MMP1

After all characterizations showing evidence that we had successfully labeled G-PEI with MMP1-TCPP consensus sequence, the next step was to optimize our prototype nanobiosensor in detecting protease activity. For these optimization experiments, the nanobiosensor was tested using a serum sample from a healthy patient that was provided from our collaborators from Hawkeye Bio. The first experiment was to optimize the amount of TCPP-peptide that needed to be loaded on the sensor to provide the highest fluorescence intensity. For this experiment, four different TCPP-peptide concentrations 7.5, 14.5, 18, and 24 mg were tested per 100 mg of nanobiosensor. The results showed that 7.5 mg TCPP-peptide gave the highest fluorescence

intensity signal, as shown in Figure 4-12. From these results, the concentration of 7.5 mg TCPP-peptide was chosen and used for subsequent experiments.

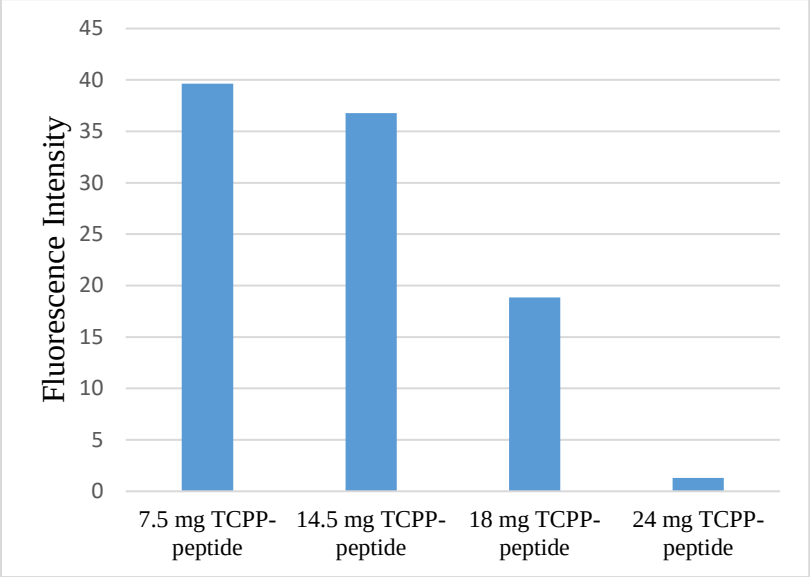

Figure 4-12 Optimization of TCPP-peptide per 100 mg of graphene-based nano-biosensor.

After optimizing the TCPP-peptide amount, the next experiment was the concentration optimization of the nanobiosensor to find the minimum concentration required to provide the highest fluorescence intensity. For this experiment, four different concentrations 0.3, 0.1, 0.01, and 0.005 mg/mL of GNB-MMP1 were tested using the same serum for all samples over a period of 60 minutes (incubation time). The results showed the optimal concentration of GNB-MMP1 was between 0.1 and 0.01 mg/mL of nanobiosensor, as shown in Figure 4-13.

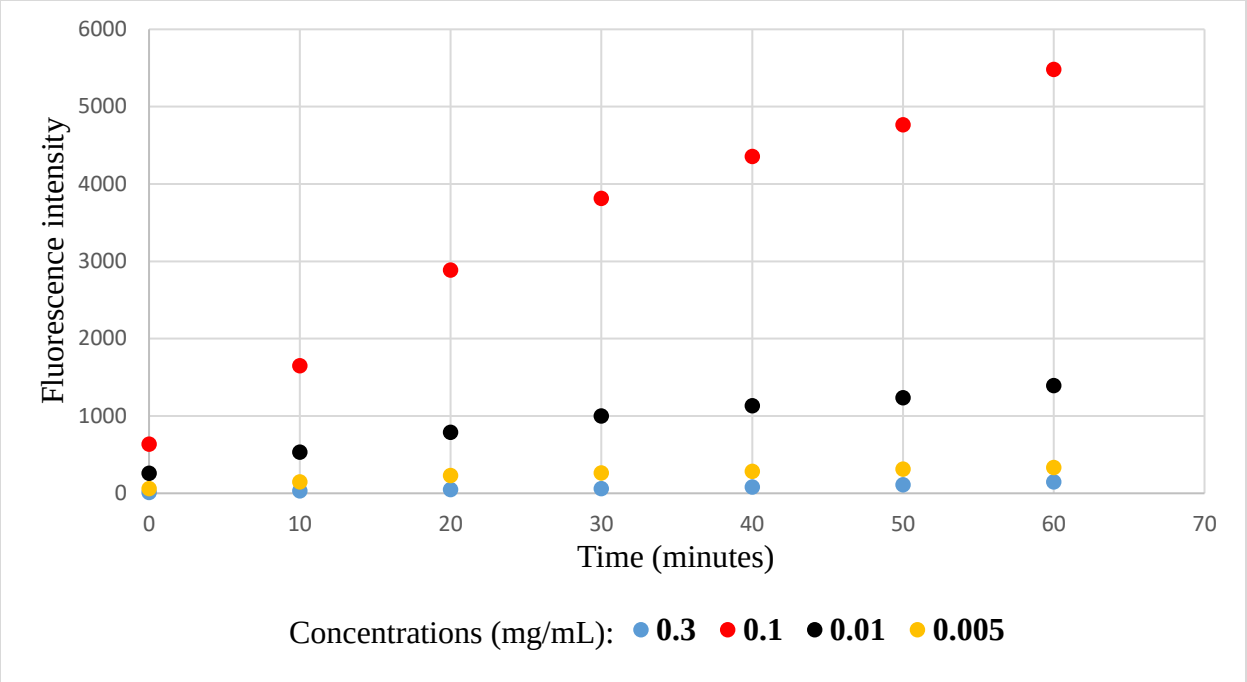

Figure 4-13 Optimization of GNB-MMP1 concentration.

After optimizing the concentration, the next experiment was done to observe the effect of pH on intensity. For this experiment, the optimized concentration 0.1 mg/mL was used, and it was observed that the pH decreased to 6, therefore, the pH was adjusted to 7.2 to ensure full enzymatic activities.[15] The results, shown in Fig. 4-14, demonstrated that in effect the fluorescence intensity significantly increased when the pH was adjusted vs not adjusted.

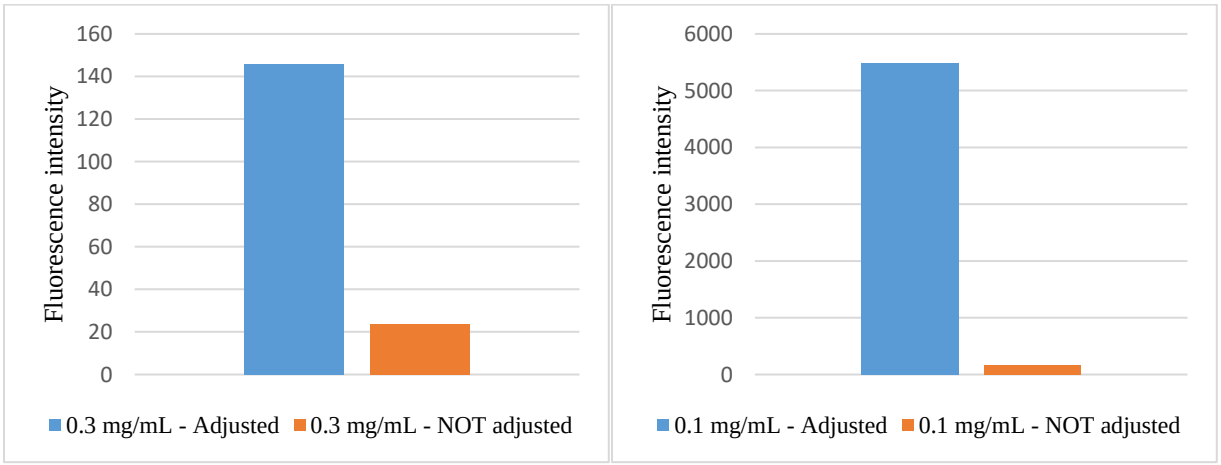

Figure 4-14 Optimization of pH (adjusted to pH = 7.2 vs not adjusted).

After optimizing the pH, the last optimization experiment was done to determine the wavelength that gave the highest fluorescence intensity because the wavelength used is dependent upon the detectable labels used in the nanobiosensor. In this case, TCPP has a maximum absorption near 420 nm. Based on the experience with our previous technology (iron/iron oxide), it was observed that TCPP detection was shifted to 421. Therefore, we wanted to verify if that was still holding true for our new GNB-MMP1, and the results demonstrated that the optimal wavelength for GNB-MMP1 was shifted to 425 nm, as shown in Fig. 4-15.

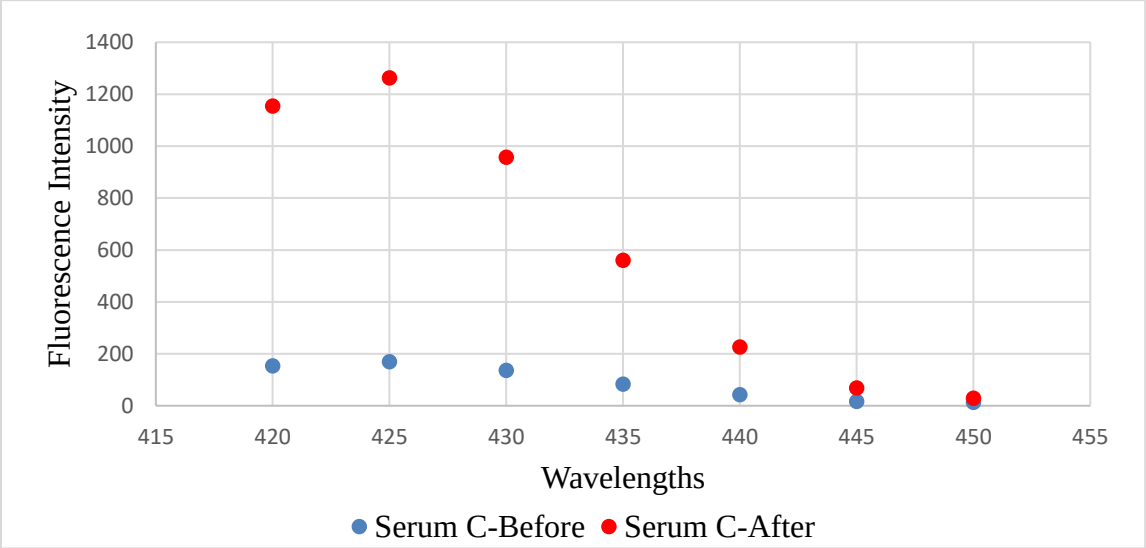

Figure 4-15 Wavelength optimization for GNB-MMP1 Prototype (before and after incubation).

Finally, once all optimizations were performed, our prototype nanobiosensor for MMP1 we tested in a sample with increasing concentration of enzyme. It was observed that the intensity of the detected signal was proportional to concentration of enzyme, as shown in Fig. 4-16. The estimated limit of detection (LOD) for this prototype nanobiosensor showed that femtomolar protease activities could be detected. When TCPP was bound, it showed virtually no fluorescence due to strong carboxygraphene quenching. Upon cleavage during 60min, the fluorophore was released escaping the quenching and resulting in a measurable increase in fluorescence. The working principle for GNB-MMP1 is illustrated by Fig. 4-17.

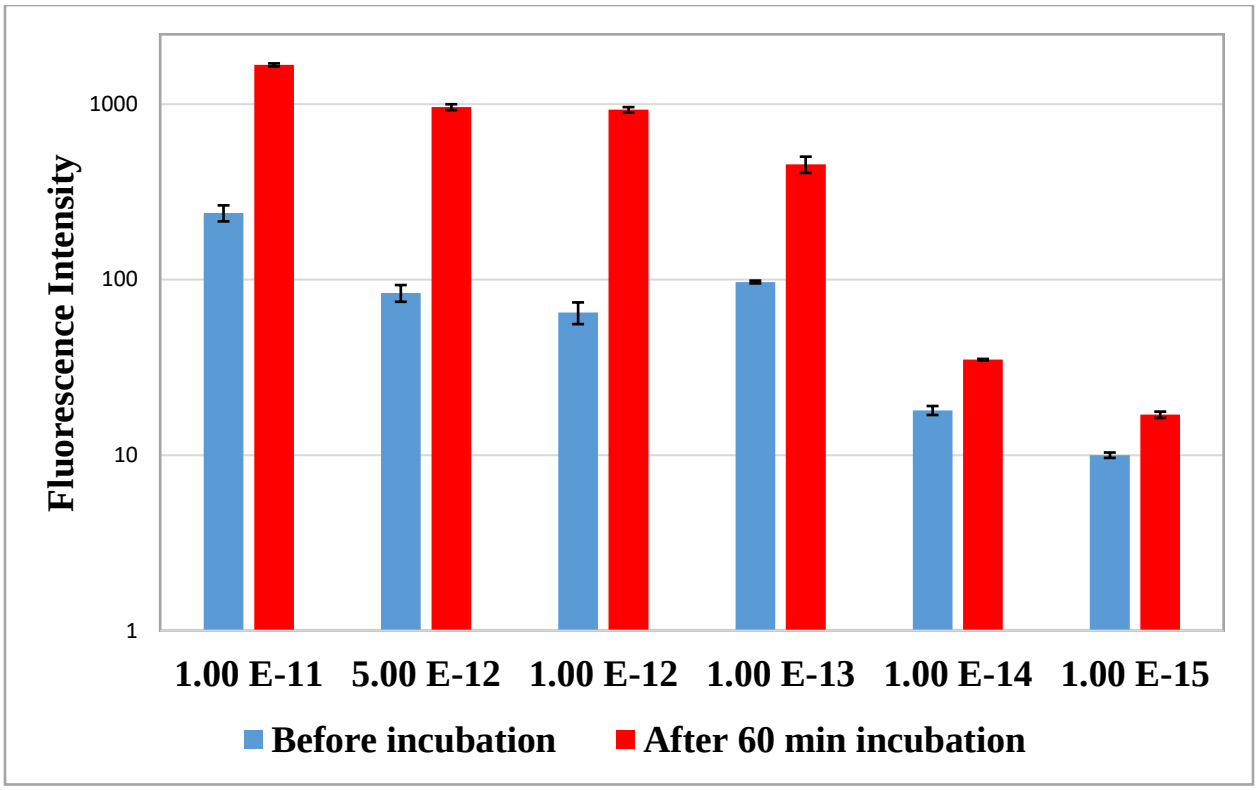

Figure 4-16 Estimation of limit of detection (LOD) as indicated by fluorescence signal (shown with a logarithmic spacing) vs enzyme concentration. (Blue bars: initial fluorescence after adding MMP1 in serum; Red bars: fluorescence reading after 60 min. incubation at 37 °C)

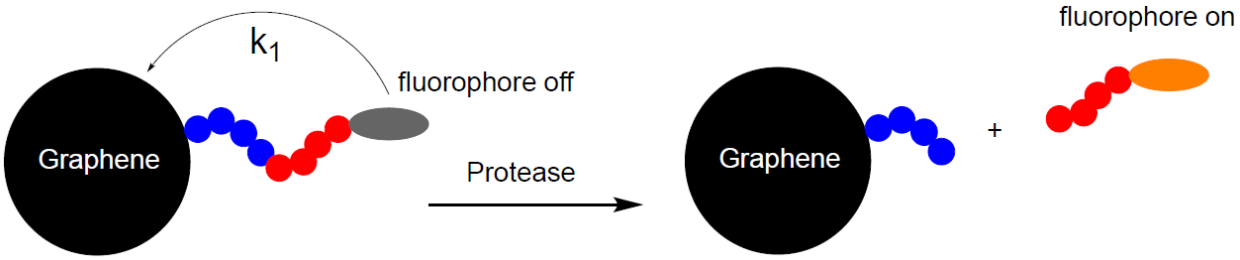

Figure 4-17 Working principle for graphene-based nanobiosensors for protease activity.

3.3. Characterization of 19 GNBs

After the promising results obtained from our GNB-MMP1 prototype, we synthesized 19 nanobiosensors for 19 different biomarkers in lung cancer. However, these 19 nanobiosensors were synthesized in our research lab and characterized by means of DLS, zeta potential, and UV-

Vis spectroscopy before sending them to our collaborators, Hawkeye Bio. The synthesis for all 19 sensors was done in two batches, and based on DLS and zeta potential results, there was minimal disparities between the two batches. Additionally, UV-vis spectroscopy showed the clear presence of the Soret band from TCPP at ~420 nm, thus indicating the sensors had been successfully conjugated with the peptide containing the consensus sequence for their corresponding biomarker. The DLS, zeta potential and Uv-Vis results are shown in Appendix C.

3.4. Replacing TCPP Dye with Rhodamine B

After the successful results from our prototype GNB-MMP1 in the detection of protease activity, we then wanted to explore the synthesis of a nanobiosensor using a different detectable label. One of the reasons was to take advantage that cyanine 5.5 was no longer needed as a quencher, and the other reason was to replace TCPP with a less expensive dye that will help reduce the cost of production thus making the nanobiosensor more affordable. We explored replacing TCPP with rhodamine B because the price of TCPP is approximately $159.00 for 1.0 gram (95% purity), whereas the price of rhodamine B is $61.40 for 100.0 grams (95% purity).[22,23] For this experiment, two nanobiosensors were synthesized and labeled with consensus peptides MMP7 and MMP9 labeled with rhodamine B. The nanosensors were then tested against serum and the fluorescence intensity was measured 60 min after incubation at 37 °C, results shown in Fig. 4-18. The results showed that both rhodamine B nanosensors had higher intensities than the assay control. Additionally, the nanosensors showed similar intensities when we compared rhodamine B against TCPP nanosensors. Therefore, results indicated the nanobiosensors could be successfully labeled with a different dye without altering the

performance of the nanosensors. However, these are early results from a rhodamine B prototype nanosensor thus more optimization studies are needed to ensure results are reproducible.

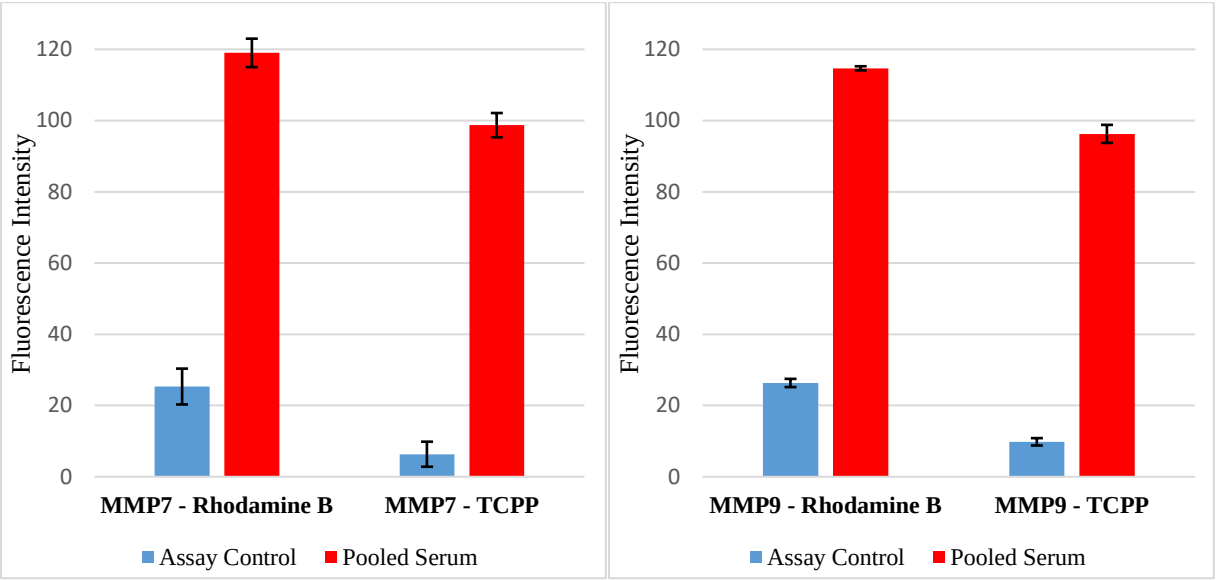

Figure 4-18 MMP7 and MMP9 nanobiosensors (rhodamine B vs TCPP labeled).

4. Conclusion

In conclusion, this chapter describes the development of a long-term stable, highly water/buffer dispersible graphene-based nanobiosensor that has overcome the limitations from our previous iron/iron oxide technologies. The synthesis of carboxygraphene and the assembly of GNB-MMP1 prototype are fully described and characterized. The results demonstrated that the GNB-MMP1 prototype was able to detect biomarkers down to the sub-femtomolar level after 1 hour of incubation. For that same reason, 19 nanobiosensors with suitable biomarkers for the detection of lung cancer were synthesized and delivered to our collaborators where their performance will be studied. Additionally, preliminary results demonstrated that changing the detectable moiety from TCPP to rhodamine B does not really have an impact in the performance of the nanosensors. Thus, it has been demonstrated that these nanobiosensors offer highly

sensitive, quantitative detection and monitoring of protease activity. Therefore, the nanobiosensors have the potential to be used in conjunction with traditional approaches or can be figured as a stand-alone tool in disease screening. This is very important in lung cancer detection because cancer survival significantly increases when it is detected at stages 0, 1 compared to 3 or 4.

5. References

[1]Lung Cancer Statistics https://www.cdc.gov/cancer/lung/statistics/index.htm

[2]Lung Cancer https://www.cancer.org/cancer/lung-cancer.html

[3]Cancer Facts & Figures 2021 https://www.cancer.org/research/cancer-facts-statistics/all-cancer-facts-figures/cancer-facts-figures-2021.html

[4]Henry, N. L.; Hayes, D. F. Cancer Biomarkers. *Mol. Oncol.* **2012**, *6* (2), 140–146.

[5]Dudani, J. S.; Warren, A. D.; Bhatia, S. N. Harnessing Protease Activity to Improve Cancer Care. *Annu. Rev. Cancer Biol.* **2018**, *2* (1), 353–376.

[6]Kessenbrock, K.; Plaks, V.; Werb, Z. Matrix Metalloproteinases: Regulators of the Tumor Microenvironment. *Cell* **2010**, *141* (1), 52–67.

[7]Dudani, J. S.; Ibrahim, M.; Kirkpatrick, J.; Warren, A. D.; Bhatia, S. N. Classification of Prostate Cancer Using a Protease Activity Nanosensor Library. *Proc. Natl. Acad. Sci. U. S. A.* **2018**, *115* (36), 8954–8959.

[8]Welser, K.; Adsley, R.; Moore, B. M.; Chan, W. C.; Aylott, J. W. Protease Sensing with Nanoparticle Based Platforms. *Analyst* **2011**, *136* (1), 29–41.

[9]Holt, B. A.; Mac, Q. D.; Kwong, G. A. Nanosensors to Detect Protease Activity in Vivo for Noninvasive Diagnostics. *J. Vis. Exp.* **2018**, No. 137, e57937.

[10]Kirkpatrick, J. D.; Warren, A. D.; Soleimany, A. P.; Westcott, P. M. K.; Voog, J. C.; Martin-Alonso, C.; Fleming, H. E.; Tammela, T.; Jacks, T.; Bhatia, S. N. Urinary Detection of Lung Cancer in Mice via Noninvasive Pulmonary Protease Profiling. *Sci. Transl. Med.* **2020**, *12* (537), eaaw0262.

[11]Chan, Y.-C.; Hsiao, M. Protease-Activated Nanomaterials for Targeted Cancer Theranostics. *Nanomedicine (Lond.)* **2017**, *12* (18), 2153–2159.

[12]Wang, H.; Udukala, D. N.; Samarakoon, T. N.; Basel, M. T.; Kalita, M.; Abayaweera, G.; Manawadu, H.; Malalasekera, A.; Robinson, C.; Villanueva, D.; Maynez, P.; Bossmann, L.; Riedy, E.; Barriga, J.; Wang, N.; Li, P.; Higgins, D. A.; Zhu, G.; Troyer, D. L.; Bossmann, S. H. Nanoplatforms for Highly Sensitive Fluorescence Detection of Cancer-Related Proteases. *Photochem. Photobiol. Sci.* **2014**, *13* (2), 231–240.

[13]Udukala, D. N.; Wang, H.; Wendel, S. O.; Malalasekera, A. P.; Samarakoon, T. N.; Yapa, A. S.; Abayaweera, G.; Basel, M. T.; Maynez, P.; Ortega, R.; Toledo, Y.; Bossmann, L.; Robinson, C.; Janik, K. E.; Koper, O. B.; Li, P.; Motamedi, M.; Higgins, D. A.; Gadbury, G.; Zhu, G.; Troyer, D. L.; Bossmann, S. H. Early Breast Cancer Screening Using Iron/Iron Oxide-Based Nanoplatforms with Sub-Femtomolar Limits of Detection. *Beilstein J. Nanotechnol.* **2016**, *7*, 364–373.

[14]Malalasekera, A. P.; Wang, H.; Samarakoon, T. N.; Udukala, D. N.; Yapa, A. S.; Ortega, R.; Shrestha, T. B.; Alshetaiwi, H.; McLaurin, E. J.; Troyer, D. L.; Bossmann, S. H. A Nanobiosensor for the Detection of Arginase Activity. *Nanomedicine* **2017**, *13* (2), 383–390.

[15]Kalubowilage, M.; Covarrubias-Zambrano, O.; Malalasekera, A. P.; Wendel, S. O.; Wang, H.; Yapa, A. S.; Chlebanowski, L.; Toledo, Y.; Ortega, R.; Janik, K. E.; Shrestha, T. B.; Culbertson, C. T.; Kasi, A.; Williamson, S.; Troyer, D. L.; Bossmann, S. H. Early Detection of Pancreatic Cancers in Liquid Biopsies by Ultrasensitive Fluorescence Nanobiosensors. *Nanomedicine* **2018**, *14* (6), 1823–1832.

[16]Udukala, D. N.; Wendel, S. O.; Wang, H.; Yapa, A. S.; Covarrubias-Zambrano, O.; Janik, K.; Gadbury, G.; Troyer, D. L.; Bossmann, S. H. Early Detection of Non-Small Cell Lung Cancer in Liquid Biopsies by Ultrasensitive Protease Activity Analysis. *J. Cancer Metastasis Treat.* **2020**, *2020*. https://doi.org/10.20517/2394-4722.2020.45.

[17]D.N. Udukala, Chemistry Protease Assays for Cancer Diagnostics, Kansas State University, Manhattan, KS, **2014**.

[18]Kasry, A.; Ardakani, A. A.; Tulevski, G. S.; Menges, B.; Copel, M.; Vyklicky, L. Highly Efficient Fluorescence Quenching with Graphene. *J. Phys. Chem. C Nanomater. Interfaces* **2012**, *116* (4), 2858–2862.

[19]Duro-Castano, A.; Conejos-Sánchez, I.; Vicent, M. Peptide-Based Polymer Therapeutics. *Polymers (Basel)* **2014**, *6* (2), 515–551.

[20]Chen, B.; Liu, M.; Zhang, L.; Huang, J.; Yao, J.; Zhang, Z. Polyethylenimine-Functionalized Graphene Oxide as an Efficient Gene Delivery Vector. *J. Mater. Chem.* **2011**, *21* (21), 7736.

[21]Song, M.; Xu, J. Preparation of Polyethylenimine-Functionalized Graphene Oxide Composite and Its Application in Electrochemical Ammonia Sensors. *Electroanalysis* **2013**, *25* (2), 523–530.

[22]Tetrakis(4-carboxyphenyl) porphyrin (TCPP) https://www.tcichemicals.com/US/en/search/?text=Tetrakis%284-carboxyphenyl%29porphyrin

[23]Rhodamine B https://www.sigmaaldrich.com/US/en/product/sigma/r6626

Chapter 5 - Summary and Future Studies

1. Summary of Results

Cancer is the 2nd leading cause of death in the United States, which on average it accounts for four new cancer cases and one death pre minute. Among most cancers, lung cancer causes a higher number of deaths than any other type of cancer in the United States, making up almost 25% of all cancer deaths. Unfortunately, there is no way to prevent cancer until this day no matter what age, gender, race, or ethnicity people might come from. For this reason, researchers have devoted a great effort in the development of early detection techniques or more effective treatments for cancer to increase the survival rate.

Thanks to the discovery of graphene's unique properties several researchers have been exploring ways to take advantage of such properties and incorporate them in the fight against cancer. However, the major issues in taking complete advantage of graphene persist in overcoming the challenges of mass-producing high-quality material and preventing the agglomeration and restacking of graphene sheets. In this work, we have offered a solution to overcoming both issues by creating the first turbostratic graphene/graphene oxide core/shell particle and demonstrating the reaction was broadly scalable while retaining graphene's remarkable property. This was done by implementing the Fenton oxidation method which only led to the oxidation of the outer graphene layers from explosion synthesized graphene, thus resulting in a unique structure that consists of an uncompromised graphene core and a highly reactive shell. Furthermore, following the concept of rational chemistry design of our turbostratic graphene oxide, we demonstrated that the carboxylic acid groups located at the outer layers of the stacked few-layer graphene assembly could be further reacted or functionalized depending

upon the desired use, to create a wide variety of GO derivatives which permits the integration of virtually intact high-value graphene into multiple new materials.

Lastly, we also developed a long-term stable, highly water/buffer dispersible graphene-based nanobiosensor for lung cancer detection that overcame the limitation from our previous iron/iron oxide technology. This was achieved by developing a novel way to derivatize graphene via azirane cycloaddition to create carboxygraphene. This offered the opportunity to add a tailored number of carboxylic acids to the surface of graphene without compromising the optical and electrical properties of graphene. The results showed that our GNB-MMP1 prototype nanobiosensor was able to detect biomarkers down to sub-femtomolar level after 1 hour of incubation. Thanks to the successful results that were obtained, a company called Hawkeye Bio from California became interested in licensing our patent. Therefore, we synthesized and delivered 19 graphene-based nanobiosensors to Hawkeye Bio. Furthermore, we explored the possibility of replacing TCPP dye with rhodamine B the make our nanobiosensor more cost effective. The preliminary results showed that replacing TCPP dye for rhodamine B does not really impact the performance of the NBs. Therefore, the nanobiosensors have the potential to be used in conjunction with traditional approaches or can be figured as a stand-alone tool in disease screening. This is very important in lung cancer detection because cancer survival significantly increases when it is detected at stages 0, 1 compared to 3 or 4.

2. Future Studies

Both derivatization procedures (Fenton Oxidation and Carboxygraphene) showed that the graphenic inner core in both materials is preserved. Therefore, one of the very next studies will be to perform biological studies on surface modified GO derivatives. We believe that these

studies will allow us to better determine what applications can these derivatives be suitable for. Furthermore, we will also be working towards expanding our library and create more GO derivatives. Additionally, one of the next objectives is to upscale the G/GO reaction up to 1 kg. This will be done to further demonstrate that our method could indeed help overcome one of the greatest challenges in mass-producing high-quality material in a reproducible way at low cost. Another future objective is to further derivatize carboxygraphene and create a library of compounds via the carboxygraphene route to integrate these compounds into different applications. Also, we will continue our work with our graphene-based nanobiosensor in hopes to optimize the rhodamine B nanobiosensor. Moreover, we will also explore the possibility to develop other graphene-based nanobiosensors with different detectable moieties for potential use in other diseases.

Appendix A - For Chapter 2

Optimal Experimental Design Methodology (OEDM)

In order to optimize the Fenton oxidation conditions of graphene, the effects of two main process variables (U_i) on oxygen content, as measured by CHO analysis, and zeta potential of the obtained graphene/graphene oxide core/shell nanoparticles (experimental responses R_1 and R_2) were determined: (I) concentration of iron(II)sulfate (U_1, milligrams per 100ml aqueous H_2O_2 solution, pH = 3.0) and (II) reaction temperature (U_2, ^oC). OEDM was used for designing an experimental matrix that is able to provide meaningful results with a minimum of experiments required.[44-50] OEDM is based on multivariate models[44-50] where experimental settings of independent variables are concurrently modified in a manner that an experimental matrix is shaped that permits statistically significant modelling and prediction of optimized variables. We have selected the so-called Doehlert matrix, which provides a very easy approach to optimized process parameters. In this design, the independent variables U_i are normalized. The center variable x_i defined as:

$$x_i = \frac{(U_i - U_{i,0})}{\Delta U_i}$$

where $U_{i,0} = (U_{i,max} + U_{i,min})/2$ is the value of U_i at the center of the experimental region (Doehlert hexagon). ΔU_i is defined as $(U_{i,max} - U_{i,min})/2$. For a Doehlert matrix, the dependent variable $Y = f(x_i)$ is represented by a quadratic polynomial model.

$$Y = b_0 + b_1x_1 + b_2x_2 + b_{11}x_1^2 + b_{22}x_2^2 + b_{12}x_1x_2$$

In the case of two independent variables, the Doehlert matrix contains 7 uniformly distributed experiments that form a hexagon containing a center variable. The experiment in the center has to be repeated at least three times to ascertain the statistical reproducibility of the results.

We used the program package DESIGN Expert 2[51] to calculate the coefficients of the polynomial model and the resulting surface response by applying the least-squares method, as well as F-tests to ascertain the validity of the quadratic polynomial model.

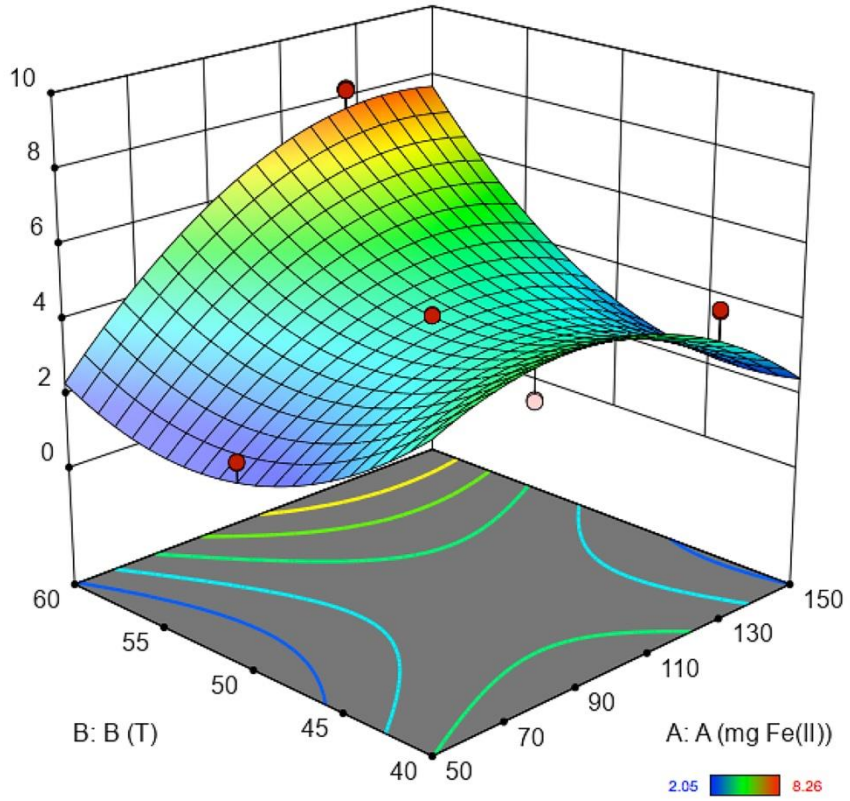

Figure A. 1. Response surface of Doehlert matrix 1 (catalyst variation: 50 to 150 mg FeSO4 x 7 H2O; temperature variation: 40 to 60 °C.

ANOVA analysis for the model shown in Figure A.1. resulted in a p-value of < 0.0001 (significant). The final response equation for this model is:

$$R_1 = 415.2 - 1.64778\ A - 9.77281\ B + 0.004744\ AB + 0.004752\ A^2 + 0.071956\ B^2$$

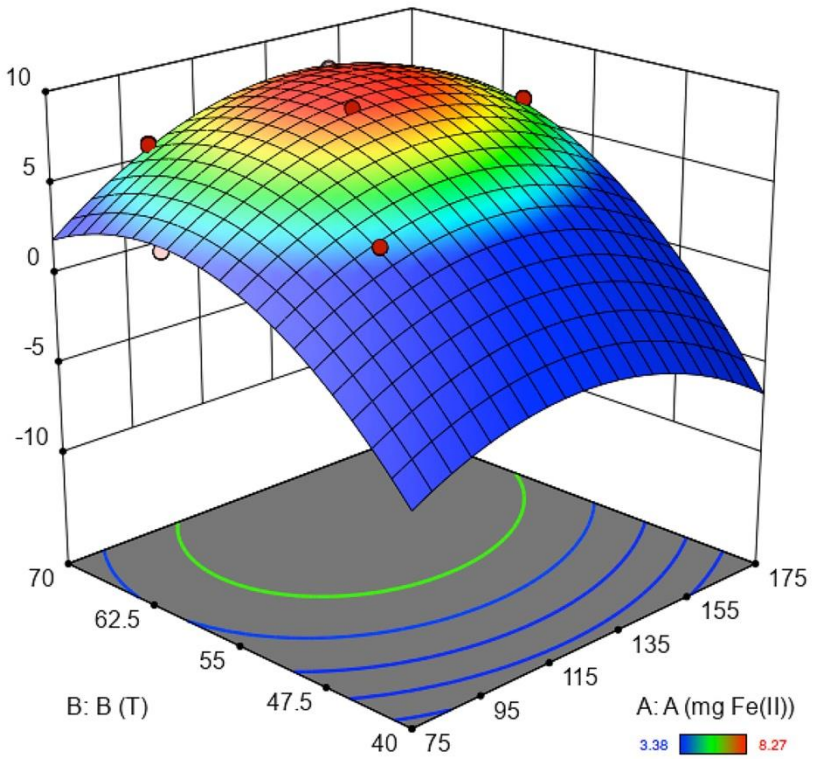

Figure A. 2. Response surface of Doehlert matrix 2 (catalyst variation: 50 to 150 mg FeSO4 x 7 H2O; temperature variation: 50 to 70 °C.

ANOVA analysis for the model shown in Figure A.2. resulted in a p-value of < 0.0001 (significant). The final response equation for this model is:

$$R_1 = -82.42597 + 0.249511\ A + 2.31817\ B + 0.001930\ AB - 0.001365\ A^2 - 0.020212\ B^2$$

The second Doehlert optimization clearly shows a maximum close to 60 ^oC and 125 mg $FeSO_4$ x 7 H_2O. This clearly demonstrates that the application of an Optimal Experimental Design Method has minimized the requirement of experiments to find optimal reaction conditions. This will be important for effective rational chemical applications of graphene derivatives, such as graphene oxide.

Appendix B - For Chapter 3

Sample	Zeta Potential (mV)
1st Upscale reaction (10 g in 1 L)	- 8.35
2nd Upscale reaction (10 g in 1 L)	- 7.79

Table B. 1. Zeta potential analysis of the first two upscale reactions (10 g GNs in 1 L H_2O_2).

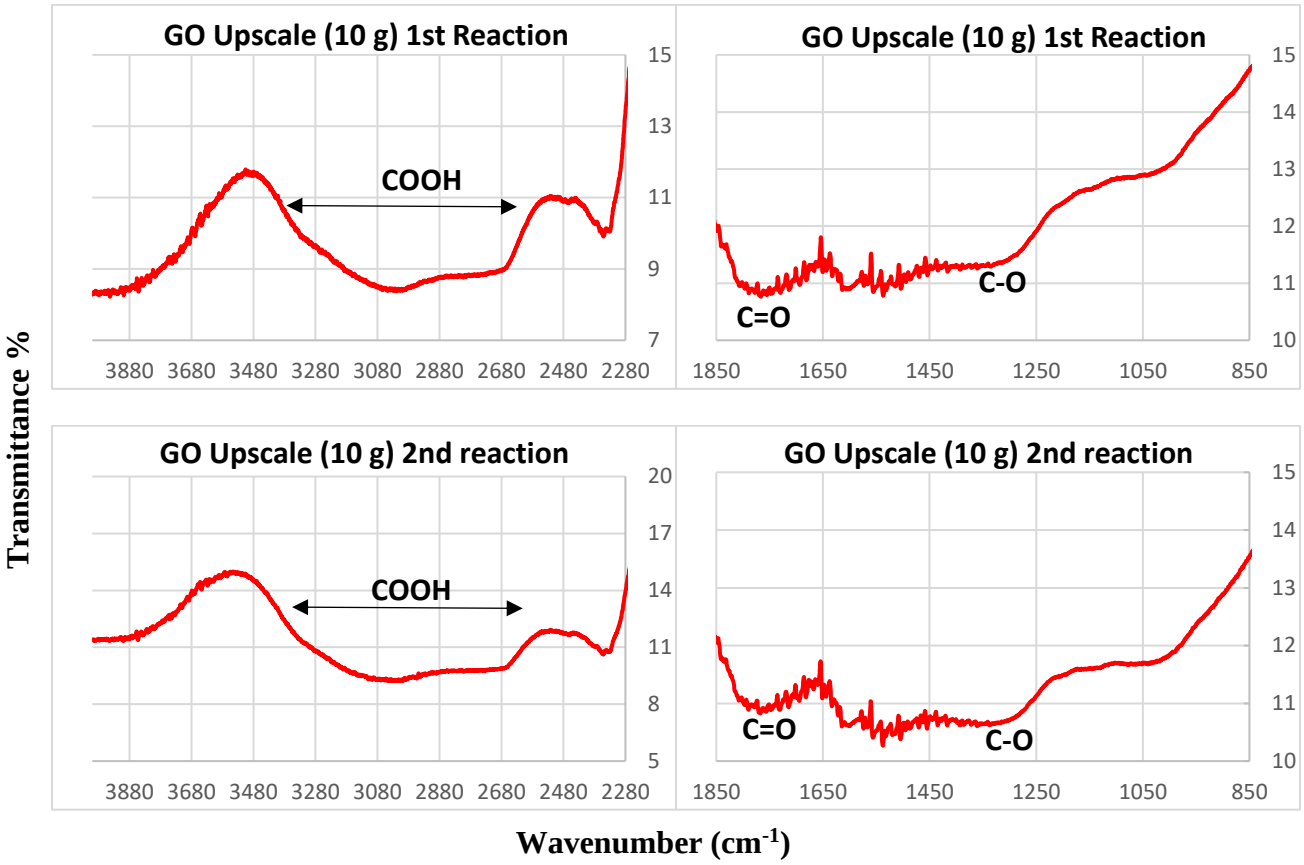

Figure B. 1. FTIR spectra of the first two upscale reactions (10 g GNs in 1 L H_2O_2).

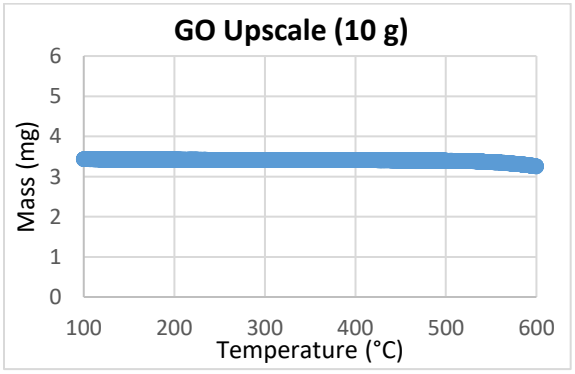

Figure B. 2. Thermogravimetric analysis of the first two upscale reactions (10 g GNs in 1 L H_2O_2).

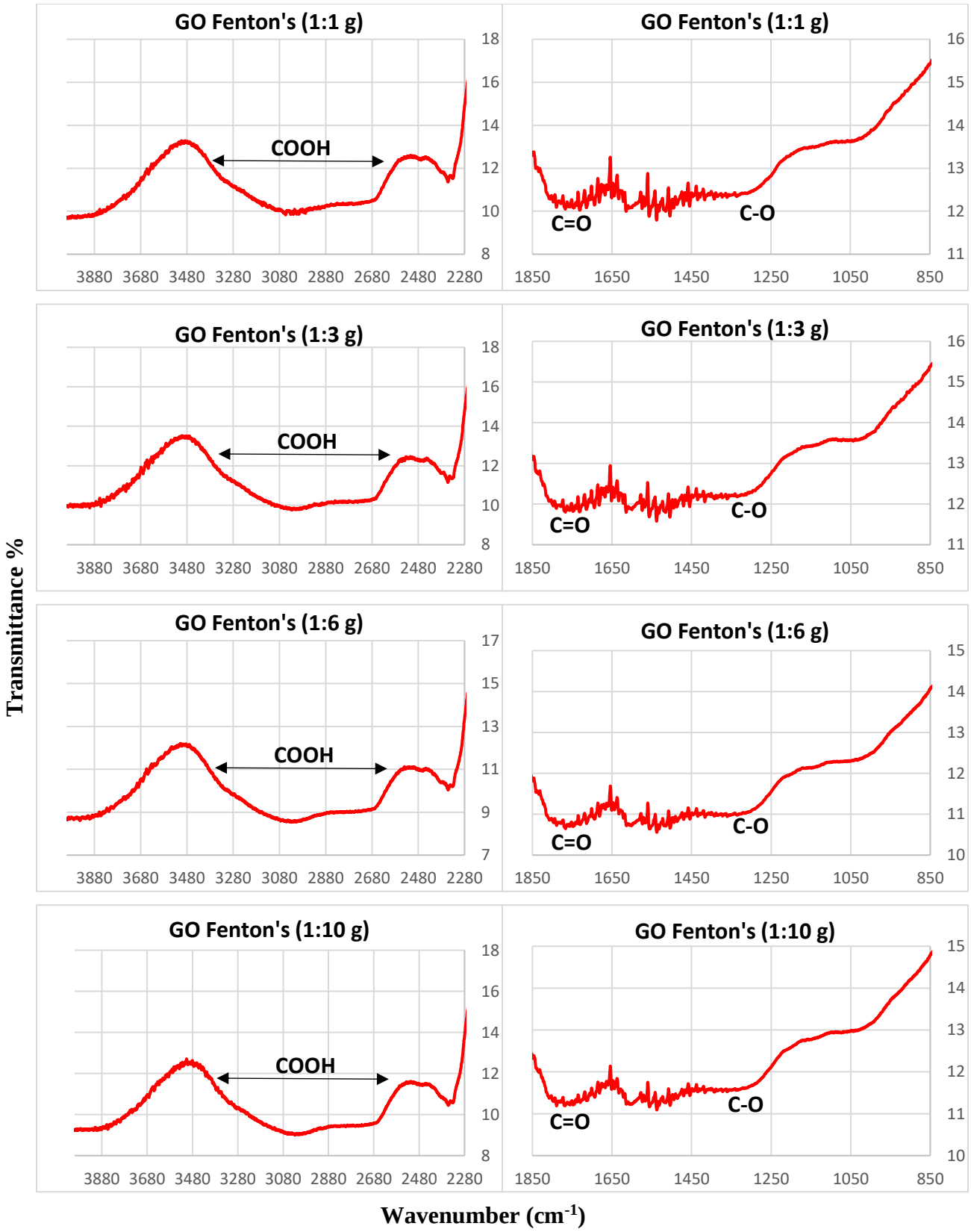

Figure B. 3. FTIR spectra of 1:1, 1:3, 1:6, and 1:10 reactions for optimization parameters.

Sample	Zeta Potential (mV)
Upscale reaction (100 g in 1 L)	**- 9.69**
Upscale reaction (200 g in 2 L)	**- 8.62**

Table B. 2. Zeta potential analysis of upscale reactions (100 g and 200 g GNs in 1 L H_2O_2).

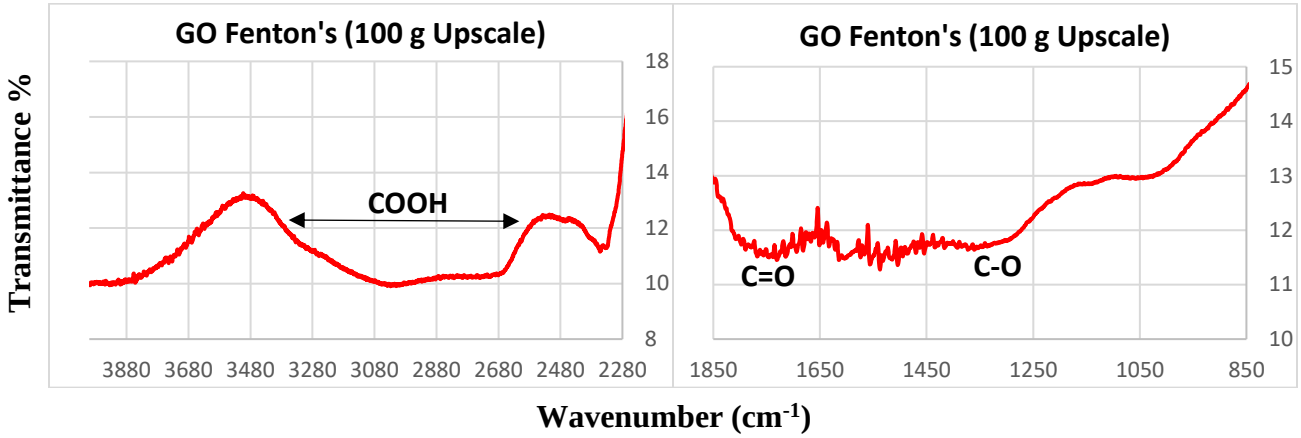

Figure B. 4. FTIR Spectra from 100g Upscale Reaction.

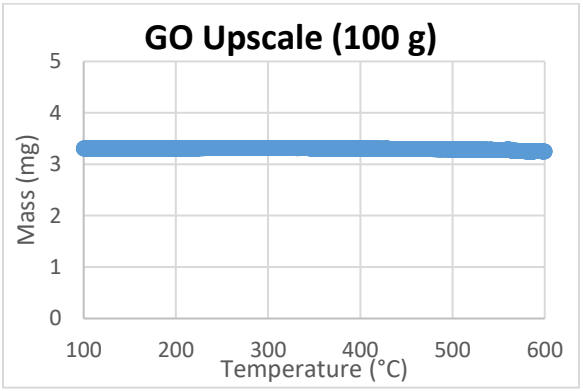

Figure B. 5. Thermogravimetric analysis of the first two upscale reactions (100 g GNs in 1 L H_2O_2).

Appendix C - For Chapter 4

	DLS (nm)		Zeta potential (mV)	
	Batch 1	**Batch 2**	**Batch 1**	**Batch 2**
MMP1	611.07	611.51	1.19	1.33
MMP2	551.19	688.17	0.37	-0.87
MMP3	551.19	603.09	3.66	1.33
MMP7	563.71	636.74	3.13	1.25
MMP9	569.27	670.57	1.68	1.52
MMP10	368.11	419.43	1.96	1.75
MMP11	401.15	44.29	3.33	1.97
MMP12	324.48	363.58	4.10	2.93
MMP13	601.67	676.28	1.85	1.26
MMP15	607.38	684.30	0.55	0.91
CTS B	563.96	657.33	1.42	1.38
CTS D	467.87	533.72	3.88	2.18
CTS E	692.28	794.73	-0.33	-1.81
CTS H	514.39	504.57	2.23	2.35
CTS K	433.65	452.68	3.88	1.42
CTS L	686.77	701.84	0.56	1.19
NE	504.69	498.07	1.68	0.25
uPA	467.57	509.31	1.92	0.68
Arginase	545.25	485.01	3.47	2.06

Table C. 1. DLS and Zeta Potentials of all 19 Nanobiosensors.

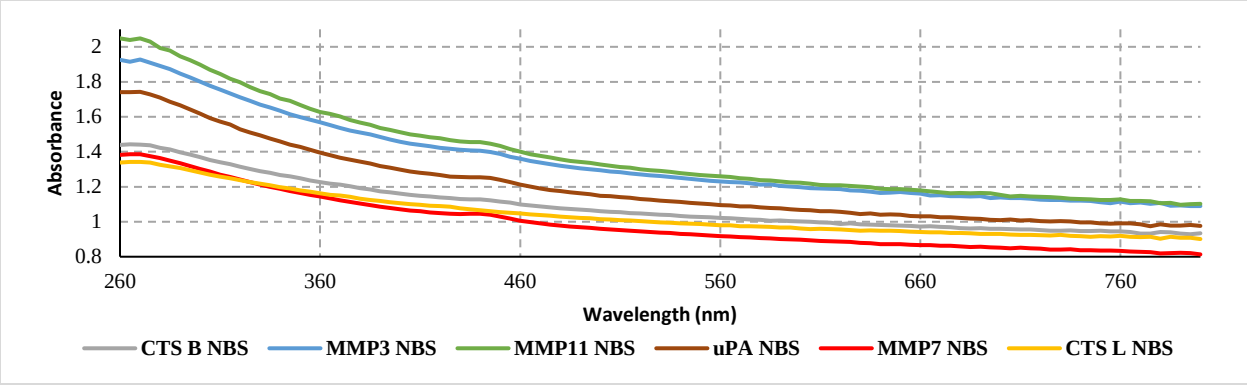

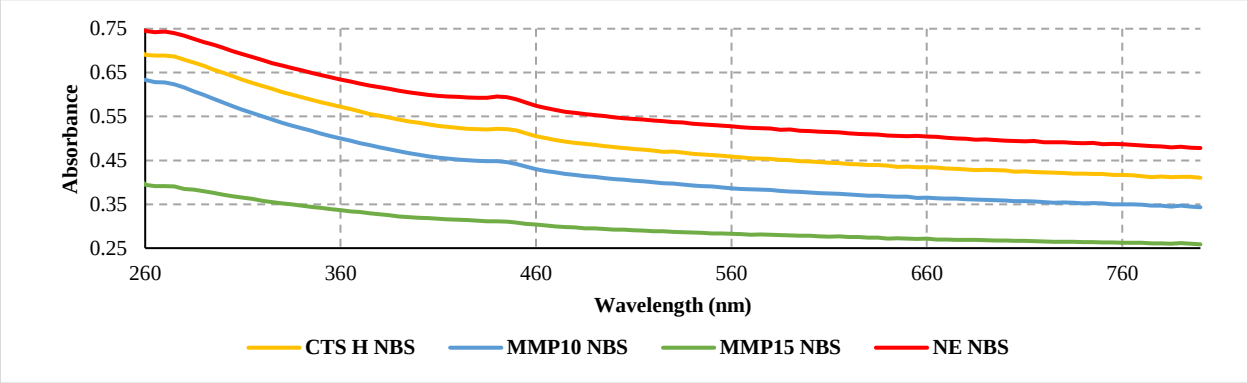

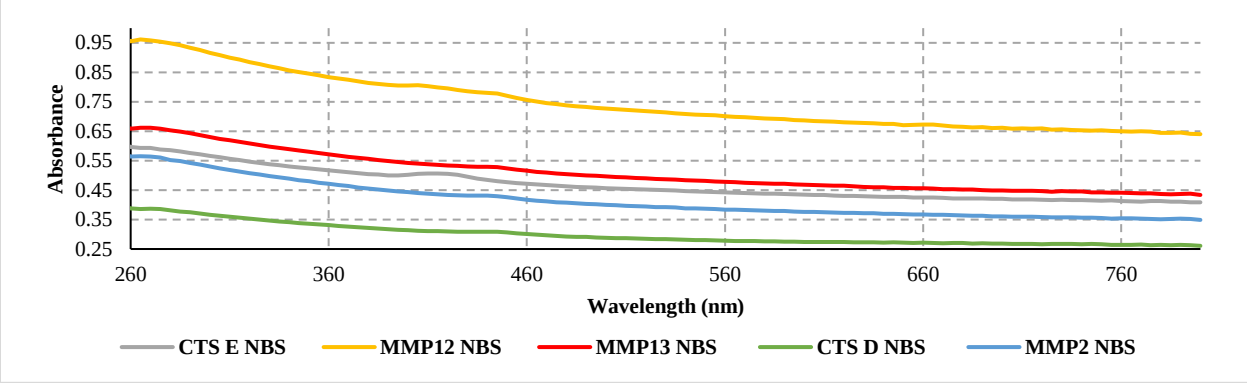

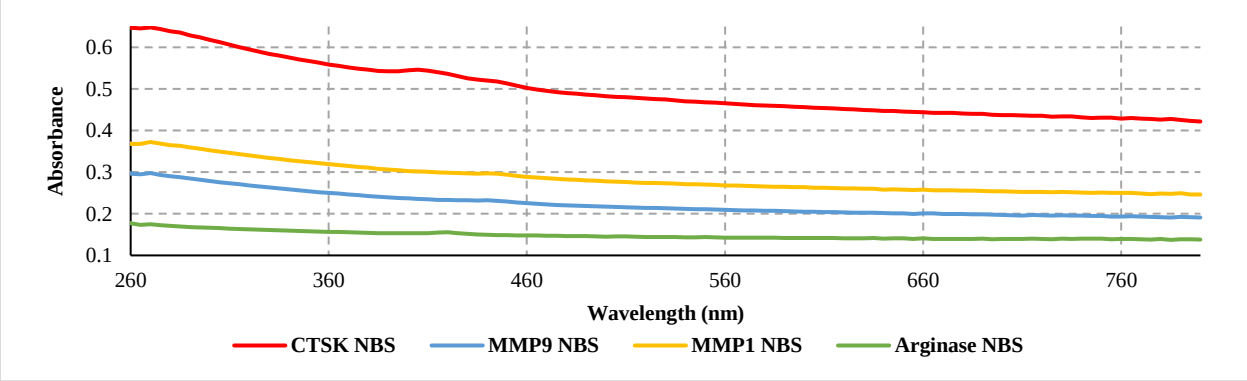

Figure C. 1. Uv-Vis spectra for all 19 nanobiosensors.

List of Terminology: Abbreviations Page

Abbreviation	*Meaning*	*Page*
G	Graphene	21
GO	Graphene oxide	22
GNs	Graphene nanosheets	24
RGO	Reduced graphene oxide	27
PTT	Photothermal therapy	28
NGO	Nanoscale graphene oxide	29
NCGO	Nanoscale carboxylated graphene oxide	29
NMR	Nuclear magnetic resonance	35
FTIR	Fourier Transform infrared spectroscopy	35
SSA	Specific surface area	35
TEM	Transmission electron microscopy	35
Gr	Graphite	36
GON	Graphene oxide nanosheets	37
STM	Scanning tunneling microscopy	38
XPS	X-ray photoelectron spectroscopy	38
OEDM	Optimal experimental design methodology	40
G/GO	Graphene/graphene oxide core/shell particles	41
XRD	X-ray powder diffraction	43
TGA	Thermogravimetry Analysis	53
mGO	Graphene oxide methyl ester	57
degGO	Graphene oxide diethylene glycol ester	59
aGO	Graphene oxide amide	61
PEI	Polyethylenimine	88
SCLC	Small cell lung cancer	89
NSCLC	Non-small cell lung cancer	89
MMP	Matrix metalloproteinase	90
CTS	Cathepsin	90
uPA	Urokinase plasminogen activator	90

TCPP	Tetrakis (4-carboxyphenyl) porphyrin	91
CG	Carboxygraphene	92
G-PEI	Carboxygraphene – polyethylenimine	94
GNBs	Graphene-based nanobiosensor	96
GNB-MMP1	Graphene nanobiosensor labeled with MMP1 consensus sequence	102